THE ROLE OF HIGH FREQUENCY OSCILLATIONS IN MEMORY AND MOTOR PERFORMANCE

by

QIAOYU CHEN

A thesis submitted to the University of Birmingham

for the degree of

DOCTOR OF PHILOSOPHY

School of Psychology

College of Life and Environmental Sciences

University of Birmingham

15 February 2024

ABSTRACT

While high frequency (in the gamma range) rhythmic sensory stimulation (RSS) mainly involves inhibitory interneurons responses, low frequency RSS drives pyramidal neurons (Cardin et al., 2009). Using high and very low frequency RSS, the current thesis explored the role of high-frequency oscillations in human episodic memory and sensorimotor synchronization (SMS). High frequency RSS was delivered by short movies. Although existing evidence suggesting the recruitment of inhibitory interneurons by high frequency RSS, our findings revealed nuanced modulations in both SSVEPs and memory performance. In contrast, low frequency appears to play a crucial role in facilitating long-distance communications and plasticity. Supporting this idea, using low frequency auditory RSS, the final study revealed a connection between the phase locking of beta bursts to slow rhythms and movement performance. Collectively, despite the distinct mechanism underlying high and low frequency RSS, this thesis sheds light on the potential of RSS in regulating brain activity. Future investigations that integrate techniques such as optogenetics, neuroimaging, and computational modelling could provide a multidimensional perspective and valuable insights into the application of RSS in both research and clinical fields.

To my dear grandparents in Happy Land.

ACKNOWLEDGEMENTS

Since embarking on my PhD journey, I have been eagerly anticipated filling this acknowledgement. I have even been roughly drafting the name list numerous times. Finally, the moment has arrived. And I find no words in my dictionary could be sufficient to express my gratitude.

I would like to take this opportunity to extend my deepest gratitude to my exceptional supervisors, Simon Hanslmayr and Kimron Shapiro. Your guidance has illuminated my path in the realm of science and revealed the joy of research to me. Irrespective of your remarkable accomplishments, your patience in mentoring your students remains unwavering. Being your student has been an immensely enjoyable journey, and words can hardly encompass the depth of my appreciation.

My heartfelt thanks extend to Danying Wang, Ole Jensen, and Maria Wimber for their invaluable insights, unwavering support, and encouragement as I navigate the pursuit of truth. I also extend my gratitude to the numerous colleagues in the lab; it has been a pleasure working alongside you.

I am deeply grateful to the China Scholarship Council for providing me with this opportunity.

Furthermore, I am indebted to my dearest friends for their unwavering support.

To 燕秋, your unwavering support over our shared twenty-four years means the world to me. To 楚华, your invaluable assistance has been indispensable. To 劉涵, thank you for being my best friend. To my younger brother, 鹏涛, for looking after my loved ones when I am not present and for being my best friend.

Lastly, my heartfelt gratitude extends to my grandparents and parents for their unwavering love. Their encouragement and support have been the bedrock of my happiness and growth.

BLANK

CONTENTS

PUBLICATIONS AND CONTRIBUTIONS

A significant portion of this thesis incorporates content that has been published or submitted to academic journals, prepared for publication, presented at conferences, or shared on preprint servers. The text from these sources has been meticulously adapted to form a cohesive narrative within this thesis.

Chapter 1: This chapter is derived and modified from a paper authored by myself (QC) as the primary author. In this capacity, QC was responsible for experiment design, data collection and analysis, and drafting the manuscript, which included creating figures suitable for publication. Simon Hanslmayr (SH) and Kimron Shapiro (KS) provided comprehensive supervision throughout all phases of the project. Danying Wang also contributed to the design of the experiment and supported data analysis.

Chapter 2: The content presented in this chapter comprises a significant portion of a study currently in preparation for publication. In this study, experiment design, data collection and analysis, manuscript drafting were carried out by myself (QC), with continuing supervision from SH and KS.

Chapter 3: The experiment in this chapter was designed by Mark T. Elliott (ME) and Craig J. McAllister (CM). Data collection was conducted by Verena Braun, and SH handled the initial data pre-processing. During the pandemic, QC undertook the data analysis under the supervision of SH and KS, with efforts to mitigate the potential impact of COVID-related disruptions. This chapter has been prepared to meet publication standards and has been shared on preprint servers. QC is the lead author responsible for data analysis and manuscript composition, while SH, KS and CM supervised the writing process.

Journal Articles

Chen, Q., Wang, D., Shapiro, K. L., & Hanslmayr, S. (2021). Using fast visual rhythmic stimulation to control inter-hemispheric phase offsets in visual areas. *Neuropsychologia*, *157*, 107863.

Chen, Q., Shapiro, K. L., & Hanslmayr, S. (in preparation). Using high gamma rhythmic visual stimulation to investigate the role of STDP in human episodic memory.

Chen, Q., McAllister, C. J., Elliott, M. T., Shapiro, K. L., & Hanslmayr, S. (2023). Beta bursts correlate with synchronization of movements to rhythmic sounds. *bioRxiv*, 2023-03.

Chen, Q., McAllister, C. J., Elliott, M. T., Shapiro, K. L., & Hanslmayr, S. (in preparation). Beta bursts correlate with synchronization of movements to rhythmic sounds.

LIST OF FIGURES

LIST OF ABBREVIATIONS

AD	Alzheimer's disease
ANOVA	analysis of variance
AUC	area under the curve
CA1	cornu ammonis 1
CA3	cornu ammonis 3
CRT	cathode-ray tube
DPSD	dual-process signal detection
EC	entorhinal cortex
EEG	electroencephalogram
EMG	electromyography
EOG	electrooculography
ERD	event-related desynchronization
ERS	event-related synchronization
FIR	finite impulse response
FS-PV+	fast spiking parvalbumin-positive interneurons
FWHM	full width at half-maximum
HEOG	horizontal electrooculography
ICA	independent component analysis
IOI	Inter-onset interval
ITPC	inter-trial phase coherence
LED	light-emitting diode
LSM	left sensorimotor cortex
LTD	long-term depression
LTP	long-term potentiation
LVF	left visual field
MEG	magnetoencephalography
NMA	negative mean asynchrony
NMDA	N-methyl-D-aspartate
PAS	paired associative stimulations
PPC	pairwise phase coherence
R matrix	reference matrix
rAA	right associative auditory cortex
RESS	rhythmic entrainment source separation
RMS	root mean square
ROC	receiver-operating characteristics
ROI	region of interest
RSS	rhythmic sensory stimulation
RT	reaction time
RVF	right visual field
RVS	rhythmic visual stimulation
S matrix	signal matrix
SD	standard deviation
SEM	standard error of mean
SMS	sensorimotor synchronization
SNR	signal-to-noise ratio
SSVEPs	Steady-state visual evoked potentials
STDP	spike timing dependent plasticity
TMS	transcranial magnetic stimulation
TOI	time of interest

CHAPTER 1: GENERAL INTRODUCTION

1.1. The oscillating brain

A century ago, the phenomenon of oscillating brain came to light through the pioneering work of Dr. Hans Berger. He named the first brain rhythm recorded from the occipital skull "alpha" (approximately 10 Hz, Berger, 1929). Similarly, he coined the term "beta" for a faster rhythm characterized by smaller amplitude. In the wake of Berger's discovery, subsequent research uncovered an expanding array of oscillatory patterns. The highest frequencies documented could be up to 600 Hz (Katz & Cracco, 1971). Among these rhythms, the most extensively studied frequency bands are delta (0.5-4 Hz), theta (4-8 Hz), alpha (8-12 Hz), beta (12-30 Hz) and gamma (30-100 Hz). However, the delineation of frequency bands can sometime overlap, depending on diverse factors, e.g., the specific brain region investigated. These rhythms were thought to server a wide variety of functions. For example, theta is involved in memory formation, attention and learning, and alpha is associated with irrelevant information inhibition. This thesis will be focusing on the role of high frequencies (>12 Hz) in episodic memory and sensorimotor synchronization.

1.2. Episodic memory, gamma oscillations and STDP

Episodic memory, as first defined by Tulving and in a series of works (Tulving, 1972; 1983; 1984; 1993), pertains to the recollection of personal experienced events. This concept underscores the significance of two integral elements: temporal and spatial information.

Tulving captured the retrieval process for episodic memory by the query, “What did you do at time T in place P?”—a statement that has gained widespread acceptance (Tulving, 1984). In his booking titled “How We Remember: Brain Mechanisms of Episodic Memory”, Hasselmo presents a model that portrays episodic memory as a spatial-temporal trajectory (Hasselmo, 2011), which is coded by the brain rhythms.

Synchronization at the gamma range is critical for episodic memory (Benussi et al., 2022; Juergen Fell & Axmacher, 2011; Jürgen Fell et al., 2001; Griffiths et al., 2019; Gruber et al., 2004; Gruber et al. 2001; Hanslmayr et al., 2016; Jutras et al., 2009; Miltner et al., 1999; Sederberg et al., 2003). Conclusive support stems from the measure of macaque hippocampus neurons revealed enhanced gamma synchronization during memory encoding predicts recall performance (Jutras et al., 2009). Spike timing-dependent plasticity (STDP) is one important candidate mechanism correlates with gamma synchronization that underlies episodic memory by supporting neural communications and plasticity (Debanne & Inglebert, 2023; Juergen Fell & Axmacher, 2011). In STDP, the efficiency of synaptic modification depends on the activation order and time delay between pre- and postsynaptic neurons (Fig. 1.1). It results in long-term potentiation (LTP) when the activation of presynaptic neuron precedes postsynaptic neuron, and long-term depression (LTD) when the order is reversed. The crux of LTP induction resides within a precise temporal window, optimally situated in the range of 10 to 30 ms, corresponding to a frequency range of 100-33 Hz — entailing the gamma band (Buzsáki, 2010).

The first documented instance of observing STDP *in vivo* dates back to 1998. Zhang and colleagues conducted experiments on retinotectal neuron in Xenopus, a type of frog, using repetitive electrical stimulation. Their research illuminated that the critical time window for l-term potentiation (LTP) and long-term depression (LTD) is approximately ± 20 ms. Notably,

the transition from the LTP to LTD peaks occurs within a mere 10 ms timeframe (Zhang et al., 1998).

A similar time window is consistently demonstrated across various species, including rodents, locusts, and cats. Numerous studies, including intracellular and extracellular recordings as well as *in vitro* studies related to perception and learning, revealed analogous short time frames from ± 20 to ± 60 ms (Bi & Poo, 1998; Cassenaer & Laurent, 2007; Fu et al., 2002; Meliza & Dan, 2006; Yao & Dan, 2001).

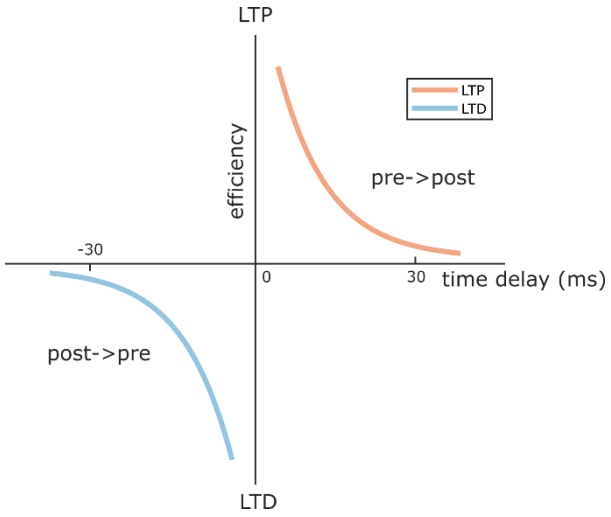

Fig. 1.1. STDP. The efficiency of synaptic modification depends on the time delay and activation order between pre- and postsynaptic neurons. It leads to LTP when presynaptic spike precedes the activation of postsynaptic neuron (orange). Oppose temporal order results in LTD (blue).

Moreover, similar findings were extended in human subjects. Using paired associative stimulations (PAS), STDP was identified in the human motor cortex (±25 ms, Stefan et al., 2002; 25 ms for LTP, -10 ms for LTD, Wolters et al., 2003) and during perception (Fu et al., 2002; McMahon & Leopold, 2012; Romei et al., 2016). However, *in vitro* studies detected a wider time window in human neocortex (Verhoog et al., 2013) and hippocampus (Testa-Silva et al., 2010).

Nevertheless, the evidence for STDP within human episodic memory remains scarce. This is mainly due to the inherent challenges in techniques and ethical concerns that it caused regarding electrical stimulation of human neurons *in vivo*.

Rhythmic sensory stimulation (RSS), as a non-invasive tool, allows safe modulation of neural groups with precise timing (Garcia-Argibay et al., 2019; Henry & Obleser, 2012; Mathewson et al., 2012; Papalambros et al., 2017; Spaak et al., 2014). Using this approach, recent studies demonstrated the causal role of theta-mediated plasticity in multisensory associative memory (Clouter et al., 2017; Wang et al., 2018). Specifically, the activation time of auditory and visual regions was orchestrated using sinusoidally modulated stimulus at 4 Hz, interlaced with four distinct time delays (equivalent to 0°, 90°, 180° and 270° phase lags). Subsequent memory performance was modulated by the time delay conditions, with enhanced memory observed in shortest time delay condition, demonstrating the causal role of the theta synchronization in associative memory. However, whether RSS is effective at high frequency demanding timing precision with several milliseconds remains uncertain.

More importantly, the extent of influence achieved by RSS remains uncertain. Exciting findings was firstly reported in a series of research of a mouse model of neurodegeneration, particularly Alzheimer's disease, AD. Repetitive RSS at 40 Hz using LED light and/or with auditory tones, resulted in gamma entrainment within visual cortex, prefrontal cortex and CA1. Remarkably, this treatment attenuated amyloid, a main biomarker of AD, and protected the mouse models from neurodegenerative factors (Adaikkan et al., 2019; Iaccarino et al., 2016; Martorell et al., 2019). Further, gamma entrainment driven by 40 Hz LED light on deep structures such as hippocampus and insular was replicated in a human subject (Khachatryan et al., 2022). In mild AD patients, a three-month multisensory stimulation treatment exhibited positive effects on cognitive function, circadian rhythmicity, and reduction of AD related biomarkers (Chan et al., 2021). Despite these promising discoveries, recent replication attempts in two independent groups failed to reveal gamma entrainment beyond V1 in mice (Schneider et al., 2023; Soula et al., 2023), thus prompting a need for further exploration.

1.3. Beta and sensorimotor synchronization

Sensorimotor synchronization (SMS) refers to the coordination of movements to sensory inputs (Pressing, 1999; Repp, 2005), for example, dancing to the beats or playing musical instruments. It reflects the ability to precisely time movements in response to external auditory, tactile or visual stimuli. This ability holds significance for daily life, as spoken language communication relies on the perception of lip movement rhythms (Park et al., 2016; Biau et al., 2021; Fujii & Wan, 2014). Furthermore, fundamental movements like walking and cycling are contingent upon sensorimotor coordination. As a result, training that involves SMS has been used for movement disorder rehabilitation (Thaut et al., 1997; Wright et al., 2014) and speech enhancement (Patel, 2011; 2014).

Unlike the aforementioned gamma frequency, for which our intention was to augment synchronization and power through rhythmic stimulation to poke elevated memory performance, excessive synchronization within the beta band (13-30 Hz) in the basal ganglia often correlates with movement disorder (Eusebio & Brown, 2009; Little & Brown, 2014; McCarthy et al., 2011). Music training for movement deficits that inherently recruits low frequency entrainment may exert an effect by coordinating motor beta oscillations. Interestingly, studies utilizing passive listening paradigms have observed the engagement of motor beta (Fujioka et al., 2012; Morillon & Bailet, 2017). In the absence of movement or intention to move, the rebound of modulated beta predicts upcoming auditory stimulus. In classic observation, movement-related beta decreases in power (event-related desynchronization, ERD) before movement, and rebounds gradually back to baseline, (van Wijk et al., 2012; Pfurtscheller & Da Silva, 1999), characterised by power increase (event-related synchronization, ERS). The rebound of beta predicting rhythmic stimulus may reflect its role beyond movement but prediction. The predictive role could elucidate the enhancement

of sensory perception during overt movements (Morillon et al., 2014; Morillon & Baillet, 2017). Providing the highly predictable nature of rhythmic sensory stimulus, it remains unclear whether motor beta also factors into SMS.

In contrast to the conventional observation of ERD and ERS, recent studies suggest that this measurement might mask the insights derived from the discrete, high amplitude and transient burst-like beta activities (beta burst, < 150 ms, Feingold et al., 2015; Little et al., 2019; Shin et al., 2017). Hence, the current study will focus on the exploration of beta burst.

1.4. Thesis objectives

In the subsequent three chapters, chapter 2 and 3 focus on the investigation of STDP in human episodic memory. In both studies, we use high frequency gamma range stimulation to rhythmically stimulate the left and right visual cortices. The inter-hemifield phase lag is modulated by the manipulating onset timing delay between movies presented in both visual fields. In chapter 2, we demonstrate the viability of using high frequency RSS to drive inter-hemifield gamma oscillations at a desired phase lag of 37.5 Hz. While we find no impact of the manipulation on episodic memory, in chapter 3, we refine the paradigm and data analysis. With 60 Hz RSS, we observe enhanced memory in the condition with the shortest time delay, which aligns with the STDP rule. However, this result cannot be simply explained by the difference of driving frequency. We discuss the results from the perspective of paradigm and cellular mechanisms.

Chapter 4 delves into the interplay between motor beta and auditory-entrained low frequency. Given the predictive role of beta and its active engagement in passive listening, it was expected that beta might contribute to SMS, potentially interacting with low frequency auditory entrainment. Results illustrate that beta bursts aligning with the phase of the entraining

frequency correlate with SMS performance, indicating a functional role of beta in sensorimotor coordination.

Chapter 5 provides a general discussion on the main findings and an outlook for future questions.

CHAPTER 2: USING FAST VISUAL RHYTHMIC STIMULATION TO CONTROL INTER-HEMIFIELD PHASE OFFSETS IN VISUAL AREAS

Spike timing-dependent plasticity (STDP) is believed to be important for neural communication and plasticity in human episodic memory, but causal evidence is lacking due to technical challenges. Rhythmic sensory stimulation that has been used to investigate causal relations between oscillations and cognition may be able to address this question. The challenge, however, is that the frequency corresponding to the critical time window for STDP is gamma (~40 Hz), yet the application of rhythmic sensory stimulation has been limited primarily to lower frequencies (<30 Hz). It remains unknown whether this method can be applied to precisely control the activation time delay between distant groups of neurons at a millisecond scale. To answer this question and examine the role of STDP in human episodic memory, we simulated the STDP function by controlling the activation time delay between the left and right visual cortices during memory encoding. This was achieved by presenting flickering (37.5 Hz) movie pairs in the left and right visual fields with a phase lag of either 0, 90, 180 or 270 degrees. Participants were asked to memorize the two movies within each pair and the association was later tested. Behavioral results revealed no significant difference in memory performance across conditions with different degrees of gamma phase synchrony. Yet importantly, our study showed for the first time, that oscillatory activity can be driven with a precision of 6.67 ms delay between neuronal groups. Our method hereby provides an approach to investigate relations between precise neuronal timing and cognitive functions. ♣

♣ *Published in:*

Chen, Q., Wang, D., Shapiro, K. L., & Hanslmayr, S. (2021). Using fast visual rhythmic stimulation to control inter-hemispheric phase offsets in visual areas. *Neuropsychologia*, *157*, 107863.

2.1. Introduction

Brain oscillations have been shown to be crucial for efficient information transmission in neural networks (Buzsáki, 2010; Draguhn & Buzsáki, 2004; Fries, 2015). Via this central communication function oscillations are key to a host of cognitive functions, such as attention and memory. A currently important question is whether oscillations are causally important for cognition, or whether they merely are a non-causal by-product of cognitive processing (Hanslmayr et al., 2019). One way to answer this question is to perturb oscillations via rhythmic stimulation and test whether such perturbation induces a change in behavior. An efficient way to drive oscillatory activity is via rhythmic sensory stimulation (e.g., flickering a visual stimulus). In the current study, we present a novel application of rhythmic sensory stimulation in a memory experiment. We demonstrate that rhythmic visual stimulation in the gamma frequency range (37.5 Hz) is capable of controlling the phase delay between left and right visual cortex in a temporally finely-grained manner.

Traditionally, rhythmic visual stimulation has been used to tag cognitive processes, which would otherwise be difficult to observe via so-called steady-state visual evoked potentials (SSVEPs, Müller et al., 2003, 2006). SSVEPs have been particularly successfully applied in the study of attention and memory. This is because in comparison with transient evoked potentials, SSVEPs provide a substantially longer time window over which a cognitive process can be monitored (Capilla et al., 2011), allowing for the tracking of attention both temporally and spatially (Adamian et al., 2020; Müller et al., 2006; Störmer et al., 2014). Frequency tagging (or SSVEPs) has also been used in memory research to elucidate reactivation of early visual signatures of a specific memory. For instance, Wimber et al. (2012) found rapid reinstatement of tagged frequencies during successful memory retrieval (but see Lewis et al., 2018; Price & Johnson, 2018 for difficulties in replicating). Together, these studies demonstrate

the power of using rhythmic sensory stimulation as an effective means to study neural correlates of cognitive processes.

Recent studies have gone beyond a mere correlational approach and used rhythmic sensory stimulation to drive a specific oscillation to induce a change in the associated behavior (Garcia-Argibay et al., 2019; Henry & Obleser, 2012; Mathewson et al., 2012; Papalambros et al., 2017; Spaak et al., 2014). For instance, interregional synchrony in the theta band is believed to be of crucial importance for memory formation. To test this hypothesis, two recent studies induced theta phase synchrony or asynchrony between visual and auditory cortices to examine if synchrony affects memory formation. Visual and auditory regions were driven at phase offsets of 0 (synchronous), 90, 180 or 270 (asynchronous) degrees. Importantly, both studies found better memory for multisensory (i.e. audio-visual) memories on trials in which auditory and visual cortices were stimulated synchronously compared to asynchronously stimulated trials (Clouter et al., 2017; Wang et al., 2018). These studies demonstrate a causal role of theta phase synchrony for memory formation. In particular, they show that subsequent remembering and forgetting depends on the relative timing of sensory information, and that this timing can be controlled through sensory stimulation. However, the extent to which this approach applies to faster frequencies (i.e., gamma), which have also been shown to play a role in synchronization, and to coordinating brain areas within the same sensory domain (i.e., visual cortex) is unclear.

Fine-grained timing of neural cell assemblies, as achieved by synchronization in the gamma frequency band, is important for effective information transmission between neurons (Fries, 2015). Precise timing is critical because neurons in the brain integrate inputs over time, with the rate of relaxation of the membrane potential dictating the length of the temporal window. For neocortical principal cells that time window is typically between 10 – 30 ms (100

– 33 Hz), therefore fine-grained temporal synchronization is necessary for an upstream cell assembly to drive a down-stream neuron (Buzsáki, 2010). Equally important, synaptic plasticity has been shown to be critically dependent on the time delay between the firing of an up-stream and a down-stream neuron, which is termed 'spike timing-dependent plasticity' or STDP. In STDP, the efficiency of synaptic modification declines exponentially as a function of time delay between the activation of a pre- and postsynaptic neuron. The optimal time window for synaptic modification is very narrow due to the exponential decay (Bi & Poo, 1998). In support of this contention, a rodent study found that spikes must co-occur in a time window of approximately 25 ms to facilitate synaptic modification, corresponding to gamma frequency at ~40 Hz (Wespatat et al., 2004). Indeed, phase synchronization at the gamma frequency range is optimal for the facilitation of STDP (Fell & Axmacher, 2011). Action potentials tend to appear in the depolarized phase of local field potential (Fries, 2005) which has been observed in the theta and gamma band (Jacobs et al., 2007; Vinck et al., 2010). As a result, synchronizing the phase of the local field potential from two distant brain regions would promote the induction of long-term potentiation (LTP; Axmacher et al., 2006; Jutras & Buffalo, 2010). Critically, higher frequencies mean tighter coupling, therefore gamma synchronization in particular leads to more precise coupling of action potentials which in turn facilitates STDP (Abbott & Nelson, 2000; Caporale & Dan, 2008; Fell & Axmacher, 2011; Jutras & Buffalo, 2010). Modulating the degree of synchrony in gamma phase between neuron assemblies arguably manipulates the time delay of action potentials and therefore, STDP between them. STDP supposedly underlies memory formation but its role in human episodic memory has been rarely studied because of the technical challenge to non-invasively control the timing of neural assemblies. Rhythmic sensory stimulation as employed in the present study may open a new approach to address these

questions, thus providing a potential link between highly invasive research in animals and non-invasive human studies.

In the current study, we aim to address two questions. The first is a technical question, namely whether it is possible that SSVEPs can be used to control neural activity in the left and right visual cortex with high temporal precision corresponding to a quarter cycle (i.e., 6.67 ms) of a gamma oscillation. Given the high temporal precision to which we aimed, we chose the hemifield approach, which controls neural activity between left and right visual hemifield. We chose this because the transduction time should vary little between the left and right visual cortex, while this is not the case between auditory and visual sensory regions. The second question is whether such stimulation has an impact on human episodic memory formation. To address these questions, we presented two sinusoidal flickering movies in the left and right visual hemifields (Fig. 2.1A). A sine wave of 37.5 Hz was used to modulate the luminance of the movies. To induce a phase offset of 0°, 90°, 180°or 270° (corresponding to a time lag of 0, 6.67, 13. 33 and 20 ms) between the left and right visual cortices, sinusoidal flickering movies were presented in the left and right visual field with a phase lag of either 0°, 90°, 180° or 270° (Fig. 2.1B). We predicted that, if STDP plays a role in episodic memory, subsequent recall of the association of movie pairs should exponentially decrease with increasing phase lags. Although the 90° and 270° offset condition may look similar from a purely circular perspective, they are very different from each other from a temporal perspective, i.e., the difference in time which indeed is 6.67 ms vs. 20 ms. According to our STDP hypothesis, this time delay, although subtle, has dramatic consequences for plasticity due to the exponential decay ((Bi & Poo, 1998).

2.2. Methods

2.2.1. Participants

Thirty-eight participants were recruited (mean age = 22.11; age range = 18-32; 71.1% female; all right-handed). Participants received course credit or financial reimbursement in return for their participation. Two participants were excluded for excessive horizontal eye movements (see below). One participant was excluded due to EEG recording interruption. This left 35 participants for further analysis (mean age = 22.37; age range = 18-32; 68.6% female; all right-handed). Ethical approval was granted by the Research Ethics Committee at the University of Birmingham (ERN_15-0335), complying with the Declaration of Helsinki.

2.2.2. Stimuli

384 randomly paired three-second movie clips were employed as movie pairs (N = 192) for associative memory. Half of the movies were drawn from the same pool as those used in Experiment 3 of Clouter et al. (2017), while the remainder were trimmed documentaries downloaded from an online resource (https://www.youtube.com) with creative commons license. Four additional movie pairs were used in a practice block. Consistent with movies used in previous work (Clouter et al., 2017; Wang et al., 2018), all movies were emotionally neutral human/natural activities.

Movies were resized to 360(W) x 288(H) pixels, with the frame rate increased to 150 Hz from 25 Hz by replicating each frame 6 times with in-house scripts written in MATLAB (R2017a; The MathWorks, Inc., Natick, MA, USA). Movies were randomly paired once resulting in 192 unique associations. The same pairs of movies were used for each participant.

All movies were luminance-modulated from 0% to 100% by a 37.5 Hz sine wave, but with different onset depending on the condition. Specifically, within each pair of movies, one always (across conditions and participants) served as the leading movie, with an onset of 0°,

while the other one served as the trailing movie, with an onset of one of the following degrees (conditions evenly distributed): 0°, 90°, 180° or 270°. This results in four phase lag conditions, i.e., 0°, 90°, 180° or 270° (see Fig. 2.1B) between the leading movie and the trailing movie, with 48 trials in each of the condition. Phase lag conditions assigned to each group of 48 movies pairs were counterbalanced across participants.

All behavioural tasks were programmed using the Psychophysics Toolbox (Brainard, 1997; Pelli, 1997; Kleiner et al, 2007) running on MATLAB (R2015b; The Mathworks, Natick, MA, USA). To make sure that the stimulus was presented at the frequency we need, precise timing of the stimulus was verified with a photodiode before the experiment was run (see Fig. S6.5 and Supplemental Material).

2.2.3. Experimental procedure

Participants were seated in a testing room and requested to complete forms for safety screening and to provide consent after they were informed with the procedure of the study and prepared for EEG data collection. Details of the memory task were explained to participants and a practice block was used to ensure familiarity with the memory task. Participants were seated at a distance of 60 cm from the screen centre with their heads resting on a chin support. A web camera was used by the experimenter to verify the subject's head position and compliance during the task. The experiment consisted of three tasks; (i) a memory task, (ii) a synchrony judgement task and (iii) an EOG calibration task with instructions provided before each task. At the end, to allow for source analysis and to provide more precise estimation for electrode interpolations, 3D geometric locations of each electrode were recorded using a Polhemus FASTRAK device (Colchester, Vermont, USA) and Brainstorm (Tadel, Baillet, Mosher, Pantazis, & Leahy, 2011) implemented in MATLAB (R2018a; The MathWorks, Inc., Natick, MA, USA).

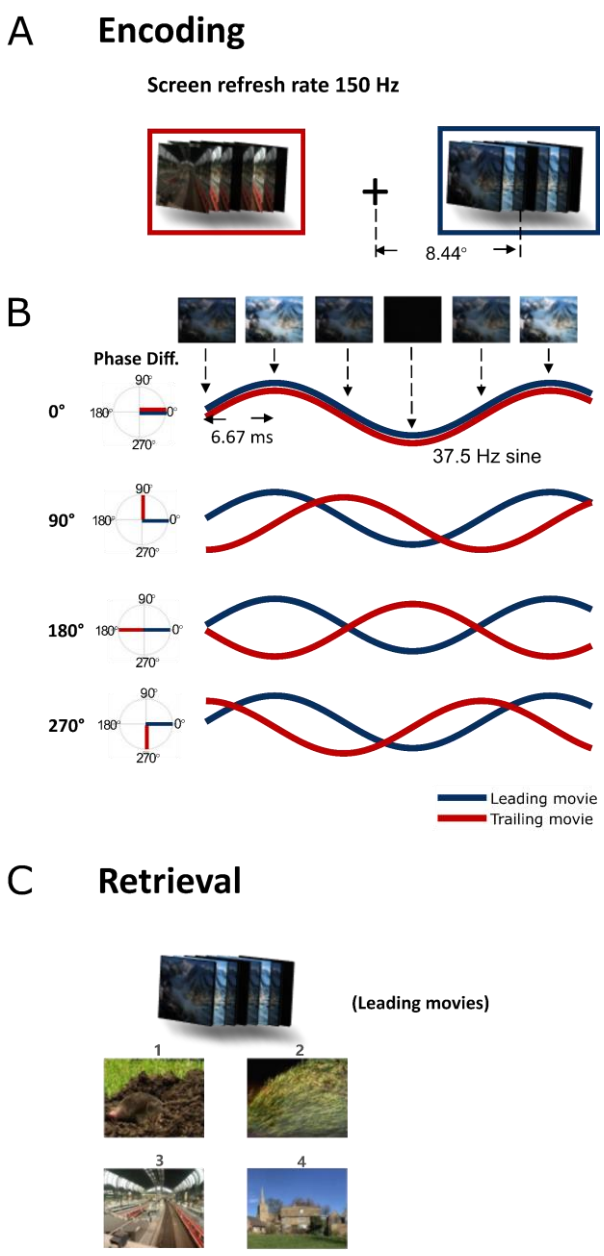

Fig. 2.1. Experimental procedure. The experiment contained 192 trials, evenly divided into 6 blocks. Each block (32 trials) consisted of an encoding phase, a distractor task and a retrieval task. (A) Encoding phase. A pair of movies was displayed simultaneously on the left and right of 8.44° off to the centre of a 21-inch CRT screen with refresh rate of 150 Hz, for a duration of 3 second. Participants were encouraged to make associations between the two movies as their memory of associations would be tested. **(B)** Modulation of pairs of movies. Movies were luminance-modulated by a 37.5 Hz sine wave but with various onset depending on the phase lag conditions (0, 90, 180 or 270 degrees). One of the movies within each pair was defined as leading movie, because it always began with onset at 0° and the other was trailing movie, beginning with onset evenly distributed at 0°, 90°, 180° and 270°. Sine waves utilized for luminance modulation for leading (blue) and trailing movies (red) showed a phase lag of 0, 90, 180 and 270 degrees for the corresponding experimental condition. Time lags between leading and trailing movies were 0, 6.67, 13.33 and 20 ms for 0, 90, 180 and 270 phase lag conditions, simulating the activation time delay between pre- and postsynaptic in STDP. The minimal time lag between leading and trailing movies for asynchrony conditions was only 6.67 ms. **(C)** Retrieval phase. The memory test was carried out after a 30-second distractor task. All 32 pairs of movies showed at encoding phase were tested for once. During the test, participants were asked to recall the associated movie cued by leading movies. Four options as a static frame taken from trailing movies were displayed below the cue. All cues and options were stimuli from the encoding phase within the same block.

Based on our previously published results (Clouter et al., 2017; Wang et al., 2018), the present experiment aimed at testing 24 participants with a minimum number of 32 trials per condition, which would lead to a power of 97.7% (alpha level=0.05, one-tailed paired sample t-test). However, given concerns on the low signal to noise ratio of gamma entrainment for this study, as compared to theta entrainment in previous studies (Clouter et al., 2017; Wang et al., 2018), we initially decided to double the sample size (48 participants), however, data collection had to stop because of the pandemic. Bayesian repeated measures ANOVA revealed a Bayes Factor (B10) of 0.076, suggesting that the null model outperformed our hypothesis.

2.2.3.1. Memory Task

The memory task was comprised of six blocks, each containing an encoding phase, a distractor phase and a retrieval phase. For each block, 32 pairs of movies were shown during the encoding phase and participants were asked to remember the pairs as they would be tested in the retrieval phase. Block order was fully randomized for each participant. During intervals between blocks, memory performance was shown to the participant on the screen to motivate good performance. After blocks of poor performance participants were encouraged to take a break.

During the encoding phase, for each trial, a pair of movies was displayed simultaneously on the left and right (see Fig. 2.1A) of a 21-inch CRT screen (150 Hz refresh rate and a resolution of 800 width x 600 high pixels) through an nVidia Quadro K600 graphics card (875 MHz graphics clock, 1024 MB dedicated graphics memory; Nvidia, Santa Clara, CA, USA). Movie pairs were resized to 250(W) x 200(H) pixels and were aligned horizontally to the screen centre, with a visual angle of 8.4° (movie centre to the screen centre; see Fig. 2.1A). The background of the experimental interface was set to grey. For trials with phase offsets of 90, 180 or 270 degrees each pair of movies consisted of one leading movie and one trailing movie

(for 0-degree phase offsets both movies flickered synchronously hence neither movie was leading nor trailing). The left vs. right position of leading movies presented on the screen was randomly assigned for each trial. Participants were instructed to maintain fixation at the screen centre and attend to both movies without shifting gaze. This is because selective attention modulates SSVEPs (Morgan et al., 1996; Kashiwase et al., 2012). Our objective was to establish and maintain sustained and equal attention toward movies presented in both visual fields (Müller et al., 2003). Participants were encouraged to link the movies via stories or visual imagery to help them learn the associations. Participants were informed that their memory of the associations would be tested in the later retrieval section. After watching each pair of movies, participants responded on a scale from 1 to 5 to which extent that the movies fit with each other, i.e., how easy it was for participant to link them (1: no fit, 5: perfect fit). This judgement task was implemented to maintain the engagement of participants during encoding.

Following the encoding phase, a 30-second distractor task was implemented to prevent active rehearsal of the movie pairs. Participants were asked to overtly count backwards from a random 3-digit number displayed on the screen by subtracting three each time.

In the final test phase, a full movie was shown which acted as a cue. Only old movies (i.e., movies that have been shown during encoding in this block) were presented. For phase offset conditions 90, 180, and 270 the leading movie always served as the cue. Below the cue, four screenshots which were taken from old encoding movies (only trailing movies within the same block) were shown as options. The participant selected which of the 4 screenshots they thought was presented with the cue during encoding. Each trailing movie served as lures for exactly three times and as matched movie (correct answer) for one time.

2.2.3.2. Synchrony Judgement

The synchrony judgement task tested whether participants were able to perceive the phase offsets between the movies, i.e., whether they could tell the difference between synchronous (0 degree) and asynchronous pairs (90, 180 or 270 degrees). To this end, 60 movies pairs were drawn randomly from the memory encoding phases (see Fig. 2.1A). Participants were asked to judge in a two alternative forced choice procedure whether a given movie pair was flickering synchronously (0 phase lag), or not (90, 180 and 270 phase lags). Responses were requested after the presentation of the movies.

2.2.3.3. EOG Calibration Task

The EOG calibration task provided a template for monitoring the occurrence of horizontal eye movements. The data from this task was used to exclude trials where overt eye movements were made to the movies. In the EOG calibration task participants were asked to visually track a black cross appearing randomly to the left or right of the fixation cross at a visual angle of 8.44°. After each movement, the fixation cross maintained its position for a duration between 800 ms to 1200 ms before moving back to the centre, which marked the onset of the next trial. There were 80 trials in total. For half of the trials the fixation cross moved to the left, and for the other half it moved to the right. 10% of trials served as catch trials during which participants were asked to report a color change of the cross (black to red) by pressing the space button as soon as possible. This ensured that participants maintained attention throughout the calibration task.

2.2.4. Data Analysis

2.2.4.1. Behavioral Data

To test whether the manipulation of phase offset had consequence on episodic memory, memory accuracy was compared between 0°, 90°, 180° and 270° phase offset conditions using

a one-way repeated measurements ANOVA. Trials with excess HEOG were excluded for this analysis. Further, to rule out perceptual factors that might have affected episodic memory, a sensitivity index *d'* was calculated for each participant to test whether they were able to tell synchronous from asynchronous movie pairs. This was estimated as follows:

$d' = Z(\text{hit rate}) - Z(\text{false alarm rate})$,

where the Z function was deployed by the normal inverse cumulative distribution function in MATLAB (R2017a; The MathWorks, Inc., Natick, MA, USA), considering synchronous movie pairs as signal and asynchronous pairs as noise. One-sample *t*-test was adopted to examine whether *d'* was statistically different from zero.

2.2.4.2. EOG calibration

The purpose of the EOG calibration was to exclude trials on which subjects made horizontal eye-movements, as such trials are detrimental to tracking the EEG response to the left/right visual hemifields independently. It is feasible to use EOG data for tracking eye movements as a result of the linear relationship between voltage and visual angle (Acuna et al., 2014). This procedure enabled a threshold for each participant to be calculated individually for the purpose of excluding trials as defined by the following procedure.

First, the EOG data from both the EOG calibration task and the encoding phase of the memory task was preprocessed using a procedure similar to that used for the EEG data. EOG data were epoched to 2000 ms before and after the onset of the fixation cross. For the memory encoding phase, the data were epoched to 2000 ms before and 5000 ms after onset of the movie pairs. Both datasets were then low pass filtered at 30 Hz and resampled at 512 Hz.

Second, erroneous eye movements were manually excluded for further analysis via trial-by-trial visual inspection. Such errors included eye movements that were made too early (i.e.,

before the fixation cross jumped) or random saccades (i.e., eye movements not reflecting tracking of the fixation cross). To detect the voltage gradients generated by saccades from the centre to the left/right centre of movie position (at visual angle of 8.44°), the first derivative was calculated using the 'diff' function in Matlab. The resulting data was then aligned according to the largest peaks that appeared within 600 ms upon stimulus onset and then averaged. A threshold was calculated by taking 50% of the averaged peak value, thus corresponding to a saccade of 4.22°. Peaks of EOG gradients were then calculated in the same way for the encoding phase of the memory task for each individual trial. Trials which exceeded the threshold (of 50%) were excluded from further behavioural and EEG analysis.

2.2.4.3. EEG recording and preprocessing

EEG data were collected via a 128-channel BioSemi ActiveTwo system. EOG recording was completed by one additional electrode placed 1 cm to each of the lateral canthus and 1 cm below the left eye, respectively. Online EEG data were sampled to 2048 Hz by the BioSemi ActiView software.

The Fieldtrip toolbox for EEG analysis (Oosenveld, Fries, Maris, & Schoffelen, 2011) was used for EEG data preprocessing. Data were first epoched from 2000 ms before and 5000 ms after stimulus onset and then bandpass filtered from 1 to 100 Hz. Line noise was removed from the raw data by bandstop filters between 48-52 Hz and 98-102 Hz. Before ICA (independent component analysis), data was downsampled to 512 Hz, followed by the removal of noisy EEG channels and trials with muscle artefacts by manual inspection. ICA components indicating horizontal and vertical eye movements and cardiac activity were removed from data. Triangulation of nearest neighbours calculated by individually recorded electrode positions were used for interpolation of rejected channels. Finally, data were re-referenced to the average reference and trials with artefacts were rejected by visual inspection.

2.2.4.4. Phase Offset Analysis

To confirm whether the phase stimulation is driving brain oscillations between left and right visual cortices at the corresponding degree of phase offset, phase comparisions were conducted by the following steps at both individual and group level.

2.2.4.4.1.ROI selection and ITPC calculation

First, for each participant, one electrode from left and right hemifield, respectively, was identified as ROI that responds strongest to the rhythmic visual stimulation. The basic rationale for the determination of these ROIs was that, in each of the left/right visual cortex, there existed one electrode that mostly responds to the visual stimulation from the contralateral visual field. Inter-trial phase coherence (ITPC) should be strongest across trials recorded from this electrode with the leading movies presented in the contralateral visual field. For example, across trials with leading movies presented at the right visual field, the ITPC was expected to be strongest in an electrode over the left visual cortex. This was because the leading movies were always starting with a same onset at 0°. On the contrary, the phases for the trailing movies (i.e. the associated stimuli) were equally distributed across 0°, 90°, 180° and 270° and thus lead to low ITPC. Since the leading movies were split between left and right hemifiled, this approach allowed us to determine one ROI (i.e. one electrode) for each hemisphere of the visual cortex. Details of this analysis is given below.

For each participant, we separated trials according to the location of leading movies. In the following statements, LeadLvsf and LeadRvsf are used to represent the conditions with the leading movies in the left and right visual fields, respectively.

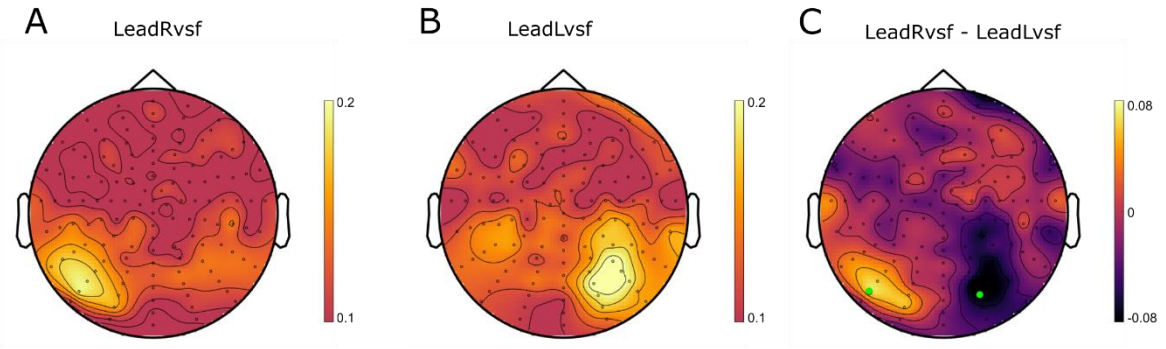

Fig. 2.2. A subject example for definition of ROI for later analysis. (A) Topography of ITPC values in LeadRvsf. ITPC across trials with leading movies presented at the right visual field were calculated. Strongest ITPC was clustered at the contralateral (left) visual hemifield. **(B)** Topography of ITPC values in LeadLvsf. Similar to (A) but for LeadLvsf with opposite pattern. **(C)** Topographic distribution of ITPC difference between LeadRvsf and LeadLvsf (LeadRvsf – LeadLvsf). One electrode showing strongest positive and negative ITPC difference was identified as ROI for the left and right hemifield, respectively, as highlighted in this example.

ITPC from 20 to 50 Hz in steps of 2.5 Hz was calculated using a dpss multitaper (1 taper for each frequency of interest, from -1s to 3.75s upon stimulus onset, with a time window of 0.5s in width, 128 channels) time-frequency transformation based on multiplication in the frequency domain. A single subject example with ITPC averaged at the band of 37.5 ± 2.5 Hz for the LeadRvsf and LeadLvsf condition is displayed in Fig. 2.2A and B, respectively. The averaged ITPC was calculated for a selected time window of interest from 1-2s upon stimulus onset. The selection of this time window was to align with previous work (Clouter et al., 2017; Wang et al., 2018) with a similar paradigm in lower frequencies, but results are also shown for the entire epoch (see Fig. S6.2). The contrast between LeadRvsf and LeadLvsf (Rvsf-Lvsf) reveal the electrodes that responded most strongly to visual stimulations from the left and right visual field (see Fig. 2.2C). This analysis was implemented for all participants, such that one electrode (as highlighted in Fig. 2.2C as an example) from each side of the visual cortex was defined as a subject-specific ROI for later analysis (except for the analysis confirming the specificity of ITPC difference at 37.5 Hz, which is decribed in the next paragraph).

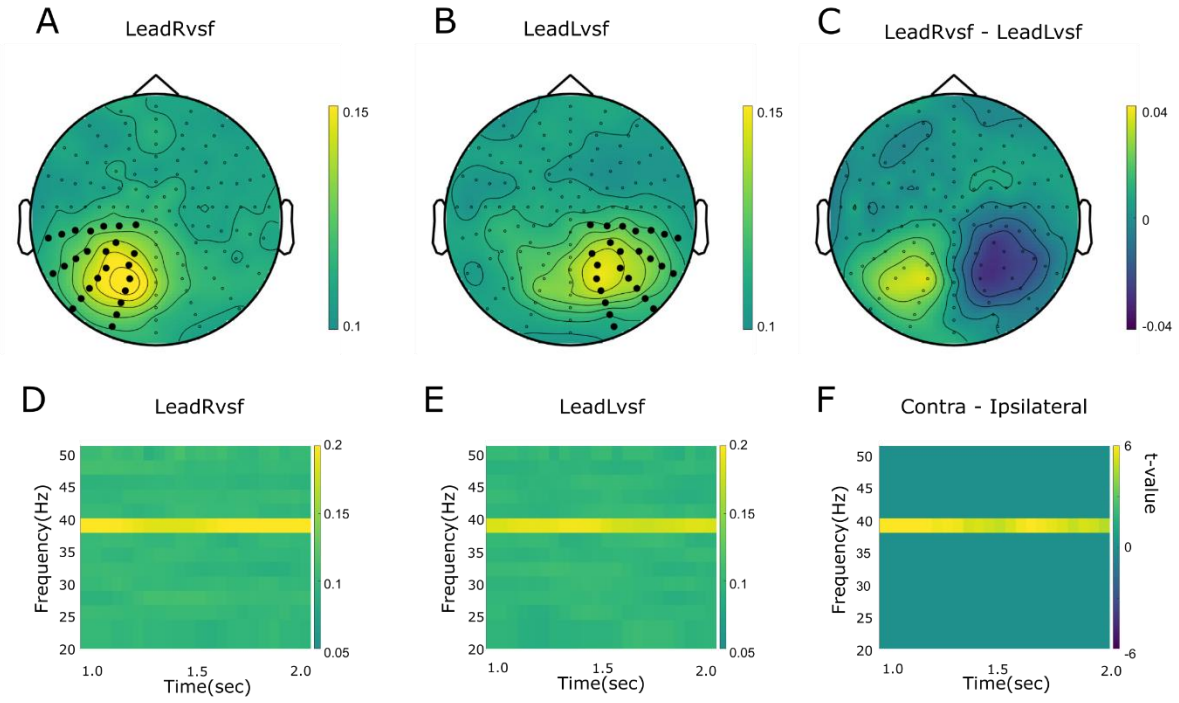

Fig. 2.3. Group ITPC distribution. (A) Topography of grand averaged ITPC values at 37.5 ± 2.5 Hz in LeadRvsf. ITPC across trials with leading movies presented at the right visual field were calculated between 1s and 2s upon stimulus onset from 35 to 40 Hz. Strongest ITPC was clustered at the contralateral (left) visual hemifield. **(B)** Same as (A), but for LeadLvsf with opposite pattern. Highlighted electrodes in (A) and (B) were channels pre-selected for averaging ITPC from 20-50 Hz as shown in (D) and (E), respectively. **(C)** Topographic distribution of grand averaged ITPC difference between LeadRvsf and LeadLvsf (LeadRvsf – LeadLvsf). Cluster-based permutation test indicated statistically significant difference ($p_{corrected}$ < 0.001) between LeadRvsf and LeadLvsf. **(D)** and **(E)** Time-frequency representation of ITPC value from 20-50 Hz averaged across electrodes highlighted in (A) and (B), respectively. The specificity of high ITPC to frequencies around 37.5 Hz can be visually seen. **(F)** The specificity was statically confirmed by comparing the difference (between ITPC values contra- and ipsilateral to the leading movies presented field) vs. zeros. A cluster of significant t-values emerged in the frequency range around 37.5 Hz ($p_{corrected}$ <0.001).

At the group level ITPC values were averaged across all subjects for LeadRvsf and LeadLvsf conditions, seperately. The difference between the two conditions was statistically assessed by means of a two-tailed (alpha = 0.025) paired-sample permutation test (number of randomizations = 2000) at the frequency of interest (37.5 Hz) across the time duration from 1s

– 2s following stimulus onset. Specifically, the significance probability was performed by Monte Carlo method and multiple comparisons were corrected by "cluster". To further confirm whether this difference was specific for the frequency of interest, we implemented another independent analysis based on posterior electrodes rather than the subject specific ROI mentioned above. We firstly averaged time-frequency structured ITPC values across 25 posterior electrodes (see electrodes highlighted in Fig. 2.3A for LeadRvsf and Fig.3B for LeadLvsf) within each hemifield. The same ROI was used for each subject. This was performed at single subject level for conditions with leading movies presented at the contralateral and ipsilateral visual fields, respectively. Then, the difference between the averaged ITPC values for the contralateral and ipsilateral conditions (contra - ipsilateral) were compared against zero, from 20-50 Hz (in steps of 2.5 Hz) and 1-2 second (in steps of 50 ms) upon stimulus onset, by using a one-tailed paired sample permutation test (number of randomizations = 2000). The p-value estimation and correction for multiple comparisons were Monte Carlo and "cluster", same as the above analysis. Parameters for the calculation of the effect size was as follows. For each participant, ITPC difference was calculated by subtracting the ipsilateral (to the leading movie position) ITPC from the contralateral ITPC in the left and right posterior electrodes (25 electrodes at each hemifield, 50 electrodes in total, as highlighted in Fig.3A and B) at each time point of toi (1-2s upon stimulus onset, 0.05 s in steps). Thereafter, ITPC difference averaged across 37.5 ± 2.5 Hz was selected for the calculation of effect size.

2.2.4.4.2. SSVEPS and Measuring Phase Offsets between Left and Right Visual Cortex

As reported above, one electrode corresponding to the left/right visual cortex was selected for each subject as a ROI, which is reflecting the strongest response to the rhythmic visual stimulation. To examine whether the phase lags between left and right ROI were consistent with the visual modulation (i.e., 0, 90, 180 and 270 phase lag conditions), we

extracted the instantaneous phase for each phase lag condition. Since gamma is notorious for its susceptibility to noise, the extraction of instantaneous phases was based on SSVEPs rather than on single-trials (Fries et al., 2008). To increase trial number for the timelocked analysis, ROI data were swapped between left and right hemifield for the trials in the LeadLvsf condition. As a consequence, the LeadLvsf condition also has the leading movie stimulation projected to the left hemifield, similar to the LeadRvsf condition. This hemisphere swapping procedure allowed us to include trials in both LeadLvsf and LeadRvsf for the timelocked analysis, with the left and right side of visual cortex corresponding to stimulation from the leading movies and trailing movies, respectively. As a result, for each participant, there was one SSVEPs for each combination of the following two factors: leading/trailing movies by 0/90/180/270 phase lags, resulting a total number of 8 SSVEPs. The number of trials for this timelocked analysis ranged between 32 and 47.

At the individual level, a bandpass filter from 35-40 Hz was then applied to the SSVEPs. To extract instaneous angles, Hilbert transformation was applied to the SSVEPs and the resulting angles were thereafter unwrapped. Instantaneous phase differences between left and right ROIs were calculated for each phase lag condition (0, 90, 180 and 270 degrees), with the time of interest (toi) from 1s to 2s upon stimulus onset, to avoid any possible contamination from stimulus onset and offset (see Clouter et al., 2017; Wang et al., 2018 for a similar rationale).

For group analysis, eight SSVEPs were calculated based on grand averaged SSVEPs across participants for each combination of the conditions (i.e. 2 by 4), leading/trailing movies by 0/90/180/270 phase lags. The instanteous angles and phase differences were generated with the same process as stated above for individuals but based on the grand averaged SSVEPs. The V test implemented in the Circular Statistics Toolbox (Berens, 2009) was used to test whether

the instantaneous phase differences were uniformly distributed at the same phase as the visual stimulation conditions (0, 90, 180 and 270 phase lags).

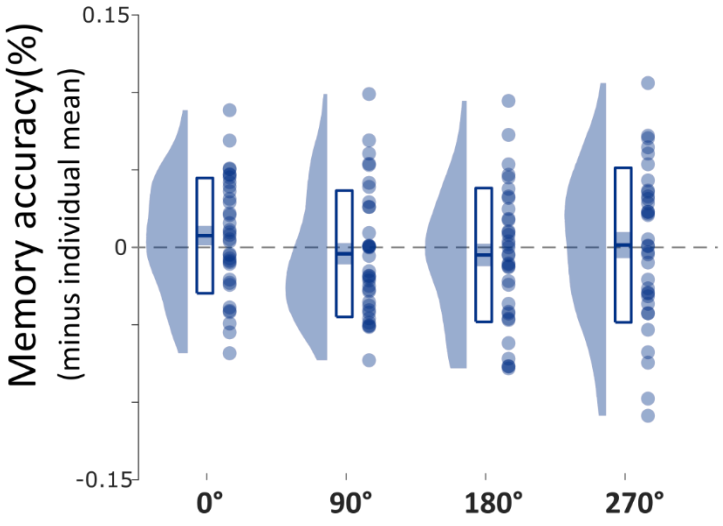

Fig. 2.4. Memory performance across conditions. Memory accuracy is shown after subtraction of individual mean performance (N =35). Although one-way ANOVA revealed no significant difference across conditions, there appeared to be a weak trend that memory performance was slightly better at 0°. Each dot represents one single subject memory accuracy in one corresponding phase lag condition. The dashed line represents zero. The thick line represents mean performance, the shaded area shows standard error of the mean, and the boxes show 95% confidence level within condition. Distributions within condition is also available. For memory performance without subtraction of individual mean, see Fig. S6.1.

2.3. Results

2.3.1. Behavioural performance

Recall accuracy did not differ significantly across the four phase offset conditions of 0°, 90°, 180° and 270° (N =35; one-way repeated measurements ANOVA; F (3,102) = 0.612, p = .609, ω^2 = 0, see Fig. 2.4 and Fig. S6.1). However, it should be noted that there was a weak trend for memory accuracy being slightly higher at the 0° phase lag condition as compared to the other three phase lag conditions (90, 180 and 270). This trend was more obvious visually when showing the accuracy for the four phase lag conditions by subtracting individual mean performance across conditions (see Fig. 2.4; and see Fig. S6.1 for data without the subtraction). Mean performance ratio for each condition ranges from 0.643 (180°) to 0.659

(0°), with *SD* ranging from 0.142 to 0.169, showing median difficulty of the task (*M* = 0.659, *SD* = 0.159; *M* = 0.646, *SD* = 0.143; *M* = 0.643, *SD* = 0.142; *M* = 0.652, *SD* = 0.169 for conditions of 0, 90, 180 and 270 degrees, respectively). The overall performance appears to be higher than previous work using a multisensory association paradigm (Clouter et al., 2017; Wang et al., 2018). Bayesian repeated measures ANOVA revealed a Bayes Factor (B10) of 0.076, suggesting that the null model outperformed our hypothesis. The largest effect size was found between 0° and 180° offset conditions (Cohen's d = 0.2331) and according to this effect size, at least 219 subjects are needed to reveal a significant difference in memory performance between 0° and 180°.

To determine if subjects were able to distinguish between synchronous and asynchronous movie pairs, *d'* was calculated for 34 participants out of 35. One subject was excluded for the analysis of the synchrony judgement task because the hit rate was zero. A one-sample *t*-test suggested that *d'* for the synchrony task was significantly different from zero, $t(33) = 14.92$, $p < 0.1e\text{-}15$, indicating that participants were well able to distinguish between synchronous and asynchronous trials.

2.3.2. ROI and ITPC

After trial rejection due to EOG thresholding and EEG preprocessing, the total number of trials at single subject level across all conditions survived ranges from 135-185 trials (out of 192), with a mean of 164.63 trials. The number of trials for LeadLvsf condition ranges from 68-95 trials (mean = 84.37), and that for LeadRvsf condition ranges from 67-96 trials (mean = 80.26). For each phase offset condition, the range of number of trials is 30 to 47, with a mean of 40.71, 40.97, 41.29 and 41.66 for 0°, 90°, 180° and 270° offset condition, respectively.

ITPC in the frequency band from 35 to 40Hz was utilized to identify ROIs in each visual hemifield for each subject (see Methods section and Fig. 2.2). As expected, stimulation from leading movies displayed at the right visual field (LeadRvsf) caused the strongest ITPC in the contralateral (left) hemifield, while at the ipsilateral (right) hemifield ITPC is lower for trailing movies with various phase onset asynchronies (Fig. 2.2A). A similar result occurred for the LeadLvsf condition (see Fig. 2.2B). To cancel out factors that may potentially affect ITPC beyond the conditioning, such as common responses to the fixation on the screen centre, a contrast between the two conditions (LeadRvsf – LeadLvsf) was calculated which revealed the most responsive electrodes for phase modulation observed in each visual hemifield (See highlighted electrodes in Fig. 2.2C).

The averaged topographic pattern of ITPC across participants in the range of 37.5 ± 2.5 Hz in the left and right hemifields showed a highly consistent pattern across subjects (Fig. 2.3A and B). Cluster-based paired-sample permutation tests between LeadRvsf vs. LeadLvsf topographic distribution revealed a significant difference during the interval from 1s – 2s upon stimulus onset (Fig. 2.3C, $p_{corrected} < 0.001$). Grand averaged ITPC from 20-50 Hz across electrodes highlighted in Figure 2.3A and B indicate strongest ITPC at the frequency around 37.5 ± 2.5 Hz for both LeadRvsf and LeadLvsf conditions (Fig. 2.3D and E, see Fig. S6.2 for ITPC in other time windows). The specificity for 37.5 Hz was further confirmed by cluster-based paired-sample permutation test by comparing the resulting ITPC difference (contralateral - ipsilateral) with zero (see Fig. 2.3F). The Cohen's effect size of ITPC difference at posterior electrodes (as highlighted in Fig. 2.3A and B) across 37.5 ± 2.5 Hz at toi (1s-2s upon stimulus onset) indicated such difference was robust ($d = 0.4145$, $M = 0.0162$, $SD = 0.0389$). These results suggested that the aligned phase activity was specific to frequencies around the entrained frequency, 37.5 Hz, $p_{corrected} < 0.001$.

2.3.3. SSVEPs and entrained gamma phase offset

Band-pass filtered (37.5 ± 2.5 Hz) SSVEPs averaged across subjects are shown in figure 2.5. These results indeed show different phase lags between leading and trailing movies for the 4 different phase lag conditions (0, 90, 180 and 270 degrees) at the group level (Fig. 2.5A). Closer inspection of the SSVEPs (see Fig. 2.5B) suggests that the phase offsets between leading and trailing movies closely followed the phase lags induced by the different stimulation conditions (0, 90, 180 and 270 degrees).

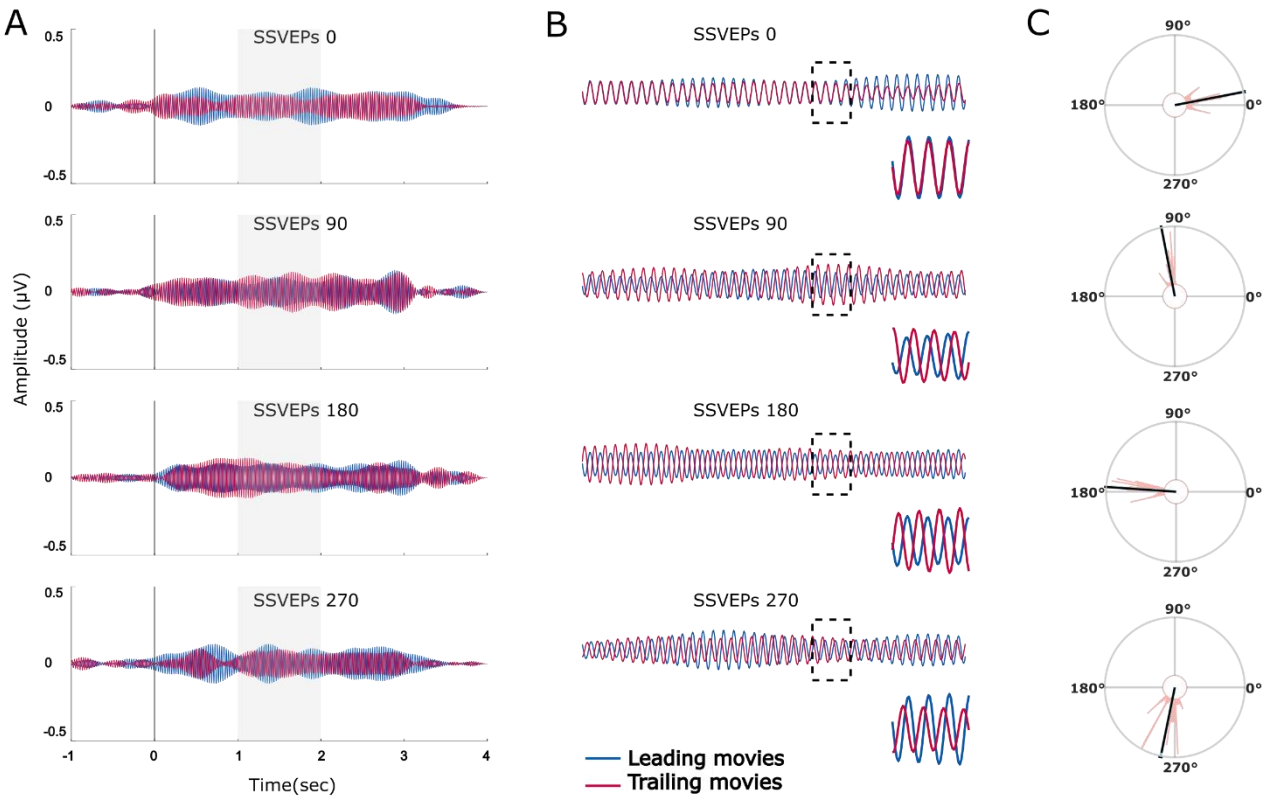

Fig. 2.5. Group SSVEPs and instantaneous phase offset between leading movies and trailing movies. (A) SSVEPs band-pass filtered at 37.5 ± 2.5 Hz from -1 to 4 second for leading (blue) and trailing movies (red) in 0°, 90°, 180° and 270° appeared to have different patterns. **(B)** A closer inspection of shaded areas in (A). For demonstration purpose, a randomly selected area was zoomed in at the right bottom. **(C)** Instantaneous phase difference between SSVEPs for leading and trailing movies for shaded areas in (A) was binned in a circular histogram. The mean resultant vector of the instantaneous phase difference in 0°, 90°, 180° and 270° phase lag conditions were represented as dark bars (resultant vector lengths are 0.98, 0.99, 0.99 and 0.95, respectively). A V-test confirmed that the phase differences were uniformly distributed around the entrained phase offset, with $p = 0$ for all conditions.

In order to statistically test whether the phase offsets between the SSVEPs elicited by the leading/trailing movies were congruent with the phase offsets induced by our stimulation, the instantaneous phase differences between trailing and leading movies were calculated (see Fig. 2.5C; for phase offsets at individual level for each condition, see Fig. S6.3; for phase offsets at group level based on group ROI, see Fig. S6.4). The mean phase differences with 95% confidence interval are 10.88° ± 1.14°, 101.06° ± 0.84°, 176.09° ± 0.66° and 258.49° ± 1.60° for 0, 90, 180 and 270 phase offset conditions, respectively. A V-test was performed on these phase differences, which tests the nonuniformity with a known mean direction of circular data. The V-test confirmed that the phases from 1s -2s upon stimulus onset were uniformly distributed around their entrained phase offset, with $p = 0$ for all conditions.

Together, the EEG results demonstrated the feasibility of inducing phase lags between the left and right visual cortex at a minimal time interval of 6.67 ms by hemispheric visual stimulation.

2.4. Discussion

Modulating brain oscillations via rhythmic sensory stimulation opened a new avenue to potentially draw causal links between oscillations and cognitive functions. However, such usage has so far been limited to low frequencies (Hanslmayr et al., 2019), while the feasibility of stimulating at higher frequencies (>30 Hz) has rarely been explored. STDP is a prominent theory of a synaptic plasticity mechanism by which synaptic efficiency declines exponentially with increasing time delay between pre- and postsynaptic neurons (Bi & Poo, 1998; Song, 2000; Caporale & Dan, 2008), and was observed within a critical time window corresponding to 40 Hz in an study using animal models (Wespatat et al., 2004). Similar observations of STDP in human participants have proved to be challenging. As a result, little is known about whether

STDP has a similar function and time course in humans compared to animals (Mansvelder et al., 2019), and indeed whether it plays an important role in human episodic memory.

Using rhythmic sensory stimulation, we aimed to drive gamma oscillations at different phase offsets between left and right visual cortex at a high temporal precision (i.e., phase delays of 90 degrees or 6.67 ms) to investigate a potential role of STDP in human episodic memory. Despite observing no effects on memory performance, EEG results demonstrate the feasibility of inducing phase offsets at high frequencies, thus preserving the precise timing of the rhythmic sensory stimulation. Previous studies demonstrated that EEG/MEG signals show steady-state potentials up to 90 Hz (Herrmann, 2001; Zhigalov et al., 2019). However, our study shows, for the first time, that phase offsets between two regions in the brain can be controlled at a high temporal resolution. We believe this is important as it opens new avenues of investigating the neural and behavioural impact of subtle timing differences between large-scale neuronal assemblies in humans.

Despite the successful manipulation of phase lags between left and right visual cortex at 0, 90, 180 and 270 degree of 37.5 Hz, only a weak trend of enhanced memory by synchronizing gamma between hemifields at 0 degree (see Fig. 2.4) was observed. While the electrophysiological results look very clear, the behavioural data are considerably noisier. Comparing with the effect size of 0.978 (24 participants and 32 trials per condition) based on our previous published results, the largest effect size reached was found between 0° and 180° offset conditions (Cohen's d = 0.2331, 35 participants and 48 trials per condition) in the current experiment. Based on the post-hoc effect size, at least 219 subjects are needed to reveal a significant difference in memory performance between 0° and 180°. Therefore, it is likely that more behavioural data is required to show an effect, while relatively fewer data are needed to show an electrophysiological effect.

In theory, one possible explanation for this null result is that the chosen frequency of stimulation may not be ideal for STDP in human visual cortex during memory encoding. Indeed, a wide STDP window determined by cellular mechanisms like NMDA receptors and voltage-dependent Ca2+ channels was revealed in vivo and vitro studies (Caporale & Dan, 2008), consistent with the observed time window for neocortical principal cells (10-30 ms, corresponding to 33-100 Hz). More importantly, fast and slow gamma oscillations are likely to serve distinct functions in the hippocampus. In rodents, the medial entorhinal cortex (for information inputs) and CA3 (essential for information storage) are phase-locked to CA1 at a fast (~65-140 Hz) and a slow gamma (~25-50 Hz) rhythm, respectively (Colgin, 2015; Colgin et al., 2009). A recent intracranial EEG study shows similar evidence in humans with increased fast (60-80 Hz) gamma power indicating successful episodic memory encoding, and enhanced slow (40-50 Hz) gamma power indicating successful memory retrieval in the hippocampus (Griffiths et al., 2019). Information encoding and retrieval therefore are likely to be implemented by different gamma frequency bands. Given the above evidence, it is conceivable that fast gamma around 60-80 Hz is critical for STDP in visual cortex for sending information to higher level structures (such as the hippocampus), which would explain why stimulating at slow gamma (37.5 Hz) did not modulate memory encoding in our study.

An alternative explanation of the absence of behavioural effects could be that gamma phase modulation affects implicit memory, rather than episodic memory (which is inherently explicit; Tulving, 1972). Critically, the hippocampus has long been believed to be pivotal for episodic memory (Milner, 1966), given that patients with bilateral damage to the hippocampus show intact implicit memory but impaired episodic memory (Bechara et al., 1995). While EEG results suggest successful gamma phase modulation at visual cortex, it remains unclear if and to what extent the hippocampus is affected by rhythmic stimulation. Indeed, SSVEPs appear to

become more focal as the frequency increases (Zhigalov et al., 2019). If this is the case, implicit memory, which is not dependent on hippocampal function, would be more likely to be modulated by gamma. Moreover, given that the stimulation in our study is limited to a single modality, it is possible that hippocampus, as the binding centre of affluent information, contributes less to unimodal binding. Consistent with this notion, evidence from TMS and fMRI studies strongly suggests that priming (a form of implicit memory) is mediated by sensory areas that process the primed feature, such as color and location (Kristjánsson & Campana, 2010). More interestingly, uni-sensory entrainment at 40 Hz was found to exert alternation on visual perception (Elliott & Müller, 1998; Helfrich et al., 2014), suggesting that gamma synchrony plays a role in visual binding. In summary, rhythmic visual stimulation at gamma may have influenced unimodal implicit memory as it relies on sensory cortex and is independent from hippocampal involvement.

There is evidence, however, that runs counter to the above assertion. Neurons in the hippocampus of mice fire when auditorily stimulated at 40 Hz (Martorell et al., 2019), indicating that sensory stimulation is able to modulate hippocampus activity; whether this is applicable to humans, however, remains unknown. It is also worth noting that Martorell et al.'s study only found multisensory stimulation to improve cognition. To further our knowledge regarding non-invasive protocols for probing neuronal activation, a better understanding of how rhythmic sensory stimulation affects sensory cortex and downstream neural assemblies needs to be developed.

Limitations may arise from the replication of each movie frame six times, potentially impacting the effectiveness of entrainment and behavioural effects due to the phenomena of repetition suppression (RS) and enhancement (RE). While the combined duration of the six duplicated frames sums up to 40 ms, most studies exploring RS and RE effects typically present

stimuli for hundreds of milliseconds (e.g., Kuehl et al., 2013; Peykarjou et al., 2014; Stefanics et al., 2020). There is limited evidence regarding RS/RE induced by stimulus of very short durations. In fMRI studies, contradictory findings were reported with the first stimulus presented for 40 ms (Zago et al., 2005) and 50 ms (Müller et al., 2013), where one study observed null effects while the other detected repetition suppression. RS/RE effects may become apparent with increased repetition frequency, and the direction of suppression and enhancement can be manipulated (Müller et al., 2013; Nordt et al., 2016). Notably, even though frames were repeated six times in this study, each frame was presented for less than 6.67 ms. Additionally, attention may play a role in enhancing responses and potentially counteracting repetition suppression (Segaert et al., 2013; Auksztulewicz et al., 2015). Despite participants directing their gaze to the screen centre, they were encouraged to actively engage and establish associations between the movies. Together, existing evidence offers incomplete explanations for the effects of repeated stimuli as presented in the current study. Future research might address the repetition issue by increasing movie frame rates using software that incorporates motion interpolation and algorithmic frame generation instead of a simple frame duplication approach.

In summary, although no memory effect was found by gamma phase stimulation, the EEG results strongly suggest the capability of gamma entrainment to modulate brain oscillations among sensory areas with high temporal precision. Our paradigm provides a non-invasive way to manipulate neural synchrony at high temporal resolution between two brain regions. We believe this method makes it possible for future studies to investigate the role of timing at high frequencies for behavioural and neural processes in human subjects. Although the present application of this method was to investigate the role of STDP on human memory formation, other applications in other cognitive domains (i.e., attention) are conceivable.

CHAPTER 3: USING HIGH GAMMA RHYTHMIC VISUAL STIMULATION TO INVESTIGATE THE ROLE OF STDP IN HUMAN EPISODIC MEMORY

In chapter 2, we conducted an experiment involving luminance modulation of movie pairs at 37.5 Hz. This modulation was implemented with four different phase lags to manipulate the timing delay between the left and right visual hemifields. The results showed for the first time that oscillatory activity can be effectively driven with a temporal precision of 6.67 ms lag between neuronal groups. Yet, we did not observe any discernible difference in memory performance across the phase lag conditions. This lack of significance could be attributed to several challenges. Given these limitations, the focus of the current chapter is on refining the experimental paradigm to address these challenges and examine the role of spike timing-dependent plasticity (STDP) in human episodic memory. ♣

♣ *In preparation for:*

Chen, Q., Shapiro, K. L., & Hanslmayr, S. (in preparation). Using high gamma rhythmic visual stimulation to investigate the role of STDP in human episodic memory.

3.1. Introduction

As introduced in Chapter 2, spike timing-dependent plasticity (STDP) is one of the critical mechanisms supporting episodic memory for its role in facilitating the precise timing and synchronization of neural cell assemblies (Cassenaer & Laurent, 2007; Debanne & Inglebert, 2023; Fell & Axmacher, 2011). Synaptic modification critically depends on the relative timing of activation between pre- and postsynaptic neurons. The optimal window within which the presynaptic neuron leads postsynaptic neuron for the induction of long-term potentiation (LTP) is typically between 10-30 ms for neocortical principal cells, corresponding to frequencies of 100 to 33 Hz (Abbott & Nelson, 2000; Bi & Poo, 1998; Caporale & Dan, 2008; Cassenaer & Laurent, 2007; Juergen Fell & Axmacher, 2011; Jutras & Buffalo, 2010; Stefan et al., 2002; Wespatat et al., 2004; Wolters et al., 2003; Zhang et al., 1998).

However, it is crucial to highlight that recordings in rodent hippocampus and entorhinal cortex suggest a different role of fast and slow gamma. Specifically, CA1 fast gamma (>60 Hz) synchronizes with entorhinal cortex, which is believed to be responsible for information encoding. Conversely, CA1 slow gamma (<55Hz) couples with slow gamma in CA3, a hippocampal subfield accountable for information storage (Colgin, 2015; Colgin et al., 2009; Zheng et al., 2016; although Schomburg et al., 2014 present slow gamma from 30-80 Hz). This was further evidenced by the observing that when freely moving rats increase their running speed, there is a frequency increment in fast gamma but not in slow gamma, suggesting a correlation between fast gamma and the increase in information coding (Zheng et al., 2015; although conflicting findings are discussed in the review by Colgin, 2015)).

Furthermore, both fast and slow gamma rhythms exhibit distinct phase-locking patterns to ongoing CA1 theta phases (Bieri et al., 2014; Colgin et al., 2009; Schomburg et al., 2014; Vivekananda et al., 2021). This might link with the findings in the theta rhythms, where

different phases of hippocampal theta rhythm are linked to memory encoding and retrieval (Hasselmo et al., 2002; Siegle & Wilson, 2014). Similarly, human intracranial EEG studies have found that successful episodic memory encoding is associated with increased power in the fast gamma range (60-80 Hz), while enhanced memory retrieval is linked to increased power in the low gamma range (Griffiths et al., 2019). These findings underscore the distinctive roles of fast and slow gamma oscillations in supporting distinct processes in memory. Additionally, this differentiation could potentially explain the 'null findings' reported in the preceding chapter, wherein slow gamma (37.5 Hz) was employed for entrainment during memory encoding.

Alternatively, the ‘null findings’ could be attributed to the type of memory measured confines to episodic memory (inherently explicit; Tulving, 1972). The formation and retrieval of episodic memory relies on the hippocampus, as revealed by studies on patients with bilateral hippocampus deficit retain intact implicit memory but impaired explicit memory (Milner, 1966; Bechara et al., 1995). It is yet to be determined how far the propagation of gamma entrainment could travel and its effect on downstream structures. Critically, whether it travels to the hippocampus, given the crucial role of hippocampus in the formation and retrieval episodic memory.

In the previous chapter, the experiment manipulation was based on high frequency rhythmic visual stimulation. Despite the attraction of developing high frequency rhythmic sensory stimulation (RSS) as a noninvasive clinical tool, its viability entraining deep structure has become a hot debate. Gamma entrainment at rat visual cortex, prefrontal cortex and hippocampus was observed by delivering 40 Hz LED flicker 1h/day, spanning from seven days to 7.5 months (Adaikkan et al., 2019; Martorell et al., 2019). Importantly, this manipulation improves cognitive function (Chan et al., 2021 in human) and protects neurons from

degenerative factors. However, using a same stimulation protocol, but with different total durations, two other independent research groups measuring spike activity in rodent V1 and CA1 report similar challenge in observing gamma entrainment beyond (Soula et al., 2023) or even within V1 (Schneider et al., 2023). Given these discrepancies, the current experiment will also include the measurement of implicit memory.

In addtion to directly testing implicit memory, using a paradigm testing recognition memory can measure both the recognition and implicit memory. The dual-process theories of recognition memory proposed that recognition memory is supported by two distinct process, i.e., recollection and familiarity. While recollection reflects a thresholdlike retrieval process, familiarity reflects a signal-detection process (Yonelinas, 1999; 2002;). The dual-process signal detection (DPSD) model in the receiver-operating characteristics (ROC) toolbox (Koen et al., 2017) was developed on the dual-process and it allows for the estimation of both explicit memory (recollection) and implicit memory (faimilarity).

In traditional analysis of steady-state evoked potentials (SSEPs), which are elicited by rhythmic sensory stimulaiton, one or a specific nubmer of electrodes/sensors were chosen as ROI. This method is subject to the quality of selected electrodes and is plagued by the subjective judgements of determining the optimal number of electrodes. In contrast to this conventialal method, rhythmic entrainemnt source separation (RESS; Cohen & Gulbinaite, 2017; Gulbinaite et al., 2019; see methods for more details) offers a solution to enhance the signal-to-noise ratio (SNR) by combining all electrodes based on a weighted approach. Specifically, RESS computes a spatial filter that maximallly differentiates the SSEPs as response to the flickers a the frequency of interest, from neighbouring frequencies. By applying this resultant spatial filter to the raw data, it allows reconstruction of single-trial data and facilitates further analysis. Taking

advantage of this method, the instantaneous phase of induced SSEPs can be extracted and compared.

Expanding on these implications, the current study utilized rhythmic visual stimulation to emulate the function of STDP, aiming to investigate the impact of stimulus time delay both implicit and explicit memory. Similar to the experiment conducted in the previous chapter, movies flickering at a high gamma frequency of 60 Hz were simultaneously presented in the left and right visual fields under synchrony (0 ms delay) and asynchrony (8.33 ms delay) conditions. The effectiveness of rhythmic visual stimulation in manipulating the inter-hemifield phase lag was quantified by the extracting of instantaneous phase from SSVEPs (steady-state visual evoked potentials, SSEPs specifically evoked through visual stimulus) reconstructed using the RESS method. Participants memorized the association between the pairs of movies, which was subsequently tested regarding both implicit and explicit memory.

Aligned with the expectations derived from the function of STDP, we anticipated that enhanced implicit memory would be observed when the time delay is attenuated (corresponds to a smaller phase lag). Furthermore, if the entrainment of gamma synchronization entrainment imposes effects in the hippocampus, we should be able to detect improved explicit memory performance with decreased time delay.

3.2. Methods

3.2.1. Participants

Thirty participants were recruited for the study, with a mean age of 23.43 years (age range: 18-33). The participant sample consisted of 56.67% males and 90% right-handed individuals. Participants were either compensated with course credit or received financial reimbursement for their involvement. However, three participants were excluded from the

analysis due to excessive horizontal eye movements, as described below. Additionally, three participants were rejected due to a high false alarm rate (>90%) in the memory task. Furthermore, one participant was excluded because of an interruption in the EEG recording. After these exclusions, a total of 23 participants remained for further analysis, with a mean age of 23.35 years (age range: 18-33). The gender distribution among the remaining participants was 43.48% male, and 86.96% were right-handed. The study received ethical approval from the Research Ethics Committee at the University of Birmingham (ERN_15-0335) and complied with the Declaration of Helsinki.

3.2.2. Experimental design

3.2.2.1. Stimuli

A total of 384 three-second movie clips were randomly paired to create 192 pairs for the associative memory tasks. Prior to the formal experiment blocks, an additional four movie pairs were used in a practice block. All movies used in the study were sourced from previous work (Chen et al., 2021) and were emotionally neutral, depicting human or natural activities. The movies were resized to 360(W) x 288(H) pixels, and the frame rate was increased from 30 Hz to 120 Hz by replicating each frame four times using MATLAB scripts (R2017a; The MathWorks, Inc., Natick, MA, USA) developed in-house. The random pairing of movies resulted in 192 unique associations, with the same pairs used across all participants.

The luminance of all movies was sinusoidally modulated from 0% to 100% using a 60 Hz sine wave. However, the onset phase of the modulation varied depending on the condition. Within each movie pair, one movie always served as the leading movie with a 0° onset, while the other movie served as the trailing movie with either a 0° or 180° onset. This created two phase lag conditions: 0° (synchrony) or 180° (asynchrony) between the leading and trailing movies (refer to Fig. 3.1B). There were 96 trials in each condition. In the synchrony condition,

both movies within a pair flickered synchronously, while in the asynchrony condition, their dynamics developed inversely. Although in the synchrony condition, neither movie was leading or trailing, to discriminate the movie used as a cue for memory (as explained below in the retrieval phase of section 3.2.2.3, where leading movies always served as the cue), the leading/trailing label was retained even in the synchrony condition. The phase lag conditions assigned to each set of 96 movie pairs were counterbalanced across participants.

For the retrieval phase of the memory task (3.2.2.3), the leading movies always served as the cue for implicit/recognition memory and remained unaltered throughout all tasks. Trailing movies were replaced by static images. These images were obtained by selecting the middle frame (the 45th frame, considering the original frame rate of 30 frames per second, and 90 frames in total for a three-second movie) from the trailing movies mentioned earlier. For implicit memory task, to generate unscrambled images, the static images were digitized from unit8 to double, and then Fourier-transformed to extract phase and amplitude information. Random noise ranging from 0% to 95% was added to the original phase information in 5% increments. The noise-added data was inverse-Fourier-transformed to create blurred images ranging from 5% to 95% noise. Each blurred image was presented for 150 ms, gradually transitioning from 95% to 0% noise, resulting in a 3000 ms unscrambling image during the implicit memory test of the retrieval phase (Fig. S7.1).

All behavioural tasks were programmed using the Psychophysics Toolbox (Brainard, 1997; Pelli, 1997; Kleiner et al., 2007) in MATLAB (R2015b; The MathWorks, Natick, MA, USA).

3.2.2.2. Experimental procedure

Fourteen of the 23 participants included in the study were assessed to be free from COVID symptoms 24 hours prior to the experiment due to pandemic restrictions, while other participants were recruited before pandemic. All participants were seated in a designated testing room, where they completed an EEG safety screening form and provided informed consent for the study after being briefed on the experimental procedure. Subsequently, the participants were prepared for EEG data collection. Prior to the main tasks, the behavioural tasks were explained to the participants, and they were given a practice block to familiarize themselves with the tasks.

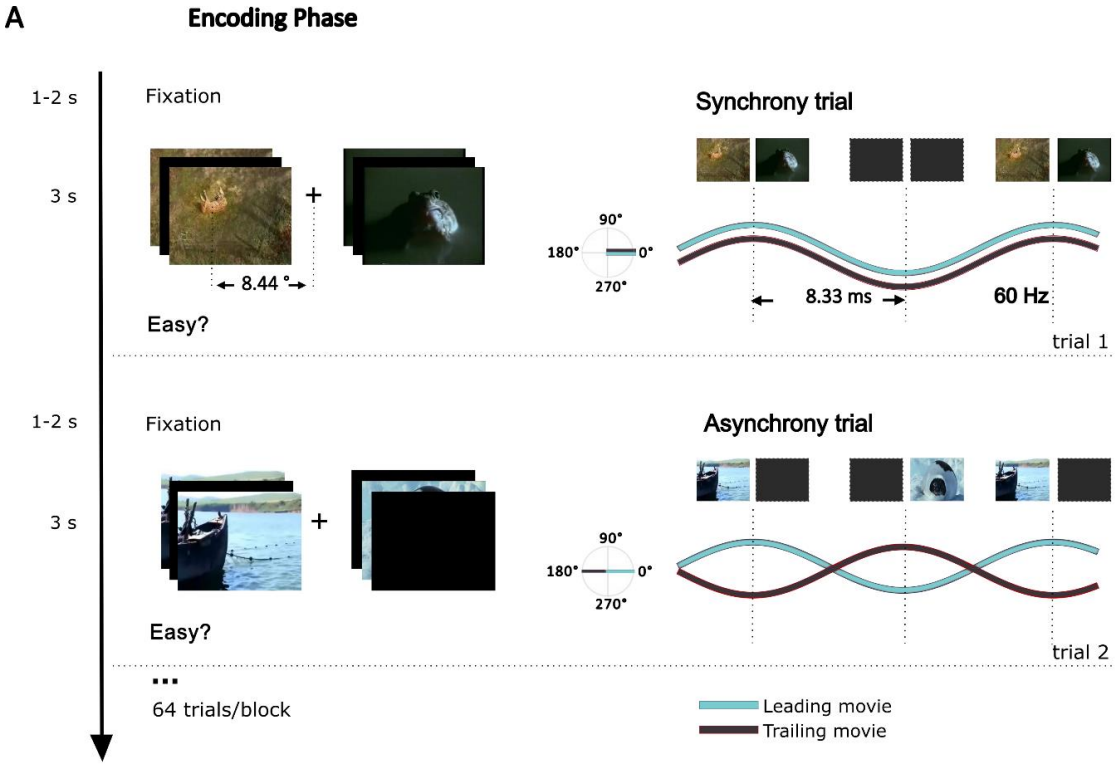
A
Encoding Phase
1-2 s
Fixation
3 s
8.44 °
Easy?
Synchrony trial
90°
180°
0°
270°
8.33 ms
60 Hz
trial 1
1-2 s
Fixation
3 s
Easy?
Asynchrony trial
trial 2
...
64 trials/block
Leading movie
Trailing movie

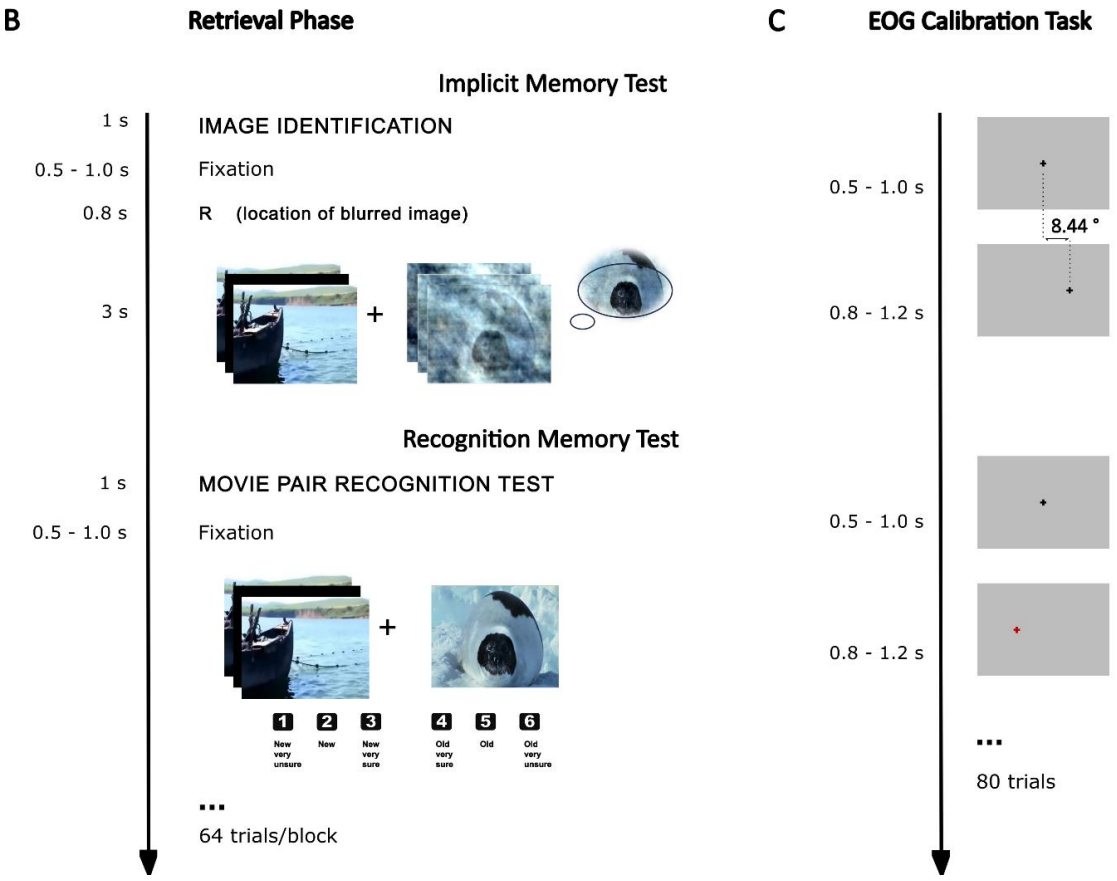
B
Retrieval Phase
Implicit Memory Test
1 s
IMAGE IDENTIFICATION
0.5 - 1.0 s
Fixation
0.8 s
R (location of blurred image)
3 s
Recognition Memory Test
1 s
MOVIE PAIR RECOGNITION TEST
0.5 - 1.0 s
Fixation
1 New very unsure
2 New
3 New very sure
4 Old very sure
5 Old
6 Old very unsure
...
64 trials/block
C
EOG Calibration Task
0.5 - 1.0 s
8.44 °
0.8 - 1.2 s
0.5 - 1.0 s
0.8 - 1.2 s
...
80 trials

Fig. 3.1. Experimental procedure. The main procedure was encompassed a memory task of 192 trials across three blocks and an EOG calibration task. Each memory block contained an encoding phase, a distractor phase and a retrieval phase. **(A)** Encoding phase. Illustrated is an exemplar trial for both the synchrony and asynchrony conditions. After a jitter fixation, a movie pair was presented for three seconds, with one displayed on the left and the other on the right visual field of a 21-inch CRT screen. The movies centre was positioned at an eccentricity of 8.44° visual angles from the centre of the screen. Participants were instructed to maintain their gaze on the central cross. Their task was to associate the movie pair for subsequent memory test, followed by indicating the ease of the association. The luminance of the movies was modulated at 60 Hz, displayed on a screen at a 120 Hz refresh rate. Within each movie pair, one led at 0° onset (leading movie), while the other followed at 0° or 180° onset (trailing movie), creating synchronous (0°) or asynchronous (180°) phase lag between them. In synchrony trials, the luminance of the movie pair began at the same phase onset (0°) and progressed at the same direction (upper right panel); while in an asynchrony trial, the onset phase and dynamics were opposite (low right panel). The leading movie always served as the cue of memory tests in (B). The leading/trailing designation was maintained even in the synchrony condition, where neither movie inherently led nor trailed, to distinguish the cue for memory. **(B)** Retrieval phase. The retrieval phase contained implicit and recognition memory tests, indicated respectively as 'IMAGE IDENTIFICATION' and 'MOVIE PAIR RECOGNITION TEST', alternating within a block. During the implicit memory test, a letter 'L' or 'R' was presented for 800 ms, indicating the location of the unscrambling image in the left or right visual field. The image was paired with a leading movie displayed at the same location as in the encoding phase. Among 64 trials in a block, 20 trials were new pairing between the leading movie and trailing unscrambling image. Participants identified the content of the unblurring image at their fastest response. The recognition memory test involved judging whether the leading movie and the trailing image constituted an old/new pair, based on the encoding phase, with three confidence levels. **(C)** EOG calibration task. This task was used for the identification and exclusion of excess eye movement made towards the movies during the memory task. For each trial, participants tracked the horizontal movement of a cross that randomly shifted left or right after a fixation of 500-1000 ms. The cross was positioned at a visual angle of 8.44°, the same distance as that between the movie and screen centre. Participants responded when the cross turned red.

During the tasks, participants were seated at a distance of 60 cm from the centre of the screen, and their heads were positioned and supported by a chin rest. Throughout the task duration, a web camera was activated to enable the experimenter to monitor the participants' head position and compliance.

The experiment comprised two main behavioural tasks: (i) a memory task and (ii) an EOG (electrooculography) calibration task. Upon completion of the experiment, to obtain more

accurate electrode interpolations, the 3D geometric locations of each electrode were recorded using a Polhemus FASTRAK device (Colchester, Vermont, USA) and Brainstorm software (Tadel, Baillet, Mosher, Pantazis, & Leahy, 2011) implemented in MATLAB (R2018a; The MathWorks, Inc., Natick, MA, USA). This additional step aimed to enhance the precision of electrode placement for subsequent data analysis.

3.2.2.3. Memory task

The memory task consisted of three blocks, each comprising an encoding phase, a distractor phase, and a retrieval phase. Each trial in the retrieval phase included both an implicit and a recognition memory test. Each block consisted of 64 pairs of movies in the encoding phase, followed by 64 implicit memory tests and 64 recognition memory tests in the retrieval phase. The order of the blocks was randomized for each participant.

During the encoding phase, each trial presented a pair of movies, with one displayed on the left and the other on the right visual field of the screen. The movies centre was positioned at an eccentricity of 8.44° visual angles from the centre of the screen (Fig. 3.1A). To ensure precise presentation timing, the movies were displayed on a 21-inch CRT screen with a refresh rate of 120 Hz and a resolution of 800 pixels width x 600 pixels height. A NVIDIA Quadro K600 graphics card (875 MHz graphics clock, 1024 MB dedicated graphics memory; Nvidia, Santa Clara, CA, USA) was used for the display. The movies were resized to 250 pixels width x 200 pixels height and horizontally aligned with the centre of the screen. The background interface was set to grey. Participants were instructed to focus their gaze at the centre of the screen and maintain central fixation throughout the presentation of the movies (3 seconds). They were encouraged to pay equal attention to both movies and remember the associations between the movie pairs by creating associative stories. This is because selective attention modulates SSVEPs (Kashiwase et al., 2012; Morgan et al., 1996). Our objective was to establish

and maintain sustained and equal attention toward movies presented in both visual fields (Müller et al., 2003). After each pair of movies, participants rated the degree of association between the two movies on a scale from 1 to 5, reflecting how easily they could associate the movies (1: no fit, 5: perfect fit). This judgment task helped maintain participant engagement during the encoding phase.

Following the encoding phase, participants engaged in a distractor task for 30 seconds to prevent active rehearsal of the movie pairs. They verbally counted backwards by subtracting three from a given random 3-digit number.

In the retrieval phase, each trial included an implicit and a recognition memory test (Fig. 3.1B). Either "IMAGE IDENTIFICATION" or "MOVIE PAIR RECOGNITION TEST" was displayed for 1000 ms before a jittered fixation (ranging from 500 to 1000 ms) to indicate the type of memory test (implicit or recognition). No fixed gaze was required during the retrieval phase. The leading movies from the encoding phase were always used as cues in the retrieval phase, although participants were unaware of which movies served as the leading or trailing ones.

During the implicit memory test, a leading movie and an unscrambling image were simultaneously displayed in the same positions as in the encoding phase for 3 seconds. Before that, the location of the unscrambling image was indicated by the letter ‘L’ or ‘R’ for 800 ms. As described above in the stimuli section, the unscrambling image was the middle frame retrieved from the trailing movie pool. For convenience, the combination of the movie and the unscrambling image was referred to as a "movie pair" in this context. Among the 64 pairs of movies in a block displayed during retrieval, 20 pairs were recombined to create new pairs. For example, in the encoding phase, pairs A (left visual field, LVF) and B (right visual field, RVF), C (LVF) and D (RVF), and E (LVF) and F (RVF) were formed. In the retrieval phase, the pair

A (LVF) paired with B (RVF) would be an old pair, while the pairs C (LVF) and F (RVF) and E (LVF) and D (RVF) would be new pairs. Importantly, the left/right positions of the movies in the retrieval phase matched those in the encoding phase. For example, if the leading movie was on the right visual field in the encoding phase (Fig. 3.1A), it remained on the right visual field in Fig. 3.1B. The number of pairs with leading movies in the left and right visual field was counterbalanced. Participants had 3 seconds to identify the content of the unscrambling image and were instructed to respond as soon as possible by pressing the spacebar. No further response was required to avoid prolonging the task excessively and maintaining attention. As a compromise, 10% of the implicit memory tests included a catch trial, in which participants were asked to select the image identical to the unscrambling image from a newly introduced lure picture. Participants with poor performance on the catch trial would be excluded. Given that no fixation was required during this test, participants were expected to utilize the presence of the leading movies as a cue to facilitate faster recall and reactivation of the associated trailing movies in the case of old pairs, as compared to new pairs.

The recognition memory test used stimuli and positions identical to those in the implicit memory test, except that the unscrambling image was replaced by the original static image without noise (Fig. 3.1B). The movie and image were displayed for 3 seconds, and participants were allowed to respond as soon as they recall the pair. Simultaneously with the onset of the movies, a scale ranging from 1 to 6 was displayed and remained visible until a response was received. Participants were instructed to judge whether the static image (from the trailing movie) was paired with the leading movie during the encoding phase. The response options included "old" or "new" with three confidence levels (1: new very unsure, 2: new, 3: new very sure; 4: old very sure; 5: old; 6: very old unsure).

3.2.2.4. EOG calibration task

The EOG calibration task provided a template for monitoring the occurrence of horizontal eye movements. The data obtained from this task were utilized to identify and exclude trials where overt eye movements were made towards the movies. During the EOG calibration task, participants were instructed to visually track a black cross that randomly appeared to the left or right of the fixation cross, positioned at a visual angle of 8.44° from the screen centre. For each trial, the fixation started at the screen centre for 500 to 1000 ms. Following each fixation movement, the fixation cross remained stationary for a variable duration ranging from 800 ms to 1200 ms before returning to the centre, indicating the onset of the next trial. In total, there were 80 trials, with an equal distribution of leftward and rightward movements. Additionally, 10% of the trials served as catch trials, in which participants were required to promptly report a color change of the cross from black to red by pressing the space button. This arrangement ensured that participants maintained their attention throughout the calibration task, contributing to the accuracy of eye movement monitoring.

3.2.3. Data analysis

3.2.3.1. EOG calibration

In order to ensure comparable tracking responses stimulated by movies presented in the left and right visual fields, we implemented an EOG calibration procedure to exclude encoding trials with overt horizontal eye movements during movie watching. It is important to note that the linear relationship between voltage and visual angle allows for the utilization of EOG data as an effective eye-tracking measure (Acuna et al., 2014). The same EOG calibration procedure was also employed in our previous related study (Chen et al., 2021). Individual thresholds were calculated for each participant to exclude trials with excessive HEOG (horizontal EOG) activity, and the procedure is described in detail below.

Initially, a similar EEG preprocessing procedure was applied to both the EOG and EEG data in the memory encoding phase. The EOG data were epoched with a time window of 2000 ms before and after the onset of the fixation cross, while the memory encoding data were epoched from 2000 ms before to 5000 ms after the onset of each movie pair. Subsequently, a low-pass filter with a cutoff frequency of 30 Hz was applied to both datasets, followed by resampling to 512 Hz.

Next, the EOG data were carefully examined, and trials with early horizontal eye movements (i.e., occurring before the onset of the stimuli movement) and random saccades that did not reflect eye tracking of the fixation cross were manually rejected. To detect the voltage gradients generated by the eye movements from the movie centre (located at a visual angle of 8.44°) to the screen centre, we calculated the first derivative using the 'diff' function in MATLAB. By identifying the largest peak voltage change within 600 ms after the onset of the fixation movement, we averaged this peak value across trials. The resulting value corresponds to the individual voltage change generated by the eye tracking from the screen centre to the movie centre. To define the threshold for HEOG exclusion, we set it at 50% of this resulting value. Encoding trials that exceeded this threshold were subsequently excluded from further behavioural and EEG analyses.

3.2.3.2. EEG acquisition and preprocessing

We utilized the 128-channel BioSemi ActiveTwo system for EEG data collection. EOG was recorded by three additional electrodes. One electrode was positioned 1 cm below the left eye, while the other two electrodes were placed 1 cm horizontally apart from the left and right lateral canthus, respectively. The online EEG data were sampled at a rate of 2048 Hz using the BioSemi ActiView software.

All EEG data analysis were performed using the Fieldtrip toolbox (Oostenveld, Fries, Maris, & Schoffelen, 2011). The processing steps for EEG data were also described in our previous study (Chen et al., 2021). Firstly, the encoding data were segmented into epochs, spanning from 2000 ms before to 5000 ms after the onset of the movie pairs. Subsequently, the data were bandpass filtered in the range of 1 to 100 Hz. To eliminate line noise, bandstop filters were applied to remove line noise between 48-52 Hz and 98-102 Hz. The data was then prepared for independent component analysis (ICA). This involved downsampling the data to 512 Hz and visually inspecting the channels and trials for muscle artifacts. ICA was used to identify and remove components associated with horizontal and vertical eye movements, as well as cardiac activity.

To address rejected channels, we interpolated the missing data using triangulation based on the individual electrode locations. Finally, the data were re-referenced to the average of all channels, and manual inspection was performed to remove trials with artifacts.

However, there were noticeable differences in preprocessing data for the calculation of spatial filters using the method of rhythmic entrainment source separation (RESS, Cohen et al., 2017). The steps were the same as the normal preprocessing routine stated above, except that 1) all ICA components were retained; 2) channels with high variance EEG signal containing EMG noise, mostly frontal and temporal, were identified and removed using the Fieldtrip ft_rejectvisual function; and 3) rejected channels were simply ignored without interpolation.

3.2.3.3. Behavioural analysis and ROC model fitting

In all subsequent behavioural and EEG analyses as detailed below, only trials passed the EOG calibration and EEG preprocessing were included. Participants with a total trial number below 100 trials were excluded from further analysis, resulting in the inclusion of a

total of 23 participants for the subsequent analysis. All behavioural analyses and data visualization were conducted in RStudio (R Core Team, 2021).

Implicit memory test

Implicit memory was accessed by measuring the reaction time when identifying the content of an unscrambling image, presented either with a paired movie or newly assigned movie. We expected participants to identify the blurred images with shorter reaction times in the condition where they were paired with familiar movies, compared to the condition with new pairings, if implicit associative memory played a role. Thus, we compared the reaction times (RT) for identifying blurred images between the old and new pair conditions. Because the number of trials in the old condition almost doubled that of new pairs, the comparison was carried out by a Wilcoxon signed rank test. For the comparison, outliers where RT was less than 1.96 standard deviation below the mean were excluded. To foreshadow the results of this analysis, no difference was found between the old and new pair conditions. Consequently, no further analysis was conducted for the implicit memory test.

Recognition memory test

In the recognition memory test, participants were required to judge whether a given static image had been paired with the preceding movie. Ratings were provided on a scale of 1-6, encompassing old/new judgments with three confidence levels (1: new very unsure, 2: new, 3: new very sure; 4: old very sure; 5: old; 6: very old unsure). These responses were fitted to the dual-process signal detection (DPSD) full model in ROC toolbox (Koen et al., 2017) which posits that recognition memory is supported by two distinct processes – recollection and familiarity. Various parameters, including recollection of oldness, recollection of newness, familiarity, and area under the curve (AUC), were estimated and compared between the

synchrony and asynchrony conditions using one-tailed paired sample t-tests. Bonferroni correction was used for multiple comparisons correction. Effect size of statistical comparisons was estimated according to the method suggested by Cohen (2013).

3.2.3.4. Validation of gamma phase entrainment

This section of EEG analysis aimed to validate the efficacy of gamma phase entrainment to both the left and right visual cortices, specifically at a frequency of 60 Hz and at phase lags of 0° or 180°. To achieve this, we first examined whether the left/right visual cortices specifically entrained to the 60 Hz movies. Next, we employed rhythmic entrainment source separation (RESS; Cohen & Gulbinaite, 2017), a spatiotemporal source separation method, to reconstruct the single-trial EEG response to the flickers. RESS functions by combining all electrodes through a weighted combination determined by the RESS filter. This method enhances signal-to-noise ratio (SNR) compared to the traditional approach of designating specific electrodes as region of interest (ROI), thereby eliminating subjectivity in ROI selection.

It is important to note that all EEG analyses conducted within this section was based on EEG data collected during the memory encoding phase, where stimulus onset refers to the onset of movie pairs. Further elucidation on the analysis protocol is provided below.

Examination of phase entrainment at 60 Hz

To investigate the EEG response to the 60 Hz flickering movies, we computed the inter-trial phase coherence (ITPC) as an indicator for consistent phase entrainment across trials. First, we organized trials based on the location of leading movies (the location was consistent between encoding and retrieval phase), either in the left or right visual field. We expected ITPC to be attenuated for the cue-at-right-visual-field condition (LeadRvsf) due to the cancellation effect caused by the 0° and 180° movies at the right visual field, while remaining robust in the left

visual field. The reverse pattern was expected for the cue-at-left-visual-field condition (LeadLvsf).

In practice, this analysis was performed for each participant. ITPC values were computed within a frequency range of 40 to 80 Hz, in steps of 2 Hz, within a time window of -1000 to 3750 ms relative to stimulus onset, across all 128 channels. We used a dpss multitaper approach for this calculation, with one taper for each frequency of interest (FOI). The multitaper method performed a time-frequency transformation by multiplying in the frequency domain with a sliding time window of 500 ms. The topographical distribution of ITPC strength at 60 Hz in the LeadLvsf and LeadRvsf conditions is shown in Figure 3.5A and B, respectively. To confirm whether the entrainment was confined to the left and right visual region, ITPC at 60 Hz was contrasted between the LeadLvsf and LeadRvsf conditions (Rvsf minus Lvsf). The inter-condition difference was subjected to a two-tailed (alpha = 0.05) paired-sample cluster-based permutation test with 2000 randomizations at the group level. The selected time window of interest (TOI) was 500-2500 ms after stimulus onset. This TOI choice was consistent with previous studies (Chen et al., 2021; Clouter et al., 2017; Wang et al., 2018) that employed a similar paradigm at lower frequencies. Additionally, this choice minimized potential interference from stimulus onset and offset effects and balanced with the low SNR of high frequency entrainment. Significance probability was estimated by means of the Monte Carlo method.

It was observed that LeadRvsf contained a greater number of trials than LeadLvsf, potentially bias the ITPC comparison between conditions. To address this, we performed supplementary analysis to compute and contrast pairwise phase consistency (PPC, Vinck et al., 2010) for LeadLvsf and LeadRvsf. PPC serves as a measure of phase coherence similar to ITPC but is unaffected by trial number bias. The PPC calculation followed by the procedure outlined

by Vinck et al. (2010), with the same dpss multitaper approach and parameters employed as those for the ITPC calculation described earlier.

While ITPC manifested a peak at 60 Hz for both hemifields (Fig. 3.5D and E), we carried out further analysis to confirm the specificity at this freuqency. This analysis was confined to channels A5-A18, D16-D17, and D24-D32 for the left hemifield (highlighted channels in Fig. 3.5B), and A26-A32, B2-B19, and C1-C16 for the right hemifield (highlighted channels in Fig. 3.5A). First, for both LeadRvsf and LeadLvsf, the ITPC difference between contralateral and ipsilateral hemifields relative to the leading movie were calculated for 40-80 Hz, following the identical dpss multitaper approach described above. The expectation was for ITPC to peak in the contralateral hemifield, while remaining low in the ipsilateral hemifield. Importantly, this ITPC difference between the two hemifields was expected to be specific to 60 Hz. Second, the ITPC difference between the two hemifields (contralateral-ipsilateral) was calculated for the 40-80 Hz range and then averaged across LeadRvsf and LeadLvsf. This resultant ITPC difference was compared against zero by a one-tailed (alpha = 0.05) paired-sample Monte Carlo cluster-based permutation test with 2000 randomizations, conducted within a TOI of 500-2500 ms upon movie onset.

The verification of inter-hemifield phase lag for synchrony and asynchrony conditions

To address the challenge of low SNR inherent to high frequency entrainment, we implemented the rhythmic entrainment source separation (RESS; Cohen and Gulbinaite, 2017) method and analyzed the Steady-State Visual Evoked Potentials (SSVEPs; Müller et al., 2003, 2006) for this part of analysis. The goal was to extract the inter-hemifield phase lag corresponding to both the synchrony and asynchrony conditions based on the reconstructed SSVEPs obtained through RESS. Below are the details of the process.

The core idea behind the RESS method is to construct a single weighted combination of all electrodes by multiplying the RESS filter – a linear spatial filter – with the EEG time series data. The RESS filter was defined as the eigenvectors with the maximum eigenvalue possessing the highest SNR, which maximally differentiates two covariance matrices (Fig. 3.2). In our study, these covariance matrices embody a signal covariance matrix centred at the frequency of interest (FOI; 60 Hz, signal, S) and a reference covariance matrix at neighbouring frequencies (60±2 Hz, reference, R). The RESS method surpasses the traditional approach of designating the best electrodes as ROI, as it substantially improves SNR by effectively mitigating potential noise from the electrodes with the maximum or minimum effect. Moreover, this approach eliminated subjectivity in determining the optimal number of electrodes for ROI.

To ensure the validity of the RESS filter, it was crucial to maintain the spatial location of the stimulus constant. Given that the movies were concurrently presented on both the left and right visual fields, albeit with distinct onset phases, we independently computed RESS filters for the left and right visual cortices to eliminate interference from each other. First, the encoding data were specifically preprocessed for the RESS filter calculation. This included retaining all ICA components and removing noisy channels affected by muscle artifacts without interpolation using the Fieldtrip ft_rejectvisual function (details in the preprocessing section). Second, based on the spatial location of the leading movies in the asynchrony condition, the data were further conditioned as LeadRvsf180 and LeadLvsf180, representing leading movies in the right and left visual fields, respectively. In the synchrony condition, where both movies began at identical onset phases, trials were concatenated irrespective of the spatial position of the leading movie. The RESS filters for the left and right hemifields were separately calculated for the LeadRvsf180, LeadLvsf180, and synchrony conditions. The left hemifield included channels A1-A25, C17-C32, and D1-D128, while the right hemifield included channels A1-A4,

A19-A32, B1-B32, and C1-C16 (see electrodes highlighted in Fig. 3.2 top panel). The channels at the antero-posterior midline were included for both hemifields.

Temporal filtering with narrow-band Gaussian filters was applied to the preprocessed data in each condition and hemifield (3 conditions x 2 hemifields). For the signal covariance matrices (S matrix), the filter centred at 60 Hz had a full width at half-maximum (FWHM) of 0.6 Hz. For the neighbouring (reference) covariance matrices (R matrix), the filter was centred at 58 and 62 Hz, respectively, with an FWHM of 1 Hz. We utilized the filtered signal and reference data from 500 to 2500 ms after movie stimulus onset to compute the S and R matrices, respectively. This time window aimed to balance between minimizing stimulus onset and offset effects on the spatial filter while ensuring a longer epoch for high SNR. As a result, each hemifield in every condition had one S matrix and two R matrices (for upper and lower neighbours, Fig. 3.2). The final R matrix was obtained by averaging the two R matrices centred at the upper and lower neighbouring frequencies (see equation (1)). Additionally, to reduce the influence of noise on the eigendecomposition results, one percent of the average eigenvalues, as shrinkage regulation, were added to the diagonals of the R covariance matrix (see equation (2); also see Gulbinaite et al., 2019). Third, we performed generalised eigendecomposition on the S and the final R covariance matrix (R in equations (2) and (3)) to construct spatial filters (W, see equation (4)):

$$covR = (covR_{upper} + covR_{lower})/2 \quad \text{(equation 1)}$$

$$R = covR + 0.01*diag(diag(covR)) \quad \text{(equation 2)}$$

$$SW = RW\lambda \quad \text{(equation 3)}$$

$$[W, \lambda] = eig(S, R) \quad \text{(equation 4)}$$

Here, W represents the matrix of eigenvectors, and λ is a diagonal matrix of eigenvalues. Each column of W represents one combination of electrode weights, and typically, the column with the largest eigenvalue is used as the spatial filter to reconstruct the RESS component time series. However, the spatial filters with the six max eigenvalues were compared in terms of SNR for maximizing EEG signals at the flicker frequency from the neighbouring frequencies. SNR was obtained by dividing the power spectra at the flicker frequency from the neighbouring frequencies, based on the reconstructed RESS component time series. The spatial filter with the highest SNR was ultimately adopted for the reconstruction of the RESS component time series (Fig. 3.2 upper right panel). The sign of the spatial filters was manually adjusted to align with the expected positive cluster in the left or right visual hemifield.

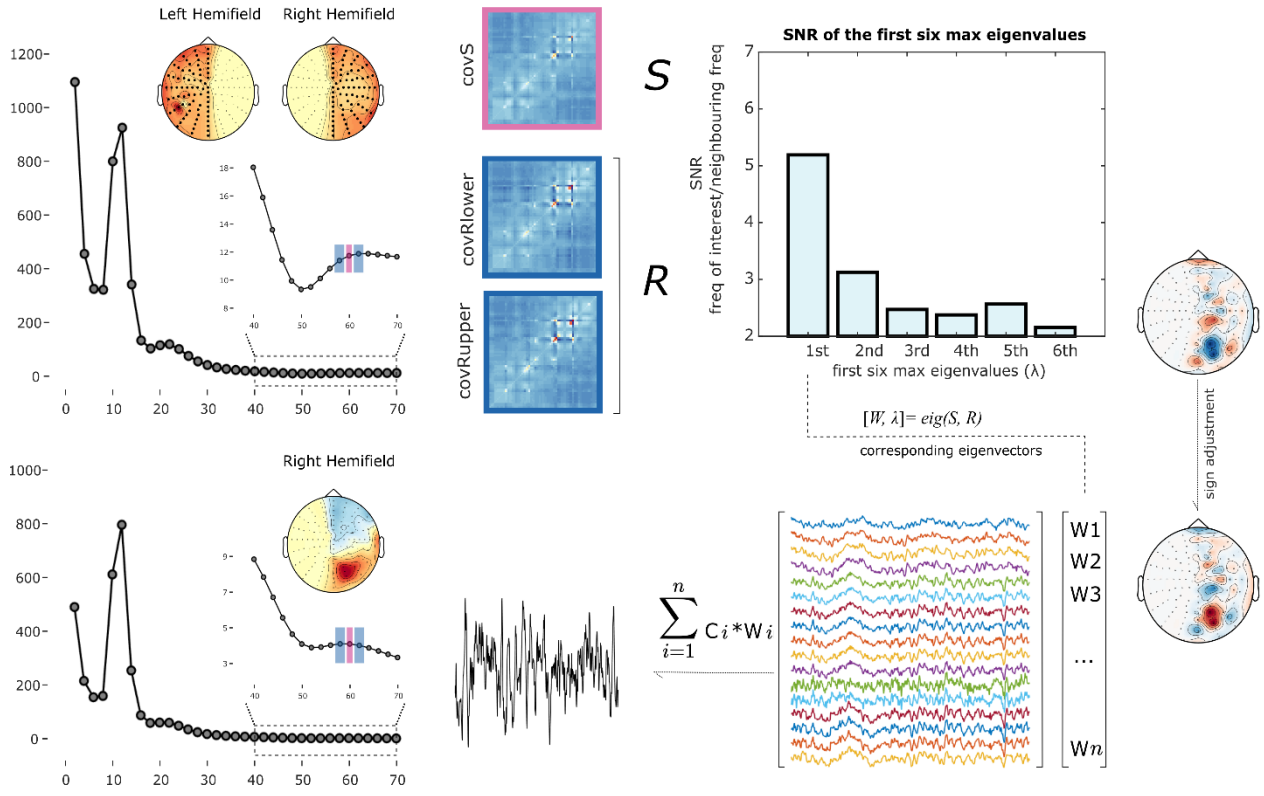

Fig. 3.2. RESS time series reconstruction procedure. The RESS filter computation was performed separately for the left and right hemifield (electrodes highlighted in the top left panel), and for the conditions of synchrony, LeadLvsf180 and LeadRvsf180, respectively. For Signal (S) and Reference (R), the channel-wise covariance matrix was calculated using Gaussian-filtered preprocessed data, centred at the FOI of 60 Hz FOR S matrix and its adjacent lower and upper frequencies for the R matrix. A generalised eigendecomposition was employed to determine the eigenvectors that effectively differentiated the S matrix from R matrix. The SNR was compared among the six highest eigenvalues (upper right). The eigenvectors corresponding to the eigenvalue exhibiting the highest SNR were chosen as the RESS filter. To ensure alignment with anticipated positive clusters in the left or right visual area, the sign of the RESS filter was manually adjusted. Subsequently, the RESS filter multiplied the raw channel data to reconstruct single time series (lower right). The power spectrum of an exemplar reconstructed time series in the right hemifield revealed a peak at FOI, while supressing other frequencies (lower left).

As a result, six spatial filters were obtained for each participant (LeadRvsf180, LeadLvsf180, and synchrony by left/right hemifield) for the reconstruction of single-trial data in each condition and hemifield. These reconstructed data were subsequently used for the

SSVEPs analysis. The single-trial data were grouped according to synchrony/asynchrony and whether the entrainment was attributed to the leading/trailing movies, yielding the synchrony-leading, synchrony-trailing, asynchrony-leading and asynchrony-trailing conditions. Time-locked analyses were conducted for each participant for these four conditions, resulting in one SSVEPs for each condition.

For each participant, the SSVEPs were prepared for Hilbert transform by applying a bandpass filter from 56 to 64 Hz. The resulting angles derived from the Hilbert transform were unwrapped to calculate the instantaneous phase difference between the leading and trailing movies in both the synchrony and asynchrony conditions. To minimize potential influence from stimulus onset and offset, the time of interest (TOI) used for analysis was set from 1000-2000 ms upon stimulus onset, following similar rationale as previous studies (Chen et al., 2021; Clouter et al., 2017; Wang et al., 2018).

In the subsequent group analysis, the SSVEPs were averaged across all participants for each condition. We adhered to the same procedure as in individual analysis to calculate the instantaneous angles and phase difference between the left and right ROIs, albeit based on the grand averaged SSVEPs. The alignment between the distribution of instantaneous phase difference (brain responses) and the phase lag conditions (stimulus lag) was assessed using the V test from the Circular Statistics Toolbox (Berens, 2009).

3.2.3.5. Single-trial phase bin sorting and ROC fitting

Alongside the behavioural analysis comparing recognition memory performance between the synchrony and asynchrony conditions, we undertook a single-trial analysis employing phase bin sorting. This approach aimed to achieve a better signal-to-noise ratio (SNR) and compare memory performance between conditions with the shortest and longest time lag

between leading and trailing movies. The single-trial analysis phase bin sorting was conducted based on the RESS-reconstructed time series, as described in the previous section (3.2.3.4).

There were six spatial filters obtained for each participant (LeadRvsf180, LeadLvsf180, and synchrony by left/right hemifield), which were utilized for the reconstruction of single-trial data for each condition and hemifield. To extract the instantaneous phase of the single-trial EEG time series data for the leading and trailing movies, the single-trial data were first band-pass filtered from 59-61 Hz. Subsequently, a Hilbert transformation and unwrapping were applied to acquire the instantaneous single-trial phase difference between the leading and trailing movies. This calculation was performed within a time window of 1000 to 2000 ms after stimulus onset. Single-trial phase bin sorting was performed based on the mean phase difference, calculated using the cir_mean function implemented in the Circular Statistics Toolbox (Berens, 2009). This resulted in the following eight phase bins: 0°-45°, 45°-90°, 90°-135°, 135°-180°, 180°-225°, 225°-270°, 270°-315° and 315°-360°.

Aligned with the function of STDP, we hypothesised that recognition performance would exhibit enhancement with decreasing delay that trailing movies tracing leading movies. Thus, we sought to compare recognition performance between the shortest and the longest delay. To ensure the robustness of comparisons, we set a threshold of at least 20 trials in each phase bin condition. However, due to the limited trial number in the 0°-45° vs. 315°-360° (N=10 out of 23) or the 0°-90° vs. 270°-360° (N=14) conditions, the subsequent ROC fitting of behavioural performance was confined to the comparison between the 0°-135° vs. 225°-360° (N=19).

During the recognition memory test, participants judged whether a given static image retrieved from the trailing movie pool was paired with the leading movie in the encoding phase, using a scale of 1-6 that included "old" or "new" with three confidence levels (1: new very

unsure, 2: new, 3: new very sure; 4: old very sure; 5: old; 6: very old unsure). The response data were fitted to the DPSD full model, which assumes that recognition memory is supported by two qualitatively distinct processes: recollection and familiarity. Parameters, i.e., recollection of oldness, recollection of newness, familiarity, and area under the curve (AUC) were estimated and subsequently compared between the 0°-135° and 225°-360° phase bins using a one-tailed paired-sample t-test (alpha = .05). Bonferroni correction was used for multiple comparisons correction. Furthermore, for each comparison, we calculated *Cohen's d* as the effect size by dividing the absolute mean difference by the standard deviation of the difference between the phase bins.

3.3. Results

3.3.1. Behavioral performance

The behavioural performance analysis includes implicit and recognition memory assessments. To ensure the analysed trials accurately reflect behaviour affected by phase modulation, a calibration procedure for horizontal electrooculogram (HEOG) was applied prior to the behavioural analysis. Additionally, any trials that were discarded during EEG preprocessing were also excluded from the analysis.

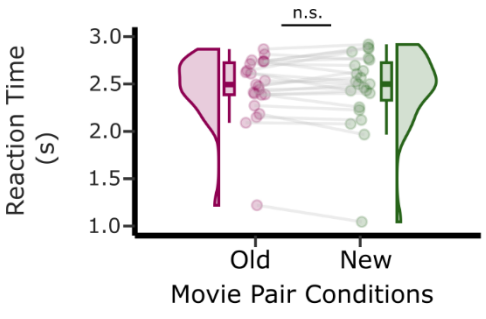

Fig. 3.3. Implicit associative memory performance. There was no significant difference in reaction time for identifying the content of unscrambling images between the old and new pair conditions. The plot includes Gaussian Kernel probability density, scatter representing individual data, and box plots. The median is indicated by the centre line, while the box boundaries correspond to the 25th and 75th percentiles. The whiskers represent 1.5 times the interquartile range.

Following the application of HEOG calibration and the removal of rejected trials, an average of 156 trials (ranging from 109-189) remained for further analysis. The trial number varied from 55-95, with a mean of 77 trials for the synchrony condition, and ranged from 54-94, with a mean of 79 trials for the asynchrony condition. It is noteworthy that fewer trials were retained in the synchrony condition compared to the asynchrony condition (t_{22} = 2.3844, p = .0262).

Regarding the implicit associative memory test, participants were expected to respond more quickly when the pair remained intact (for trial numbers, M=109, range from 89-131) compared to newly assigned pairs (M=49, range from 41-60). However, the Wilcoxon signed-rank test indicated no significant difference between the old and new pairs (Z = 0.2281, p = 0.5902, one-tailed, Cohen's d =0.0693, Fig. 3.3). Consequently, no further comparison of implicit associative memory performance was conducted between the synchrony and asynchrony conditions due to the absence of implicit associative memory observed in the test.

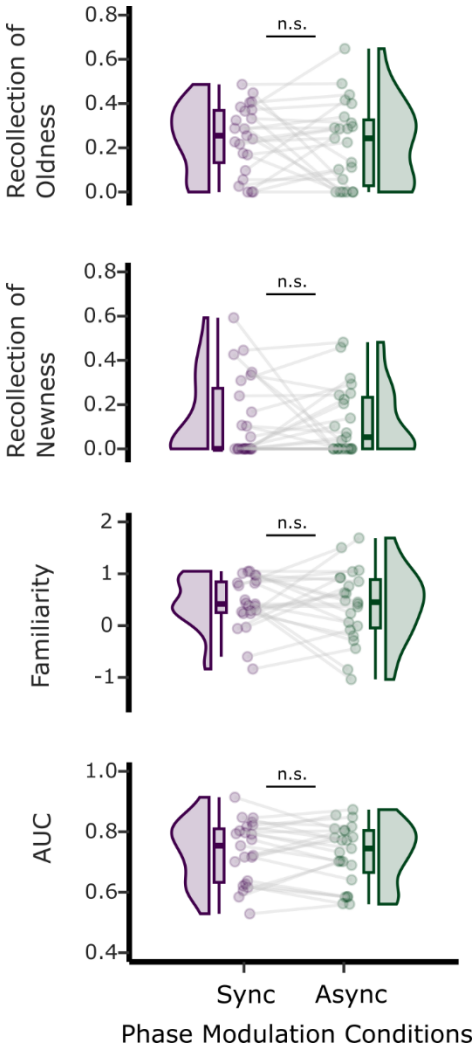

Fig. 3.4. Comparison of estimated recognition memory parameters using ROC analysis between synchrony and asynchrony conditions. The ROC toolbox was employed to fit recognition memory performance (old/new with three confidence levels), allowing estimation of recollection of oldness, recollection of newness, familiarity, and AUC. No significant differences were observed between the synchrony and asynchrony conditions for these four parameters. The median is indicated by the centre line in the box plot, while the box boundaries correspond to the 25th and 75th percentile. The whiskers represent 1.5 times the interquartile range.

During the recognition memory test, participants' responses were categorized into six levels including old/new, with three confidence levels. These responses were then fitted to the dual-process signal detection (DPSD) full model, which estimated several parameters including recollection of oldness, recollection of newness, familiarity, and the area under the curve (AUC). Subsequently, these parameters were compared between the synchrony and asynchrony conditions (Fig. 3.4). However, paired-sample t-test analysis indicated no significant difference in the estimated parameters between the synchrony and asynchrony conditions ($t_{22} = 0.4954$, $p = 0.3126$, Cohen's d = 0.1033 for recollection of oldness; $t_{22} = 0.2476$, $p = 0.4034$, Cohen's d

=0.0516 for recollection of newness; t_{22} = 0.3239, p = 0.3745, Cohen's d = 0.0675 for familiarity and t_{22} = 0.4952, p = 0.3127, Cohen's d = 0.1033 for AUC; one-sided; Bonferroni corrected p = 1 for all parameters). Therefore, no significant variations were observed in the measured parameters regarding memory performance between the two conditions.

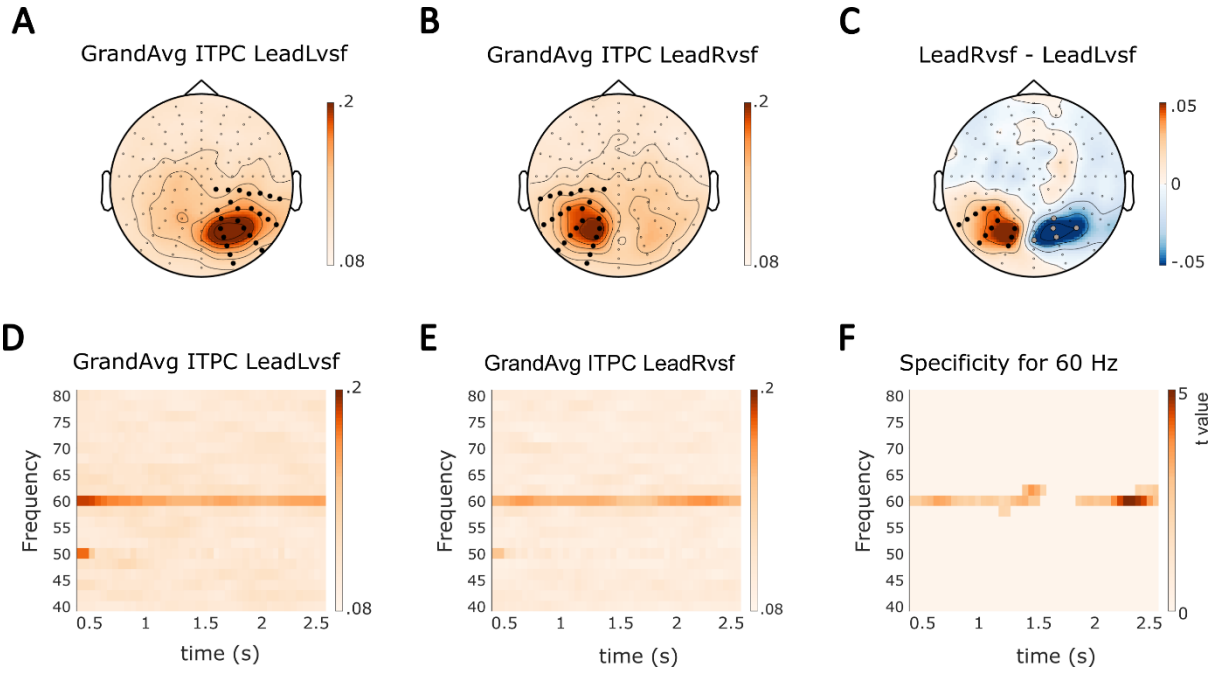

Fig. 3.5. Group ITPC distribution. (A) The topography of grand-averaged ITPC across participants at 60 Hz for the LeadLvsf condition. ITPC values were computed across trials where leading movies were presented in the left visual field, spanning from 0.5s to 2.5s post-stimulus onset. As anticipated, the most pronounced ITPC values manifested in the contralateral (right) visual hemifield. **(B)** Similar to (A), but for the LeadRvsf condition, a reversed pattern emerged. Highlighted electrodes in (A) and (B) were channels pre-selected for averaging ITPC in the 40-80 Hz range, as depicted in (D) and (E), respectively. **(C)** Topographic distribution of grand averaged ITPC difference between LeadRvsf and LeadLvsf (LeadRvsf – LeadLvsf). Cluster-based paired sample permutation test indicated difference between the two conditions in the left hemifield ($p_{corrected}$ < 0.01, electrodes highlighted in thick black dots), but not the right hemifield ($p_{corrected}$ = 0.0970, electrodes highlighted in thick grey dots). **(D)** and **(E)** ITPC from 40-80 Hz extending from 0.5s to 2.5s showed a peak at 60 Hz for both the LeadLvsf and LeadRvsf conditions. **(F)** The specificity at 60 Hz was statically validated by comparing the difference (between ITPC values contralateral and ipsilateral to the leading movies' presented field) versus zeros ($p_{corrected}$ < 0.0001 for the left cluster; $p_{corrected}$ < 0.001 for the right cluster).

3.3.2. ITPC and SSVEPs revealed gamma phase entrainment at 60 Hz

To validate gamma entrainment to both left and right hemifield, we used inter-trial phase coherence (ITPC) as an indicator for consistent phase entrainment across trials. Preprocessed EEG trials were concatenated according to the location of the leading movie, either in the left or right visual field. This yielded two distinct conditions, denoted as LeadLvsf and LeadRvsf. Anticipating that ITPC would be more pronounced in the contralateral hemifield to the side of the leading movies, we observed a stronger ITPC in the right hemifield for LeadLvsf (Fig. 3.5A) and in the left hemifield for LeadRvsf (Fig. 3.5B), aligning with our expectations.

Further, a cluster-based paired sample permutation test revealed significant differences in the ITPC topographical distribution at 60 Hz between LeadRvsf vs. LeadLvsf. Specifically, the LeadRvsf exhibited stronger ITPC in the left posterior area compared to LeadLvsf ($p_{corrected}$ <0.01), suggesting robust phase tracking to the lead movies when presented at the right visual field. However, the permutation test did not reveal significantly stronger ITPC in the right posterior area in the LeadLvsf condition compared to LeadRvsf ($p_{corrected}$ = 0.0970).

The enhanced ITPC found in the left posterior area in the LeadRvsf might be attributed to the difference in trial numbers between conditions. Indeed, LeadRvsf contained more trials than LeadLvsf (for LeadLvsf, M = 72.4348, range from 51-86; for LeadRvsf, M = 83.7391, range from 58-105; t= -5.7019, p < 0.0001, two-sided), and ITPC tends to be more stable with a larger number of trials. To survey this possibility, we carried out an additional analysis comparing pairwise phase consistency (PPC) between the two conditions. Since PPC is similar to ITPC but unbiased by trial number disparities, the results corroborated the ITPC findings (Fig. S7.3). Specifically, PPC exhibited stronger phase coherence in the left posterior area for LeadRvsf vs. LeadLvsf ($p_{corrected}$ <0.01), while no significant difference was observed in the right posterior region (($p_{corrected}$ =0.0935), where stronger PPC was expected for LeadLvsf.

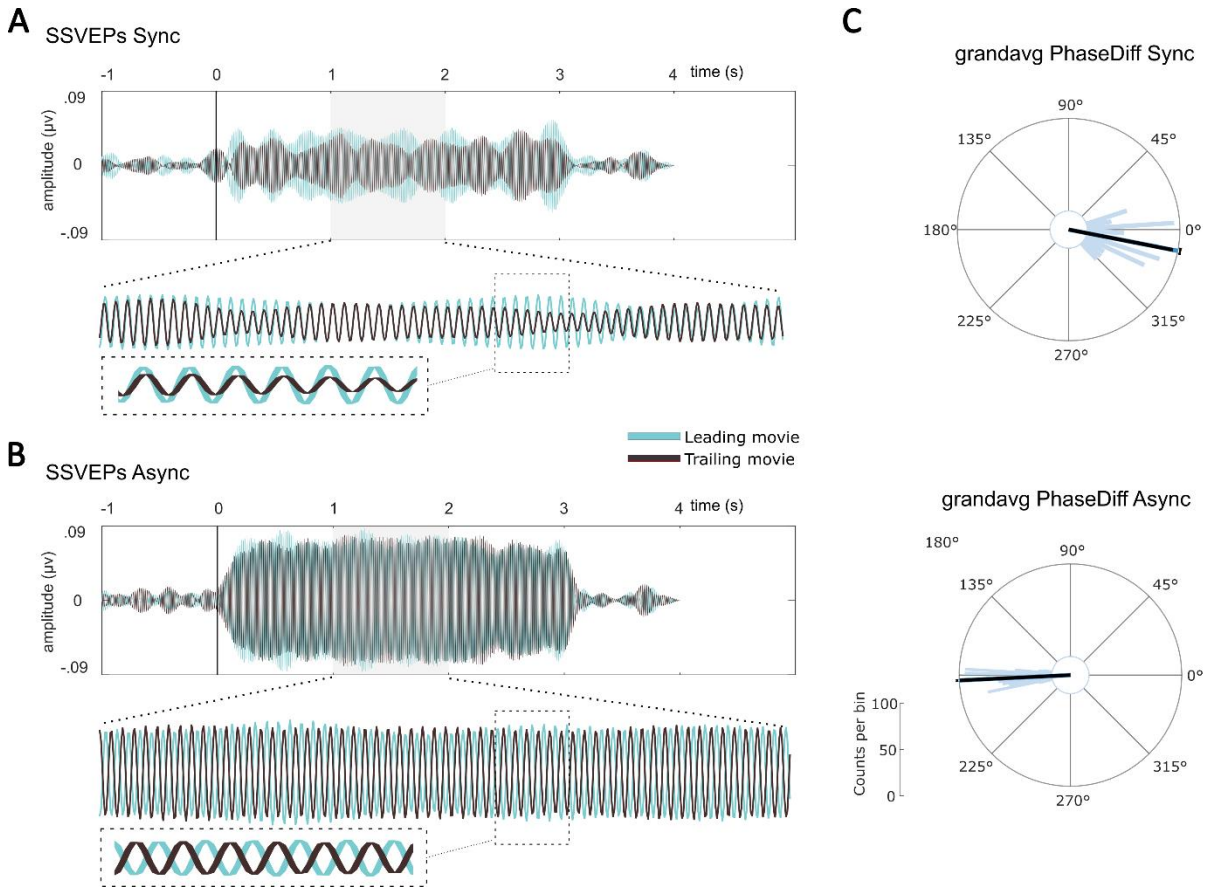

Fig. 3.6. Group SSVEPs and instantaneous phase lag between the leading and trailing movies in the synchrony and asynchrony conditions. SSVEPs band-pass filtered at 60 ± 4 Hz from -1 to 4s for leading (turquoise) and trailing movies (brown) in the synchrony **(A)** and asynchrony **(B)** conditions. **(C)** Instantaneous phase difference between SSVEPs for leading and trailing movies spanning from 1-2s post-stimulus (shaded area in (A) and (B)) was binned in a circular histogram (blue bars). The mean resultant vector of the instantaneous phase difference in the synchrony and asynchrony conditions were represented in black bars (resultant vector lengths were 0.9558 and 0.9938, respectively). The uniformity of phase difference distribution was confirmed by V-test for both conditions.

Illustrating the gamma entrainment further, the grand averaged ITPC across the highlighted electrodes in Figure 3.5A and B exhibited the most pronounced ITPC at 60 Hz for both the LeadRvsf and LeadLvsf conditions (Fig. 3.5D and E, refer to Fig. S7.2 for ITPC in a full epoch window). This specificity of gamma phase entrainment at 60 Hz was further

confirmed by additional analysis (Fig. 3.5F). The ITPC was expected to peak at the contralateral hemifield to the location of leading movies, while remaining low at the ipsilateral hemifield. Accordingly, the anticipated peak of ITPC difference between contralateral and ipsilateral hemifields was confirmed at 60 Hz in the comparison of differences within 40-80 Hz range, corroborated by paired-sample Monte Carlo cluster-based permutation test (Fig. 3.5F; $p_{corrected}$ <0.0001 for the left cluster; $p_{corrected}$ <0.001 for the right cluster).

The inter-hemifield phase lag at 60 Hz was verified by the extraction of instantaneous phase from the reconstructed Steady-State Visual Evoked Potentials (SSVEPs) using rhythmic entrainment source separation (RESS). RESS filter aims to separate rhythmic activity at the frequency of interest (FOI; 60Hz, as the signal covariance matrix, S) from neighbouring activity (60±2 Hz, as the reference covariance matrix, R) by finding the eigenvectors that maximize their difference. The resulting eigenvectors are then multiplied by the original EEG data to reconstruct a single weighted combination of all channels time series. A pivotal prerequisite for RESS reconstruction is to maintain the flickering stimulus location constant across trials. Nevertheless, our study presented movies at both the left and right visual fields, with opposing phase onsets in the asynchrony condition. To ensure the fidelity of the reconstruction, the RESS filters were computed separately for the left and right hemifields. Moreover, the asynchrony condition was further subcategorized into LeadRvsf180 and LeadLvsf180, representing the spatial location of leading movies at the right and left visual field, respectively. As a result, for each participant, there were six RESS filter calculated (synchrony/LeadRvsf180/LeadLvsf180 by left/right hemifield).

For the RESS reconstruction, there was an average of 77 trials (ranging from 55-95) included for synchrony trials, an average of 42 trials (ranging from 31-56) for LeadRvsf180 trials, and an average of 37 trials (ranging from 23-44) for LeadLvsf180 trials.

The reconstructed single-trial data were grouped into four conditions, based on the synchrony/asynchrony condition and whether the entrainment was attributed to the leading or trailing movies. These conditions were synchrony-leading, synchrony-trailing, asynchrony-leading and asynchrony-trailing. Subsequent time-locked analysis showed that in the synchrony condition, the SSVEPs (56-64Hz) of leading and trailing movies were in-phase, while in the asynchrony condition, they exhibited opposing phases (Fig. 3.6 A and B). The V test (Berens, 2009) confirmed that the instantaneous phase lag between 1000-2000 ms aligned with the phase lag conditions (V = 481.221, p = 0 for synchrony; and V =509.1903, p = 0 for asynchrony, Fig. 3.6 C).

3.3.3. Single-trial analysis found improved recognition memory with shortest phase delay

Even though no significant difference in recognition memory performance was observed between the synchrony and asynchrony conditions, we speculated that this could be attributed to the challenges of low SNR in effectively modulating phase lag at single-trial level. To address this, we employed a single-trial phase bin sorting approach based on the previously reconstructed time series using RESS.

Single-trial neural responses at 60 Hz were separately reconstructed for the left and right hemifields (highlighted electrodes in Fig. 3.2 top panel) using RESS. Instantaneous phase extraction followed a similar procedure to the SSVEPs analysis but with a narrower band width of 59-61 Hz. The resulting phase differences, obtained by subtracting the phase entrained by trailing movies from that by leading movies (leading movies – trailing movies), were then sorted into eight distinct phase bins, i.e., 0°-45°, 45°-90°, 90°-135°, 135°-180°, 180°-225°, 225°-270°, 270°-315° and 315°-360°.

In line with the principles of STDP, we hypothesized that recognition performance would exhibit enhancement as the delay between leading movies followed by trailing movies

decreased. With this rationale, we aimed to compare recognition performance between the conditions representing the shortest and the longest delays. In order to ensure the robustness and reliability of the comparisons, we established a criterion of having at least 20 trials in each phase bin condition. The number of trials in each phase bin is available in Fig. S7.4. However, due to the limited number of trials available in the 0°-45° vs. 315°-360° (N=10 out of 23) and the 0°-90° and 270°-360° (N=14) conditions, our subsequent analysis of behavioural performance was restricted to the comparison between the 0°-135° vs. 225°-360° conditions (N=19, Fig. 3.7A). This comparison represented delays of 0-6.25 ms vs. 10.41-16.67 ms. Behavioural responses from the recognition memory test were fitted to the DPSD full model using the ROC toolbox. A one-tailed paired-sample t-test revealed improved recognition memory performance in the 0°-135° condition compared to 225°-360°, as evidenced by a larger AUC ($t_{18} = 2.3406$, $p = 0.0155$; Cohen's d = 0.5542; Fig. 3.7B).

However, it is important to note that this AUC difference did not survive Bonferroni multiple comparison correction ($p_{corrected} = 0.0619$). No difference was found for recollection of oldness ($t_{18} = 0.7215$, $p = 0.23$; Cohen's d = 0.1303), recollection of newness ($t_{18} = -0.9739$, $p = 0.8285$; Cohen's d = -0.2430) or familiarity ($t_{18} = 1.4644$, $p = 0.0802$, Cohen's d = 0.3772). For recollection of oldness, recollection of newness and familiarity, the corrected p-values were 0.9596, 1 and 0.3207, respectively. Nonetheless, both the AUC and familiarity comparisons showed a medium effect size.

Collectively, our study effectively manipulated gamma phase lag at the group level by presenting movies pairs with luminance modulation. However, despite this manipulation, we did not observe any significant impact of this phase lag modulation on immediate implicit memory or recognition memory. However, findings from the analysis of reconstructed single-trial phase bin sorting disclosed a noteworthy trend, i.e., shorter time delays linked to enhanced

recognition memory, aligning with the function of STDP. Nevertheless, it is worth noting that this observed advantage in memory performance did not withstand correction for multiple comparisons.

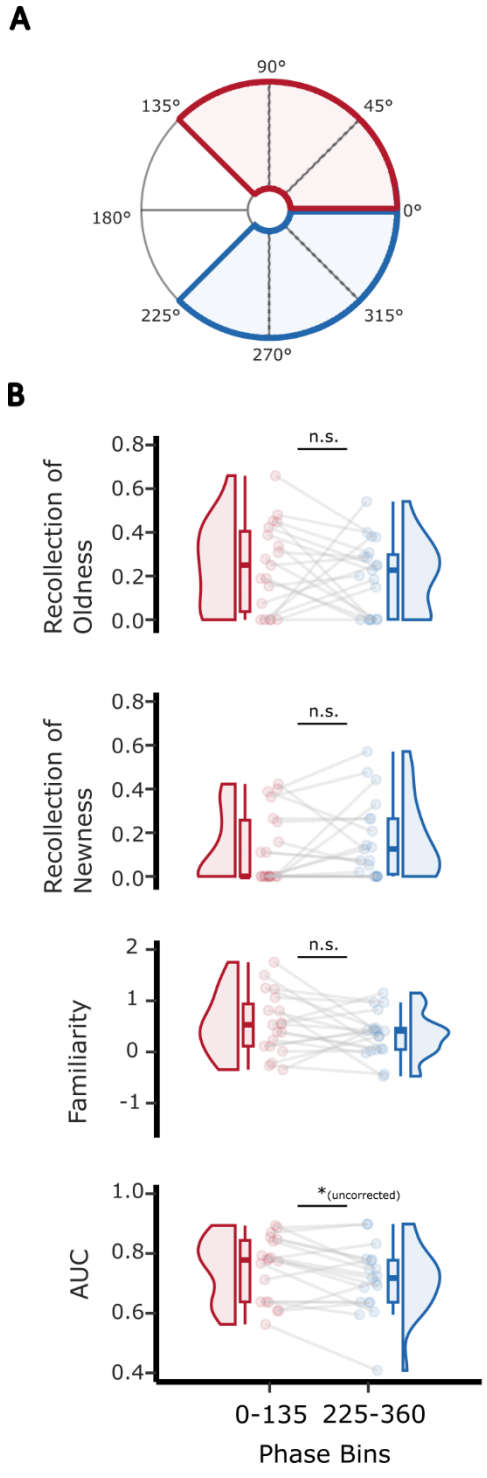

Fig. 3.7. Single trial phase bin sorting and behavioural performance fitted in ROC. (A) The single-trial instantaneous phase differences between leading and trailing movies, reconstructed using RESS, were categorized into eight distinct phase bins: 0°-45°, 45°-90°, 90°-135°, 135°-180°, 180°-225°, 225°-270°, 270°-315° and 315°-360°. To ensure a comparison of memory performance between conditions with the shortest and longest phase lags, while maintaining a balanced inclusion of sufficient trials, the phase bins of 0°-135° and 225°-360° were contrasted. **(B)** A notable enhancement in recognition memory performance was observed in the 0°-135° condition when contrasted with the 225°-360° condition, as evidenced by a notably larger AUC. There were no discernible differences found in terms of recollection of oldness, recollection of newness or familiarity. However, the difference in AUC did no remain significant after multiple comparison correction.

3.4. Discussion

Spike timing dependent plasticity (STDP) plays a pivotal role in neural communications and plasticity between assemblies (Debanne & Inglebert, 2023; Juergen Fell & Axmacher, 2011). The efficiency and direction of synaptic plasticity depend on the activation time delay between pre- and postsynaptic neurons. Operating within a very narrow time window, even within this range, the efficiency of synaptic modification drops dramatically with increased delay (Bi & Poo, 1998; Cassenaer & Laurent, 2007; Fu et al., 2002; Meliza & Dan, 2006; Yao & Dan, 2001). Despite being observed across various species and brain regions (Bi & Poo, 1998; Cassenaer & Laurent, 2007; Meliza & Dan, 2006; Testa-Silva et al., 2010; Verhoog et al., 2013; Wolters et al., 2003; Yao & Dan, 2001; Zhang et al., 1998), evidence supporting for STDP in human episodic memory is limited. To bridge this gap, we employed fast gamma rhythmic sensory stimulation (RSS) during the encoding phase to explore the potential impact of inter-hemifield time delay on implicit and recognition memory. This manipulation seeks to simulate the long-term potentiation (LTP) window of spike timing-dependent plasticity. Results revealed a lack of implicit associative memory in the context of the blurred image identification task. In contrast, a noteworthy enhancement in overall memory performance is evident in the condition with the shortest time delay, indicated by the area under the curve (AUC). This finding aligns with the function of STDP that predicts declined synaptic modification with long delays.

Our study shed light on the potential of high frequency RSS to manipulate inter-hemifield evoked gamma phase lag and its impact on memory performance. However, it is important to approach the results with caution due to the lack of significance after multiple comparisons correction and the challenges posed by low signal-to-noise ratio (SNR) in high frequency stimulation and analysis. In the following sections, we discuss findings related to

methodological enhancements, the feasibility of using high frequency RSS to investigate deep structures, and potential explanations for the memory enhancement observed in our study.

The improved SNR, facilitated by accessing single-trial phase lag through reconstructed time series using the rhythmic entrainment source separation (RESS) method, enabled us to observe the memory enhancement. Yet, this enhancement trended towards significance after multiple comparisons correction. This may be attributed to the small sample size and low SNR in RESS reconstruction for high frequencies. To address this, future studies could implement a single-source stimulation session to enhance spatial localization of activity at the flickering frequency, potentially improving SNR for high frequency RESS time series reconstruction.

During the implicit memory task, participants swiftly identified the content of the unscrambling images presented alongside leading movies. However, observed reaction time exceeded our initial expectations, potentially due to the slow progression of unscrambling (Fig. S7.1). This prolonged progression might diminish the sensitivity required to detect implicit associative memory. In addition, the consolidation-dependent nature of implicit associative memory (Tompary & Davachi, 2022) suggests that immediate testing might be unsuitable to capture its effects.

The enhanced recall performance cannot be simply attributed to the use of fast gamma for the rhythmic visual stimulation, especially when contrasted with the previous experiment using slow gamma (37.5 Hz) in chapter 2. It likely arises from differences in methodology between the two experiments. The previous chapter directly tested associative memory using three accompanying lure pictures, while the current experiment employed a recognition memory test that incorporates both explicit recollection and inherently implicit familiarity, which aligns with the dual process theory (Yonelinas, 1999; 2002). Additionally, the RESS method was inapplicable in the previous chapter due to limited trials caused by doubled

conditions. Hence, the enhanced SNR for single-trial analysis in the current study could contribute to the observed differences. Interestingly, recent research involving multisensory RSS presented contrasting findings. Wang and colleagues (2023) detected enhanced associative memory in the shortest delay condition using the same slow gamma (37.5 Hz) frequency stimulation. Despite their larger sample size (around 50), achieving statistical significance in our chapter 2 experiment that requires 219 participants indicates the influence of other factors.

Stimulus complexity and multisensory engagement emerge as likely candidates for these different outcomes. Recent studies indicate a distinct favourable effect in the medial prefrontal cortex (mPFC) during multisensory stimulation compared to unimodal stimulation (Martorell et al., 2019). Human studies also revealed the modulatory impact of multisensory stimulation on behaviour (Drijvers et al., 2021; Chan et al., 2021).

Regarding the hypothesis that unimodal associations may not involve the hippocampus, as mentioned in the introduction, our results challenge this assumption. Instead of indicating hippocampus-independent familiarity, we observed enhanced general memory. However, it remains uncertain whether the hippocampus is driven by the 60 Hz rhythmic visual stimulation, leading to enhanced memory, hindered by the low spatial resolution of scalp EEG recordings.

On one hand, recent findings suggested limited propagation of RSS to downstream structures. Drifting gratings-induced endogenous gamma remains unaffected by high frequency visual flickers, suggesting distinct mechanisms governing induced gamma and flicker-evoked gamma (Duecker et al., 2021). Additionally, 40 Hz LED light stimulation predominantly activates V1 fast spiking parvalbumin-positive (FS-PV+) interneurons (Schneider et al., 2023), which is inhibitory in nature and is sufficient to generate gamma oscillations (Cardin et al., 2009). In contrast to the active engagement of FS-PV+, Schneider and colleagues (2023) noted

weak phase-locking of excitatory spikes to rhythmic stimulation, implying a suppression of information feedforward. This was validated by weak propagation from input layer 4 to layer 2/3 (Schneider et al., 2023). Recent studies also detected no evidence of propagation in the hippocampal CA1 (Schneider et al., 2023; Soula et al., 2023), suggesting challenges in using high frequency RSS to investigate deep structures and in developing RSS-based treatments for degenerative diseases.

On the other hand, optogenetic-driven FS-PV+ in CA1 demonstrated attenuation of degenerative disease-related biomarker (Iaccarino et al., 2016). Importantly, akin results were produced by high frequency RSS (Adaikkan et al., 2019; Martorell et al., 2019), suggesting shared mechanisms between CA1 and V1 involving FS-PV. Noticeably, these studies detected gamma entrainment in somatosensory cortex, hippocampal CA1 and prefrontal cortex, indicating propagation beyond the primary visual cortex. It is suspected that the observed entrainment in deep structures might be influenced by volume conduction in the measurement of LFP (local field potential) -LFP coherence.

To be noticed, there is a distinction between the current study and the above-mentioned research regarding stimulus. In our study, the high frequency RSS was delivered with natural scenes, rich in information that potentially engaged more excitatory responses. In contrast, studies involving simple graphical stimulus or light pulses might primarily activated fast spiking interneurons. This is supported by a study involving pairing whisker stimulation across different evoked gamma phases (Cardin et al., 2009). When presented with rhythmic light only, FS-PV+ interneurons drove gamma oscillations while suppressing excitatory responses. However, when paired with whisker stimulation, excitatory responses regarding amplitude and spike timing precision were modulated by the evoked gamma phases. This underscores the role of interneurons in gating inputs and constraining the optimal window for relevant inputs, thus

might facilitate the feedforward process. Collectively, these mechanisms offer plausible but unexplored insights into using high frequency RSS combined with complex stimuli to generate dynamics of STDP and investigate the impacts on downstream assemblies. Similarly, it raises the possibility to use high frequency RSS to track the dynamics of feedforward and feedback process. In addition, future experiments may also consider the influence of the timing relation between the rhythmic flickers and complex stimulus. Nevertheless, it remains an open question whether the hippocampus is entrained due to the methodology limitation in nature.

In summary, this study demonstrates the behavioural modulation on overall memory performance by manipulating the inter-hemifield gamma phase at 60 Hz, which aims to simulate STDP as a function of the time delay (phase lag) in human episodic memory. Via high frequency RSS embedded with natural stimulus, relative timing of inter-hemifield excitatory response may be regulated by the engagement of local fast spiking neurons. Further inquiries into the cellular and molecular mechanisms that underlie high frequency RSS when coupled with complex stimuli provides invaluable insights of its application in both research and clinical domains.

Interim Conclusion

Despite existing evidence indicating that high frequency RSS primarily targets inhibitory interneurons, Chapter 2 and 3 demonstrated the effectiveness of regulating brain activity by delivering rhythmic stimulation via movies. Notably, Chapter 3 observed a tendency to modulate memory performance, although this did not withstand correction of multiple comparisons. In contrast to the mechanism underlying high frequency RSS, low frequency RSS predominantly recruits pyramidal neurons and involves long-distance communications. The subsequent chapter focuses on the relationship between low frequency RSS, beta oscillations and motor performance.

CHAPTER 4: Beta bursts correlate with synchronization of movements to rhythmic sounds

Accumulating evidence indicates transient beta bursts play an important role in the representation of temporal information and prediction. However, the role of beta bursts in sensorimotor synchronization (SMS) involving active interactions between motor and sensory systems to synchronize predictive movements to periodic events remains unclear. To answer this question, 15 participants were invited to complete a finger-tapping task whilst high-density EEG (128 channels) was recorded. Participants tapped with their right index finger in synchrony with 1 Hz and 0.5 Hz tone trains. In line with previous findings, we found a negative mean asynchrony between tone and tap time, i.e., taps preceded tones for both tone frequencies (1 and 0.5 Hz). In the EEG data, beta bursts were detected and their timing in relationship with tapping and auditory tracking was examined. Results revealed that beta bursts tracked tapping and were modulated by the low frequency phase of the tone frequency (i.e., 1 Hz or 0.5 Hz). Importantly, the locking of beta bursts to the phase of auditory tracking correlated with the behavioural variance on a single trial level that occurred while tapping to the tones. These results demonstrate a critical role for an interplay between beta bursts and low frequency phase in coordinating rhythmic behaviour. ♣

♣ *Published in:*

Chen, Q., McAllister, C. J., Elliott, M. T., Shapiro, K. L., & Hanslmayr, S. (2023). Beta bursts correlate with synchronization of movements to rhythmic sounds. *bioRxiv*, 2023-03.

And in preparation for:

Chen, Q., McAllister, C. J., Elliott, M. T., Shapiro, K. L., & Hanslmayr, S. (in preparation). Beta bursts correlate with synchronization of movements to rhythmic sounds.

4.1. Introduction

Sensorimotor synchronization (SMS), defined as the coordination of movement to external periodic events (Pressing, 1999; Repp, 2005; Repp & Su, 2013), is argued to play an important role in the evolution of music and even of language (Merker, 2000; Colling et al., 2017; Fujii & Wan, 2014; Park et al., 2016). Predictable rhythms optimize rhythmic movement. This improvement in behaviour cannot be explained by a reduction in reaction time but instead is a reflection of predictive timing, as the time gap between movement and auditory stimuli is shorter than the fastest reaction time (Repp, 2005; Repp & Su, 2013). Finger-tapping to an isochronous auditory metronome is amongst the most popular paradigms to investigate SMS because of their simplicity. These tasks usually show that the tap occurs before the tone, often referred to as negative mean asynchrony (NMA; Repp, 2005; Repp & Su, 2013). Moreover, synchronising movements to auditory cues has been applied in motor therapies for movement disorders caused by stroke and cerebral palsy (Thaut et al., 1997; Wright et al., 2014; Wright et al., 2017). However, how the sensory and motor systems interact, and support SMS with temporal predictions, remains uncertain.

Sensory entrainment occurs when ongoing brain oscillations in the stimulated region adapt to the phase of sensory rhythmic stimuli (Hanslmayr et al., 2019; Lakatos et al., 2008, 2019; Wang et al., 2018; Chen et al., 2021). Sensory entrainment has been proposed to coordinate temporal predictions by temporally modulating the excitability of relevant neural assemblies, thus optimizing perceptual analysis of periodic stimuli (Schroeder & Lakatos, 2009; Large & Jones, 1999; Stefanics et al., 2010; Cravo et al., 2011; but see Breska & Deouell, 2017).

Besides its role in temporal prediction, entrainment was observed to facilitate movement (but see Morillon et al., 2016 and Cope et al., 2012 for dissociating the role of periodic stimuli in temporal prediction), especially in the auditory domain (Arnal, 2012; Arnal & Giraud, 2012;

Lakatos et al., 2019; Schroeder & Lakatos, 2009). Auditory entrainment may improve movements by affecting the motor system. Passive listening studies confirmed this assertion by observing that the motor system, which serves as a core network that supports timing and time perception, is involved in beat and rhythm processing (Fujioka et al., 2012; Grahn & Brett, 2007; Morillon & Baillet, 2017). Evidence from studies involving rhythmic movements, however, suggests an opposite direction of influence, where overt movements enhance the perception and precise temporal anticipation of upcoming auditory stimuli (Morillon et al., 2014; Morillon & Baillet, 2017). Critically, SMS has been shown to be associated with bursts of beta oscillations (18-24 Hz) directed to the auditory system from the left sensorimotor cortex in a functional connectivity study (Morillon & Baillet, 2017). Together with the enhancement from entrainment, these findings collectively suggest that the auditory and motor systems actively interact during auditory-cued tasks involving SMS.

Although the timing of beta bursts correlates with reaction time (Little et al., 2019), it is unclear whether it plays a role in the coordination between auditory and motor systems during SMS. To answer this question, we tested whether the timing of beta bursts phase-locked to the auditory stimulation frequency reflects functional coordination between auditory and motor systems in SMS. The relationship between beta bursts and movement timing and auditory tracking was examined in an EEG study while participants performed a finger tapping task. The term entrainment has recently been hotly debated because it assumes the interaction between a physiologically meaningful brain rhythm with an externally presented rhythm which is difficult to establish (Capilla et al., 2011; Hanslmayr et al., 2019; Helfrich et al., 2019). Therefore, we here prefer the term tracking over entrainment to simply denote the locking of brain activity to an external auditory rhythm, thus being agnostic about the underlying neural mechanisms that give rise to that phase locking.

4.2. Methods

4.2.1. Participants

Fifteen healthy participants were recruited (mean age = 21.07; age range = 18-32; five males; all right-handed) and completed the experiment, whereas three were excluded because of a failure to be able to define the frequency of interest for beta burst detection (see below). This left twelve participants reported in all data analysis (mean age = 21.08; age range = 18-32; three males). All participants were compensated with £8 per hour. Ethical approval (ERN14-0950) was obtained from the Research Ethics Committee at the University of Birmingham.

4.2.2. Experimental design and procedure

Metronome beats were presented isochronously in two frequency conditions. One contained 60 tones per trial at 1 Hz and the number of tones was 30 in the other condition at 0.5 Hz. These two conditions corresponded to an interonset interval (IOI) of 1 and 2 seconds, respectively (Fig. 4.1). Hence, they are designated as IOI1 and IOI2 in descriptions of later sessions for convenience. For the same purpose, trials locked to each tap/tone were assigned as *tap/tone trials*, while trials locked to the first tone in a stimulus train were referred to as *trials*.

The experiment comprised 60 trials, with 30 of IOI1 and 30 of IOI2. To ensure participants were able to maintain attention, the 60 trials were presented equally in six blocks, with each containing five trials of IOI1 and five trials of IOI2, with a short rest in between blocks. Trials within each block were randomized. Each trial started with a 15s rest period which was used as a baseline for EEG analysis.

Before the experiment, participants were seated in an EEG testing room and instructed to complete an EEG screening form. After the acquisition of consent, preparation of EEG capping and task briefing, participants were seated in a comfortable position with their right

hand in a pronated position resting on a wooden pad incorporating a force sensor. Auditory stimuli were delivered through a regular closed back headphone (Sennheiser, Germany). Participants were instructed to tap onto the force sensor with their right index finger in synchrony with the tones. Finger taps and timing of tones were recorded using a National Instruments data acquisition card (DAQ) controlled by the MatTAP toolbox (Elliott et al., 2009) in a MATLAB environment (The MathWorks, Inc., Natick, MA, USA). At the end of experiments, 3D geometric locations of each electrode were recorded by a Polhemus FASTRAK device (Colchester, Vermont, USA) and Brainstorm (Tadel_2011) in MATLAB.

4.2.3. Data analysis

4.2.3.1. Behavioural analysis

Descriptive statistics, including mean and standard deviation of the asynchrony between each tap and corresponding tone time (tone minus tap time) were calculated by in-house scripts written in MATLAB (R2018a; The MathWorks, Inc., Natick, MA, USA). This analysis was implemented for IOI1 and IOI2 separately. To evaluate the evolution of adaptation during trials, the asynchrony was first averaged across tap/tone trials at the same time position of a trial for each participant. The group mean was calculated by averaging resulting asynchrony dynamics across participants.

4.2.3.2. EEG acquisition and preprocessing

EEG data was recorded with a 128-channel BioSemi ActiveTwo system. Three extra electrodes were placed at 1 centimetre to the left and right from the lateral canthus, and 1 centimetre below the left eye. Online data were sampled at 2048 Hz via the BioSemi ActiView software.

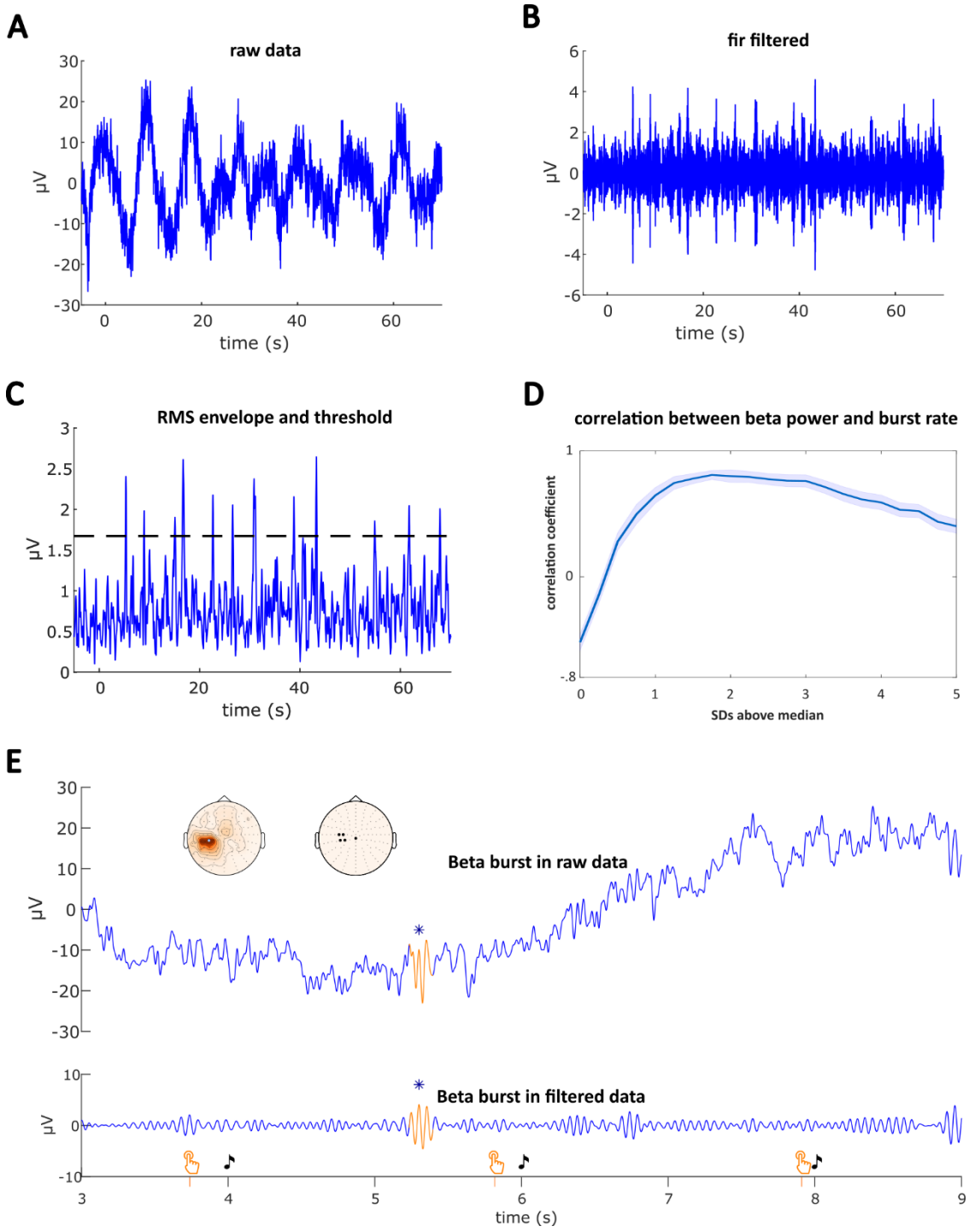

The preprocessing and analysis of EEG data was conducted in the Fieldtrip toolbox (Oostenveld et al., 2011) in MATLAB. EEG data was first epoched to the first tone of each trial, with 5 s before and 70 s after the onset. The epoched trials were then filtered with a low

Fig. 4.1. Procedure of algorithm Detection. (A) One trial of raw data locked at the first tone of a train. **(B)** Bandpass filtered of the trial with band width of ± 3 Hz centred at individual frequency of interest (18.64 Hz in this example). **(C)** The root mean square (RMS) of the filtered signal. Activity remains above the threshold (the dash line) for 0.1 to 0.5 second were detected as beta burst events. **(D)** The correlation between burst rate and beta power peaked at 1.75 SD above the median of the RMS envelope. **(E)** A detected beta burst event (orange) showed in a zoomed in window from three to nine seconds in the same trial. The orange finger tapping signs denote tap time, while the music notes sign tone onset time. The maximum peak of a detected beta burst was marked by star, both for raw data (upper panel) and filtered data (lower panel). The left topography illustrated the curve fitting resulted ROI for this example, and the right topography demonstrated the ROIs for all participants. Overlapping ROIs were represented by a single dot; one ROI was in electrode A2, two ROIs were in D18, three ROIs were in D17, D19, D28, respectively (128 channel Biosemi layout).

pass filter of 40 Hz, and a high pass filter of 0.1 Hz. The sampling rate was reduced to 500 Hz before ICA (independent component analysis), followed by manual rejection of noisy channels and trials. ICA components indicating cardiac activity and eye movements were removed. Next, channel interpolation implemented triangulation of the nearest neighbours by calculating the individually recorded electrode locations. Finally, data were re-referenced to the average, and trials with artefacts were rejected by manual inspection.

4.2.3.3. Beta burst detection

Defining parameters for burst detection

Before applying the algorithm for beta burst detection, the frequency of interest (FOI) and channel of interest were defined for each participant. To this end, EEG data locked to the tap after pre-processing was first resampled to 250Hz, in the time interval 1 s before and after the tap onset. Then, baseline corrected ('relchange', relative change to mean power) power was calculated using wavelet time frequency transformation based on convolution in the time domain, from 1 to 30 Hz in steps of 0.5 Hz with a time resolution of 50 ms at each channel. The

FOI for beta burst detection was determined as the frequency in the beta band that was primarily modulated by the tone/tapping rate. Hence, the resulting baseline corrected power data from the previous step was fit to a sine wave at the auditory stimuli rate using the *fit* function in the Curve Fitting Toolbox in MATLAB (R2018a; The MathWorks, Inc., Natick, MA, USA). Specifically, fitting was performed from 10 to 30 Hz (from 15-30 Hz for two participants because of a strong alpha peak at 10-11 Hz) in steps of 0.5 Hz at each channel. Frequencies with max absolute amplitude from the resulting fits were recorded for each channel and scale parameters were then compared across channels within participants. Three out of fifteen participants were excluded from further analysis because their fitting results yielded no peak in both IOI conditions, i.e., three out of fifteen participants failed to show a peak at the beta frequency, while 11 participants showed similar peaks for both IOI conditions. Lastly, one participant showed a peak in the IOI2 condition but failed in the IOI1 condition. Given the above, the FOI for algorithm detection was centred (± 3 Hz) at the frequency with the channel which contained the largest fitting scale in the IOI2 condition. In addition, this channel served as region of interest (ROI) in the later calculation for detection of beta bursts (Fig. 4.1E, the left topography showed the ROI for the example; the right topography showed the ROI for all participants, overlapping ROIs were represented by single dot; one ROI was in electrode A2, two ROIs were in D18, three ROIs were in D17, D19, D28, respectively; labels were defined from the 128 channel Biosemi layout, see https://www.biosemi.com/pics/cap_128_layout_medium.jpg).

Algorithm for beta burst detection

The detection of beta bursts was based on an established algorithm for detecting fast and slow spindles (Molle et al., 2002; Mölle et al., 2011; Staresina et al., 2015). The algorithm was applied to the trial segmented EEG data starting 5 s before and ending 70 s after the onset of the first tone of a train (see Fig. 4.1A for an example of raw data). First, trials were filtered with a bandpass filter (FIR filter) of ± 3 Hz centred at the FOI (18.64 Hz in this example, mean

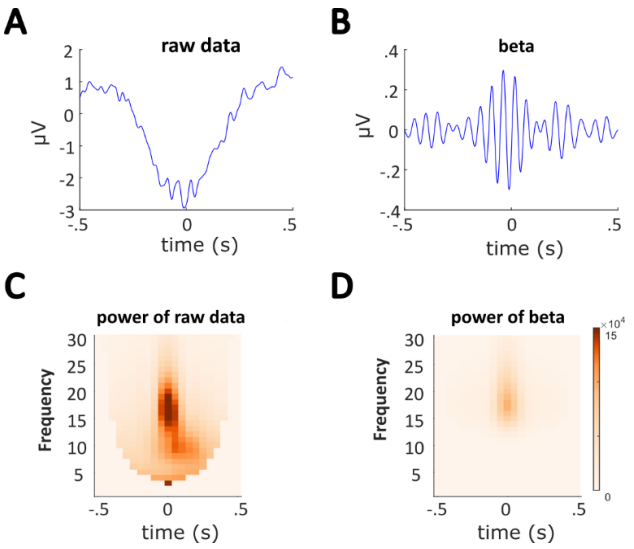

Fig. 4.2. An example of detected beta burst events. Data was incorporating IOI1 and IOI2 conditions and centred at beta burst max time. **(A)** ERPs of Raw data of the detected beta burst events for one subject. Time zero indicates beta burst max time. **(B)** FIR bandpass filtered raw data of ± 3 Hz centred at individual frequency of interest (18.64 Hz). **(C)** Time frequency representation of power of raw data (A) from 1-30 Hz revealed a peak at beta range. **(D)** Time frequency representation of FIR filtered data (B).

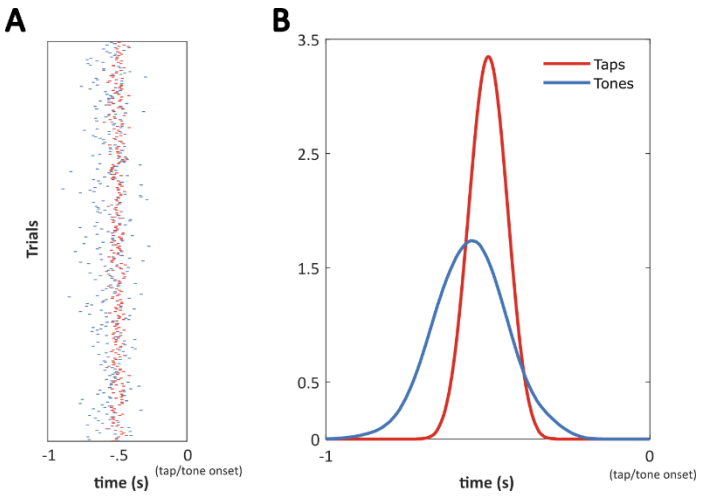

Fig. 4.3. Simulated beta burst events relative to taps/tones time in IOI1. Time stamps of detected beta burst events (max time) locked to taps/tones time were recorded for each subject. **(A)** Distribution of beta burst time stamps across trials locked to taps (red) and tones (blue) time. The example illustrates a case where beta bursts are more closely locked to the taps, than tones. **(B)** Density plot resulting from convolution between Beta burst counts and a gaussian window for taps/tones onset, illustrating higher variance for the tones compared to taps.

FOI is 19.36 Hz) calculated in the above section (Fig. 4.1B). To prepare the data for burst detection, the root mean square (RMS) of the filtered signal was calculated (Fig. 4.1C) and smoothed with a moving average of 200 ms. The threshold for burst detection was data driven by finding the maximum correlation between beta burst rate (counts of beta burst) and baseline corrected beta power locked at taps. The correlations were acquired at steps of .25 standard deviations (SD) from 0 to 5 SD (above median), at single trial level and then averaged across participants (Fig. 4.1D). The resulted maximum correlation was 1.75 SD above the median of filtered signal envelope and was set as the threshold. Events were defined as time points where the resulting RMS signal remained above threshold for 0.1 to 0.5 seconds. For each event, maxima and minima were calculated as peaks and troughs, while the highest peak was designated as the beta burst time (max time). An example of detected beta burst events is demonstrated in Fig. 4.2.

4.2.3.4. Comparing beta burst timing to taps vs. tones

To explore the relationship between the timing of beta bursts, taps and tones, the timing of beta burst events relative to the tap or tone was calculated separately. First, a time stamp was recorded for the last detected beta burst event that fell within the 1-second window (for IOI1 and 2 seconds for IOI2) before a tap, or a tone, respectively. In other words, when two bursts were detected within the time window before a tap (or a tone), only the last one was counted. A simulated example is illustrated in Fig. 4.3, which shows time stamps of beta bursts relative to the taps and tone onset time at IOI1. This example illustrates the distribution of beta bursts when they are more locked to the tap, as opposed to the tone time. Next, the standard deviation of the time information aligned to tap/tone was statistically compared between locking to the tap and tone condition using a paired samples t-test. Standard deviation was used as a measure of the distribution of beta burst activity in relation to tap and tone onset, with a lower standard

deviation indicating a stronger relationship between beta burst timing to either taps or tones. Additionally, we also carried out a similar analysis taking all beta bursts within 1 second (for IOI1 and two second for IOI2) before a tap, or a tone.

4.2.3.5. ITPC analysis for auditory tracking

After the confirmation that beta bursts track movements (see results 3.2), we aimed to measure neural response tracking of the auditory stimulus. For this purpose, we compared the tone-tap difference in ITPC (inter-trial phase coherence, a measure of the uniformity of phase angles across trials) between the first and last tap/tone trials. During the first few tap/tone trials, as participants were unaware of the stimulation frequency and were still learning the rhythm, the timing of taps varied greatly, although it rapidly improved within three tap/tone trials on average (see Fig. 4.4B). As revealed by previous findings that phase at low frequencies tracks auditory entrainment (Calderone et al., 2014; Lakatos et al., 2008, 2013; Morillon & Baillet, 2017; Stefanics et al., 2010), phase locking to the tones is predicted to be stronger than that to the taps in the first few tap/tone trials. However, since the taps in the last few tap/tone trials were well timed to the tones, a similar amount of phase locking should be obtained for taps and tones as they essentially became the same event. Hence, a comparison of the tone minus tap ITPC difference (tone-tap ITPC difference) between the first and last five tap/tone trials was taken to reflect auditory tracking. It was expected that the tone-tap ITPC difference would be greater in the first five tap/tone trials than that in the last five tap/tone trials. By contrasting the tone-tap ITPC difference between the first and last five tap/tone trials, this measure theoretically reflects the effect of auditory tracking for the first five tap/tone trials. The number of trials selected was a balance between a quick behavioural adaption found in SMS (see Fig. 4.4B) and the number of trials needed to establish tracking.

Preprocessed EEG data was downsampled to 250 Hz and epoched to tap/tone time 10 s before and after onset for the IOI1/IOI2 condition, respectively. Only trials with taps were included in this analysis. In other words, tap/tone trials where subjects missed the tone were excluded. ITPC values for the four conditions (first tones, first taps, last tones, and last taps) were computed by the following procedure individually for IOI1 and IOI2. Complex Fourier-spectra implementing a three-cycle Morlet wavelet time frequency transformation was computed with a moving window of 100 ms (FOI was 0.2 to 1.6 Hz in steps of 0.2 Hz for IOI1 and 0.1 to 1 Hz in steps of 0.1 Hz for IOI2). Next, the resulting complex Fourier-spectra were divided by their amplitude for the calculation of phase angles, which was then summed across trials. This sum of phase angles was then divided by the number of trials to generate ITPC values for each channel. The following analysis used a time window of 2 s centred at tap/tone onset at IOI1 (FOI 1 Hz) and 4 s in IOI2 (FOI 0.5 Hz). For each participant, ITPC locked to first five taps was subtracted from those locked to the first five tones, with this process repeated for the last five taps and tones, resulting in tone-tap differences for the first and last tap/tone. To measure auditory tracking, the difference between the first and last differences at group level was assessed by a one tailed (alpha = 0.01) paired samples cluster-based permutation test (Maris & Oostenveld, 2007) with 2000 randomizations across the time window preselected for IOI1 and IOI2. The significance probability was estimated by the Monte Carlo method.

Phase locking to rhythmic sensory events could be due to entrainment, i.e. locking of a neurophysiological oscillation to an external rhythmic stimulus (Meyer et al., 2020), or it could be due to stimulation artefacts, neural resonance (Helfrich et al., 2019), or superposition of transient event-related potentials (ERPs, Capilla et al., 2011). We explored this issue by measuring entrainment echoes, where phase locking outlasts for several cycles after the termination of a rhythmic stimulus (Hanslmayr et al., 2019). As each trial begins with a 15-

second break, this allows enough time for the measurement of echoes. ITPC was calculated 15 seconds before and after the last tone onset across trials for each participant. A three-cycle Morlet wavelet was used to extract phase information from 0.1 to 2 Hz, in steps of 0.1 Hz, with 100 ms time resolution. If entrainment occurs, we expected to observe stronger post-stimulus ITPC at the stimulation frequency comparing to other frequencies. In other words, in IOI1, ITPC at 1 Hz would be stronger than that at 0.5 Hz and vice versa for IOI2. Therefore, a two-way repeated measures ANOVA was carried out to explore the interaction effect between the stimulation frequency conditions (IOI1/IOI2) and the tested frequency (1 Hz/0.5 Hz). A significant interaction effect would be supportive of entrainment. To avoid interference from temporal smearing of the filters applied and the offset effect from the last tone, the time window used for statistical analysis was one to four seconds after the last tone onset for IOI1 and one to seven seconds for IOI2. The selection of time windows of interest allows an observation of three cycles at the FOI.

4.2.3.6. Calculation of PPC aligned to motor beta burst

Following the identification of neural responses to taps (motor system) and tones (auditory system, see results), it is critical to examine whether there is an interaction between the two systems. To investigate the relationship between motor beta burst timing (max time) and the stimulation frequency (1/0.5 Hz), pairwise phase consistency (PPC) locked to beta burst timing was measured. PPC was preferred over ITPC because it is bias-free with respect to the number of trials and thus allows comparisons between conditions with different numbers of observations (i.e. beta bursts in our case)(Vinck et al., 2010). Preprocessed EEG data with a time window of 14 s, centred at beta burst time for both IOI conditions, were prepared for the computation of PPC. Only the last beta bursts locked to a tap or a tone within 1 second for IOI1 and 2 seconds for IOI2 were included. Phase information was extracted by a three-cycle Morlet

wavelet time frequency transformation with a moving window of 100 ms and frequency resolution of 0.1 Hz from 0.1 Hz to 2 Hz and PPC was calculated following the procedure from Vinck et al. (2010). Channel ROIs were selected as the five channels of maximum PPC value averaged across IOI conditions, centred at the beta burst in a time window of 1 second for IOI1 and 2 second for IOI2. Thereafter, a repeated measures ANOVA analysis was carried out to investigate the interaction effect of the IOI condition and the frequency measured (at 1 Hz/0.5 Hz) on PPC. It was expected that the PPC was not only enhanced universally at low frequencies but also affected by the tone frequency (i.e., 1 Hz vs 0.5 Hz), by showing a significant interaction where PPC at the measured frequencies is higher when the measured frequency matches the IOI frequency.

4.2.3.7. Measuring PPC contrast between high vs. low variance conditions

As the analysis above indicated an interaction between motor and auditory systems (refer to results 4.3.4), our interest moved to whether such interaction accounts for behavioural differences. Although in finger-tapping tasks, participants often tap before the tone onset, where the time gap is termed NMA (negative mean asynchrony), this gap narrows with training (Repp, 2005; Repp & Su, 2013). Critically, NMA only provides information at the average level, while a large portion of trials (17.67% for IOI1 and 23.25% IOI2) reveals positive asynchrony in our data. This, importantly, could still be interpreted as anticipatory response as it is shorter than the fastest reaction time (Repp, 2005; Repp & Su, 2013). Therefore, to account for the positive asynchrony, we used the absolute value of the asynchrony as a measure of behavioural variance. Tap/tone trials were divided into low and high variance conditions depending on whether the absolute asynchrony was below or above the median for each participant. The exact scheme of PPC calculation from the above section was applied to the low and high variance conditions, respectively. PPC at the stimulation frequency depending on IOI condition (1 Hz and 0.5 Hz

was measured for IOI1 and IOI2, respectively) were statistically compared between low and high asynchrony conditions with repeated measures ANOVA.

4.2.4. Data and code availability

The pre-processed EEG data and the code used to generate the results reported in this manuscript can be downloaded from

https://osf.io/ancqm/?view_only=3099faaab84e4713828991a104801259

4.3. Results

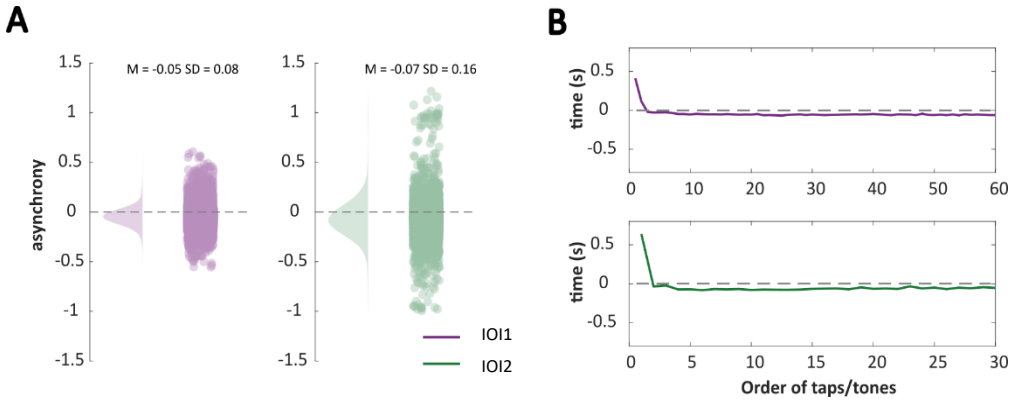

Fig. 4.4. Behavioural asynchrony. The asynchrony performance was calculated by tap minus tone time. Asynchrony of 0 as a baseline was denoted by a dash line. **(A)** Both IOI1 and IOI2 observed a negative mean asynchrony across all subjects (M = -.0459, SD = .0793 for IOI1; and M = -.0693, SD = .1646 for IOI2). Each dot represents one difference between a tone and a tap. **(B)** Time course of asynchrony between tap and tone averaged across trials for IOI1 (60 taps/tones, upper panel) and IOI2 (30 taps/tones, lower panel). The first two taps/tones in the train showed a positive mean asynchrony, but it rapidly declined and stabilized around a negative value for both IOI1 and IOI2.

4.3.1. Behavioral results

Three out of fifteen participants were excluded from further analysis because their fitting results yielded no peak in both IOI conditions at the preparation of beta burst detection, i.e., three out of fifteen participants failed to show a peak at the beta frequency. This left 12 participants in the following analysis. The asynchrony calculated by tone minus tap time

revealed a negative mean asynchrony (Fig. 4.3A) for both IOI1 (M = -.0459, SD = .0793, N = 13068, unit in second) and IOI2 (M = -.0693, SD = .1646, N = 6513). There was less asynchrony variance in IOI1 compared with IOI2. In 17.67% and 23.25% of tap/tone trials we observed positive asynchrony in IOI1 and IOI2, respectively. The asynchrony declined quickly within trials (i.e., a series of 60/30 taps for IOI1 and IOI2 respectively), indicating rapid adaptation to the entraining frequency, despite participants being unaware of the IOI condition. Noticeably, this rapid adaptation occurs within only three taps/tone iterations on average (Fig. 4.4B).

4.3.2. Beta burst is stronger locked to taps than tones

After EEG preprocessing, a mean number of 39 (from 24 to 56) trials remained for later analysis. IOI1 and IOI2 contained a same average number of trials (19, both ranging from 11 to 29). There was an average of 263 (from 68 to 376) beta burst events locked to tones detected in IOI1 and 268 (from 133 to 479) events in IOI2. For beta burst events locked to taps, this number is 263 (from 66 to 377) in IOI1 and 268 (from 135 to 478) in IOI2. There is no difference regarding the number of beta bursts between trials locked to taps and tones (t (11) = -.3427, p = .7383 for IOI1 and t (11) = -.4419, p = .6671 for IOI2).

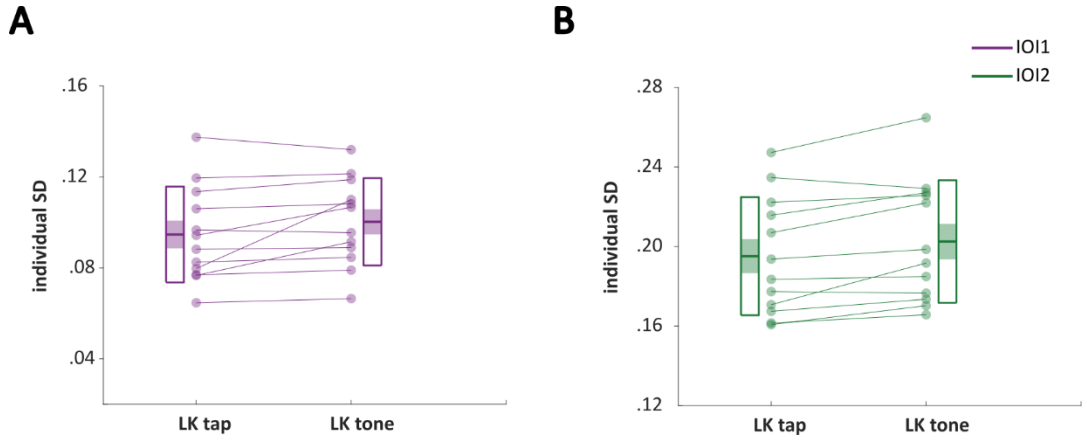

Fig. 4.5. Comparisons of distributions of beta burst events between tap and tone onset. Standard deviation of beta burst time stamps locked to tone/tap were calculated for each subject for IOI1 **(A)** and IOI2 **(B)**, respectively. Each dot represents one subject. Within subject tendency between tap and tone was showed by linked dots. The top and bottom line of the boxes represent 95% percentiles above and below the mean (middle line of the boxes). Shaded areas denote SEM. A paired samples t-test confirmed that the beta burst timing tracks taps significantly better than tones in both IOI conditions. Although the difference was marginally significant in IOI1, the main effect of burst timing locked to tap vs. tone was confirmed by a repeated measures ANOVA taking both IOI conditions together. Surprisingly, a main effect of IOI condition was also observed, but no interaction.

To investigate the timing relationship between beta bursts and taps or tones, the distribution of beta burst timing locked to taps and tones was compared by examining the standard deviation of the beta burst time stamps. A higher standard deviation was interpreted to reflect greater temporal variance and therefore less locking to the taps or tones. Findings indicated that the standard deviation was lower when beta bursts were locked to taps as compared with tones at both IOI1 and IOI2 (t (11) = -2.0266, p = .0676 for IOI1 and t (11) = -3.2607, p = .0076 for IOI2). Despite the marginal significance in IOI1, the effect was further confirmed by a repeated measures ANOVA, indicating that beta burst timing tracked the taps significantly better than tones in both IOI conditions (F (1, 11) = 10.1313, p =.0087), see Fig. 4.5). Surprisingly, we also observed a main effect of IOI condition, where IOI1 demonstrated a closer relationship between burst, tap and tone timing (F (1,11) = 210.5132, p =.0000). Although we were unable to disentangle the relationship of beta burst timing and taps from

potential interference from tones, the observed pattern across IOI conditions suggests that beta burst timing is more closely related to the movement than to the periodic auditory stimuli.

Additional analysis counting all beta bursts before the same time window before a tap (or a tone) revealed similar results but with weaker effects (t (11) = -1.6374, p = .1298 for IOI1 and t (11) = -2.3839, p = .03266 for IOI2).

4.3.3. Phase of stimulation frequency is more strongly locked to tones than taps, but no evidence for entrainment

After confirming a relation between beta burst and tap timing we aimed to measure the neural correlates for auditory tracking. Participants were not informed of the stimulation frequency before the start of each trial. Therefore, the timing of taps in the first few tap/tone trials varied greatly. Given the findings that the ongoing phase tracks auditory stimuli

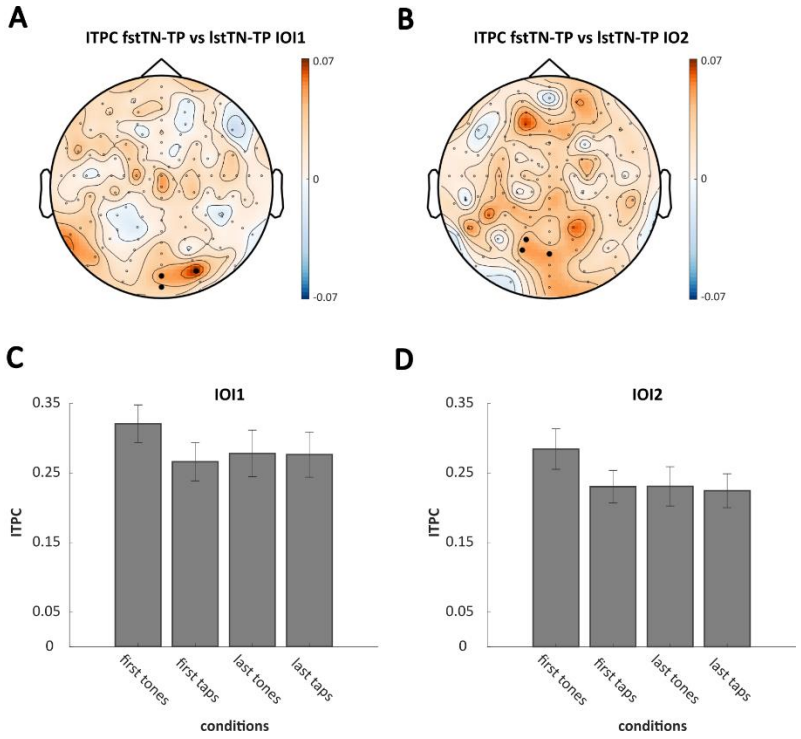

Fig. 4.6. Auditory tracking. The auditory tracking of tones was measured by the comparisons of the tone minus tap ITPC difference (tone-tap ITPC difference) between the first and last five taps/tones of a train. **(A)** and **(B)** Cluster-based permutation test indicated statistically significant differences between the first and last five taps/tones of a train regarding tone-tap ITPC difference. Electrodes with the most pronounced differences were highlighted. **(C)** and **(D)** ITPC averaged across highlighted electrodes in (A) for IOI1 and (B) for IOI2 were calculated for the first five taps/tones, respectively. In both IOI1 and IOI2, the averaged ITPC for the first tones is the highest comparing with first taps, last tones, and last taps.

(Calderone et al., 2014; Lakatos et al., 2008, 2013; Morillon & Baillet, 2017; Stefanics et al., 2010), ITPC locked to tones was expected to be stronger compared to ITPC locked to taps particularly in the first few tap/tone trials. In contrast, ITPC for taps and tones should not differ in the last few tap/tone trials, because of the nearly perfect timing of taps towards the end of the trial (see Fig. 4.4B). Hence, the auditory tracking could be measured by comparing the tone-tap ITPC difference between the first and last five tap/tone trials. We used five trials for this comparison because it represented a good balance between a quick behavioural adaption found in SMS (see Fig. 4.4B) whilst allowing for long enough segments to establish tracking. Following this logic, auditory tracking was evaluated by a cluster-based paired-samples permutation test in the comparison of tone-tap ITPC difference between the first and last five tap/tone trials. There was an average of 74 (ranging from 44 to 109) and 79 (ranging from 52 to 105) tap/tone trials involved in the calculation of ITPC locked to the first 5 tap/tone in IOI1 and IOI2, respectively. In the last five tap/tone condition, there were 91 (ranging from 32 to 145) and 91 (ranging from 54 to 135) tap/tone trials available for calculating ITPC. This analysis resulted in two clusters (channels highlighted in Fig. 4.6A and B) with significant t-values ($p_{corrected}$ = .0100 in IOI1 and $p_{corrected}$ = .0014 in IOI2), indicating stronger phase-locking to the tone at the beginning of a trial compared to the end of the trial. As predicted, the averaged ITPC within clusters for the first tones is higher than that for the first taps, while the last tones and last taps showed similar ITPC (Fig. 4.6C and D for IOI1 and IOI2, respectively). Together, these results show that phase tracks the auditory activity elicited by the tones, as opposed to motor activity elicited by taps.

To establish whether the phase locking to the auditory stimulation frequency was due to neural entrainment, we measured entrainment echoes, i.e., where phase locking lasts for several cycles even after the rhythmic stimulus stops (Albouy et al., 2017; Hanslmayr et al., 2014). ITPC from 0.2 to 2 Hz is shown before and after the last tap onset (time 0) in Fig. 4.7A and B. Support for entrainment would be if post-stimulus ITPC is stronger at the stimulation frequency compared to other frequencies. Hence, post-stimulus ITPC in IOI1 and IOI2 at the two tested frequencies (0.5 and 1 Hz) were compared using a two-way repeated measures ANOVA. Statistical results revealed a significant main effect of IOI condition (F (1,11) = 8.2960, p = .0150) such that ITPC is stronger in IOI1 compared with IOI2 for both tested frequencies. This was further confirmed by Bayes factor indicating evidence for H_+;

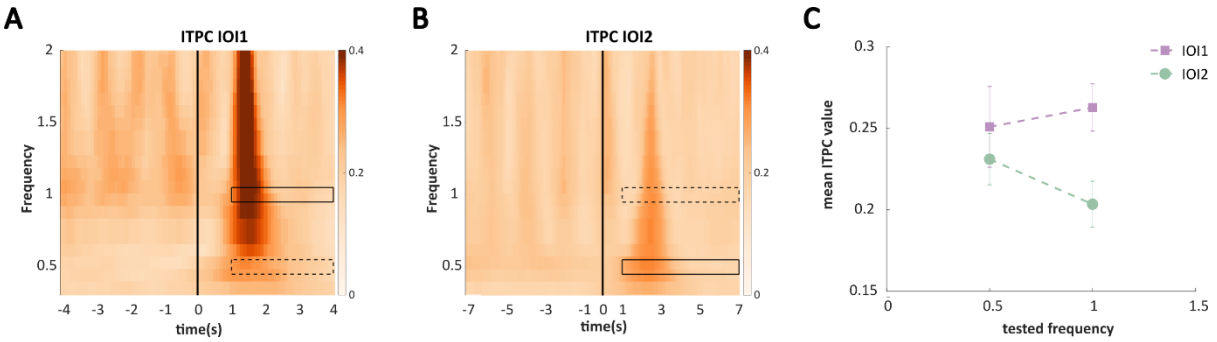

Fig. 4.7. ITPC before and after the last tone. (A) ITPC from 0.2 to 2 Hz in IOI1, in a time window of four seconds before and after the last tone onset (time 0, as indicated by the solid vertical line). **(B)** Same as (A) but for IOI2 and with a time window of seven seconds before and after the last tone onset. Black boxes in both (A) and (B) indicate TOI and FOI used for the two-way repeated measures ANOVA. While the solid-line boxes indicate congruence between stimulating and tested frequency, the dashed-line boxes indicate incongruence between them. **(C)** Averaged ITPC within corresponding FOI and TOI in both stimulating and tested frequencies. The two-way repeated measures ANOVA revealed a significant main effect of the stimulation frequency conditions, showing stronger ITPC in IOI1 comparing to IOI2. No significant interaction as evidence of entrainment was observed.

specifically, BF_{+0} = 11.52, which means that the data are approximately 11.52 times more likely to occur under H_+ than under H_0. The error percentage is 1.207%, which indicates a good

stability in obtaining the result. However, the non-significant interaction between IOI condition and tested frequency (F (1,11) = 2. .8224, p = 0.1211, BF_{+0} = .878) does not lend support to an entrainment process).

4.3.4. Beta bursts are locked to the phase of the auditory stimulation frequency

The above analyses suggest that the timing of beta bursts tracked tapping, whereas the phase at the stimulation frequency tracked the auditory stimulus. Since the task required participants to synchronise their taps to the stimulation frequency, we analysed if the timing of beta bursts is locked to the phase of the auditory stimulation frequency. Such phase locking would be an indication for an interaction between the motor (movement, i.e., taps) and sensory (auditory, i.e., tones) systems. To this end, we calculated the pair-wise phase consistency (PPC, a measure of phase locking that is unaffected by different trial numbers; Vinck et al., 2010), averaged across all channels, time-locked to beta bursts from 0.1 to 2 Hz. ROIs for statistical

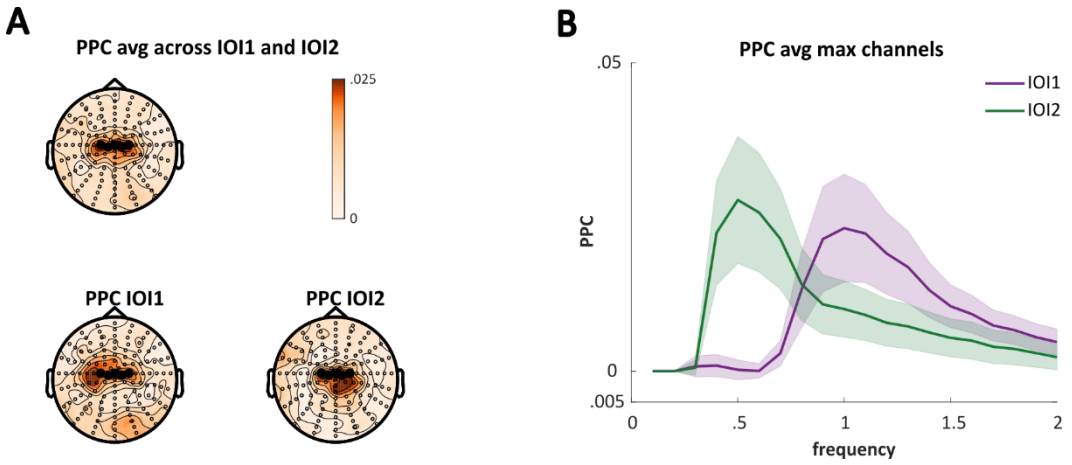

Fig. 4.8. PPC locked to motor beta burst. (A) Topographical distribution of the grand averaged PPC showing peaks at central areas in both IOI conditions (lower panels) and the average across conditions (top panel). The five maximum channels averaged across IOI conditions were used as ROI for statistical analysis (highlighted). **(B)** Pairwise phase consistency (PPC) time-locked to beta burst averaged at the ROI from 0.1 to 2 Hz is shown. Peak PPC can be observed at stimulation frequency in both IOI1 (purple line, peaks at around 1 Hz; shaded areas indicate SEM) and IOI2 (green line, peaks at around 0.5 Hz).

analysis were then later chosen as the five channels with maximum PPC values averaged across IOI conditions (Fig. 4.8A). This analysis revealed a peak at the stimulation frequency for both IOI1 and IOI2 conditions (Fig. 4.8B). This finding was further confirmed by the result of a two-way ANOVA revealing a significant interaction between IOI condition (IOI1 vs. IOI2) and PPC at the measured frequency (1 Hz vs. 0.5 Hz; F (1,11) = 8.1009, p =.0159), suggesting that beta burst phases were specifically locked to the stimulation frequency. No significant main effects were found. Grand averaged PPC across participants show peak PPC at central areas (Fig. 4.8A) for both IOI1 and IOI2. Together, these results show that beta bursts are phase locked to the stimulation frequency, suggesting a synchronization between the motor and the auditory systems during SMS.

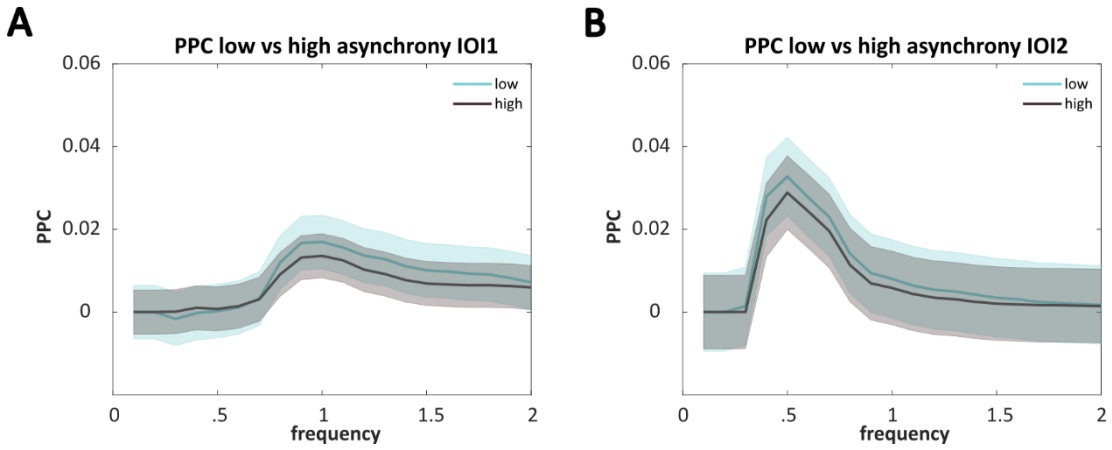

Fig. 4.9. Comparisons of PPC between low and high asynchrony conditions. PPC time-locked to motor beta burst was compared between low and high asynchrony conditions, which was conditioned by individual median of tap-to-tone absolute asynchrony. Shaded areas indicate SEM. **(A)** The difference in PPC from 0.1 to 2 Hz peaked at the entrainment frequency in IOI1 (peaked at 1 Hz) and **(B)** in IOI2 (peaked at 0.5 Hz).

4.3.5. Timing of beta bursts explains variance in behavioural performance

The above results showing beta burst phase locking to the stimulation frequency, point towards an interaction between the neural response accounting for movements and the auditory stimulus. If this interaction indeed reflects synchronization between the motor and auditory

system, then this effect is expected to correlate with variations in tapping behaviour. To test this, tap/tone trials were conditioned as low and high variance taps (i.e., good or bad timing, respectively), depending on whether the absolute value of asynchrony was above or below the median across trials (absolute asynchrony) for each participant. PPC locked at beta burst was then compared between low and high variance trials at the stimulation frequency of IOI condition using a repeated measures ANOVA. As expected, this analysis revealed stronger PPC in the low compared to high variance condition (F (1,11) = 5.2966, p =.0419, Fig. 4.9), indicating that beta bursts tend to peak at a consistent phase at the stimulation frequency when taps are temporally more accurate. Surprisingly, we also observed a main effect of IOI condition (F (1,11) = 4.9190, p =.0485), but no interaction.

Together, these results indicate that beta burst timing is closely related to taps and is phase locked to the stimulation frequency of the auditory stimulus. Importantly, beta burst phase locking accounts for tapping variations on a trial-by-trial level. These results suggest that phase-locked beta bursts may act as an internal link between the motor and auditory systems during SMS.

4.4. Discussion

Accumulating evidence suggests that both rhythmic sensory stimulation and the timing of movements contribute to SMS, which requires interaction between the motor and auditory systems. However, the underlying neural correlates remain unclear. We hypothesized that the timing of beta bursts and the phase of the stimulation frequency play an important role in the synchronization of the motor and auditory systems and that an interaction between beta burst timing and the phase of the stimulation frequency relates to behavioural performance. To test

our hypothesis, we explored the neural representation for taps and tones, which were related to beta burst timing and auditory tracking, respectively. Importantly, we observed an interaction between beta burst timing and phase locking at the stimulation frequency (1 Hz for IOI1 and 0.5 Hz for IOI2), where the degree of such phase locking correlated with behavioural performance. Together these results suggest a functional role of beta bursts and their phase locking at the stimulation frequency for synchronizing movements to a rhythmic sensory stimulus.

Behaviourally, the finding of negative mean asynchrony (NMA) is consistent with previous findings (Repp, 2005; Repp & Su, 2013). In general, participants adapted to the rhythm quickly, and anticipated the next tone within three stimuli. Additionally, tapping performance is generally better in IOI1 compared to IOI2 by showing a shorter NMA and less variance in tap-tone gaps. These behavioural results indicate higher difficulty in IOI2, consistent with previous findings showing that when IOI is longer than 1800 ms, performance drops significantly (Miyake et al., 2004). Although approximately 20% of trials showed a positive mean asynchrony, i.e., 20% taps occurred following tone onset, reaction times shorter than 150 ms (about the shortest reaction time, Repp, 2005; Repp & Su, 2013) should still be considered as predictive behaviour as opposed to reactive response. When this is taken into consideration, the proportion of trials with taps following tones by more than 150 ms is similar between IOI1 (5.85%) and IOI2 (6.26%).

Before studying the interaction between motor and sensory systems during SMS, it is critical to investigate the mechanisms underlying the phase locking to the auditory stimuli. Measuring entrainment echoes, where phase locking continues for several cycles after the termination of a rhythmic stimulus is one way of disentangling neural entrainment from other phase-locked neural responses (Hanslmayr et al., 2019). However, our results show no evidence

for entrainment. ITPC in IOI1 after stimulus offset was higher than IOI2 in general, indicating that the stimulation frequency of .5 Hz may be too slow to trigger strong entrainment. Interestingly, the ITPC at 1 Hz is significantly higher in IOI1 comparing to IOI2 (t (11) = 3.4008, p = .0059), but not at 0.5 Hz. Future designs may employ higher frequencies to test entrainment. However, it is also a challenge to distinguish whether the functional role of beta bursts, i.e., a prediction role as part of pre-movement activity, or other functional roles (e.g., facilitating responses back to baseline) as post-movement response. This becomes more of a concern when the stimulation rate increases.

Beta oscillations (13-30Hz) are considered a default mode of the motor system (Niso et al., 2016) and have been shown to be related to the representation of temporal information, with (Arnal et al., 2015; Arnal & Giraud, 2012; Kulashekhar et al., 2016; Morillon & Baillet, 2017) and without overt movements (Fujioka et al., 2012, 2015; Morillon & Baillet, 2017). Classically, beta activity is characterized by power decreases or event-related desynchronization (ERD) before movement, and power increases (event-related synchronization, ERS) gradually back to or even above baseline following the movement (van Wijk et al., 2012; Pfurtscheller & Da Silva, 1999). However, the conventional method of averaging beta signals across trials was recently challenged by studies investigating trial-wise dynamics of beta oscillations (Feingold et al., 2015; Little et al., 2019; Shin et al., 2017). These studies suggest that discrete, high amplitude, transient (typically last <150 ms, Feingold et al., 2015) and infrequent beta bursts, which are tightly locked to movements, are dominant in motor systems across humans and animals (Sherman et al., 2016). Importantly, transient beta fluctuations, which could be masked out in conventional power observation, can help the discrimination of brain states associated within movements (West et al., 2022). This research motivated us to investigate the relationship between beta burst timing with tap and tone timing.

In parallel with the better behavioural performance in IOI1, beta burst timing was more closely related to the taps (and tones) in IOI1 compared to IOI2 (Fig. 4.5). One may interpret such a result as beta burst timing predicting better behavioural performance. However, on the one hand, since taps were also closely tracing tones, we were unable to disentangle the effects of tones and produce a pure effect of beta burst timing on taps. On the other hand, while the shorter averaged gap between burst timing before tap in IOI1 than IOI2 relates to better performance, this is in violation with earlier findings showing that earlier pre-movement beta timing behaviourally correlates with fast responses (Little et al., 2019). To reconcile this discrepancy, here our results suggest that in SMS, it is the interaction between the sensory tracking phase and beta burst timing correlates with prediction performance, rather than beta burst timing per se.

By analysing directed functional connectivity, previous studies found that even during passive listening with no movements, left sensorimotor (lSM) beta (18-24 Hz) directs towards the right associative auditory cortex (rAA) in a temporal prediction task. Reversely, neural responses corresponding to auditory stimulus rates directs from rAA to lSM (Morillon & Baillet, 2017). However, whether such directional interplays relate to the prediction of behavioural performance remains unknown. Despite the equivocal role of beta burst timing in prediction of tapping performance, we found that the beta burst locking to the stimulation phase was functionally correlated with better behaviour in both IOI conditions. Limited by the EEG method we used in this study, we were unable to investigate the origin of beta bursts and the time course of interactions between motor and sensory cortices during SMS. Noticeably, in our study with movements, the frequency band of beta ranges from 18-23 Hz (except one subject at 13 Hz), similar to the beta range revealed by the above-mentioned study examining functional connectivity with passive listening (Morillon & Baillet, 2017).

Although delta (<4 Hz, Molinaro et al., 2018) entrainment was frequently studied, it was scarcely studied at frequencies less than 1 Hz in auditory entrainment. Our experiment contained two conditions implementing inter stimulus intervals of one and two seconds, corresponding to 1 and .5 Hz, respectively. Although in both IOI conditions we observed a stronger beta burst phase locking at the stimulation frequency related with shorter tap-tone gap, PPC in general is higher for IOI2 compared to IOI1, regardless to tapping accuracy. There is little existing evidence to explain this result. On a behavioural level, prediction performance in finger tapping drops when IOI is greater than 1800 ms compared to the control condition (Miyake et al., 2004). One possible explanation is that the tapping prediction may be more reliant on the phase locking between the beta burst and the stimulus when the task becomes more challenging.

In summary, our study found that the degree of phase-locking of beta burst timing to the auditory stimulation rate accounts for the accuracy of predictive tapping at the single-trial level. These results provide first evidence supporting a functional role of beta burst timing in the coordination between motor and auditory systems during SMS. However, the origin of this functional beta burst and the dynamic interaction between the motor and auditory systems during prediction need further exploration.

CHAPTER 5: GENERAL DISCUSSION

This chapter generally discusses three subjects. First, the distinct role of fast and slow gamma in the hippocampus and visual cortex that may explain the results in chapter 2 and 3. Second, the effect of high frequency RSS is discussed from a cellular perspective. It also renders the factors that may help explain different findings across similar stimulation protocol. The last part discusses the low frequency RSS as a contrast to the previous point. The end gives final summary of our findings and future questions.

5.1 The role of fast vs. slow gamma in human episodic memory

A fruitful of recordings from rat hippocampus have shed light on the distinctive roles of fast and slow gamma in tasks involving spatial memory and maze running (Bieri et al., 2014; Colgin, 2015; Colgin et al., 2009; Schomburg et al., 2014; Zheng et al., 2015, 2016, but see conflicting findings in the review in Colgin, 2015). Fast gamma (>60 Hz) coherence has been observed in the entorhinal cortex (EC)-CA1 connection. The EC is thought to be critical for memory encoding by bridging information from the neocortex to CA1 in the hippocampus (Lee et al., 2021; Suh et al., 2013). In contrast, slow gamma (<55 Hz) synchronization emerges between CA3 and CA1, with the intact CA3-CA1 circuit serving memory retrieval (Brun et al., 2002). Notably, fast and slow gamma align with distinct CA1 theta phases (Bieri et al., 2014; Colgin et al., 2009; Schomburg et al., 2014; Zheng et al., 2016), which are believed to route the memory encoding and retrieval process (Hasselmo et al., 2002; Siegle & Wilson, 2014). These together suggest fast and slow gamma is likely to play a unique role in memory

encoding and retrieval. This idea is supported by intracranial EEG recordings in human hippocampus performing memory tasks (Griffiths et al., 2019).

While this thesis employs rhythmic visual stimulation (RVS) at 37.5 Hz (chapter 2) and 60 Hz (chapter 3) to explore the role of STDP in human episodic memory, inconclusive outcomes regarding fast and slow gamma entertainment effects on recall performance persist. Although both frequency entrainment was proved to be effective at the group level, slow gamma entrainment has no effect on memory performance, while results revealed larger area under the curve (AUC) in the shortest delay condition with 60 Hz. However, the results between chapter 2 and chapter 3 are not comparable, because of the difference in memory task and data analysis. Recent studies applying RVS in associative memory tasks offer contradictory findings. Wang et al. (2023) induce STDP-like associative memory using audio-visual rhythmic stimulation at 37.5 Hz, while Griffiths and colleagues (2023) reveal varied effects with different stimulation frequencies during encoding and retrieval phases. The enhanced recall is unique to the slow gamma entrainment at retrieval, whereas there is no effect with fast or slow stimulation at encoding. It is worth noted that the rhythmicity in Wang and colleagues' study was embedded within the stimulus, similar to experiments presented in the current thesis, instead of being a background in Griffiths and colleagues (2023). As evoked gamma activity is modulated by spatial selective attention, this may account some of the inconsistent findings (Kashiwase et al., 2012; Morgan et al., 1996). Nevertheless, replications and improvements, for example, ruling out confounding factors, are needed for further understanding.

One may question that the division of fast and slow gamma may not apply in visual cortex. Actually, this dichotomy has been reported in other structures, including the visual cortex. Rodent visual cortex demonstrates distinct co-existence of fast and slow gamma. Although both regulated by recurrent inhibition, slow gamma resides in deeper layer than fast gamma and is differentially affected by pharmacomodulations (Oke et al., 2010). In primates, gamma synchronization (~60-80 Hz) corresponds to feedforward communication, while beta (~14-18 Hz) links with feedback communication (Bastos et al., 2015). The slower frequency in beta compared to slow gamma in human may be drawn to the requirement of longer distance communication in larger brain (Zheng et al., 2015). This is likely

suggesting the dissociation of fast and slow gamma as a common mechanism across structures. Human MEG studies also highlight their roles in various aspects of visual perception (Hoogenboom et al., 2006). Slow gamma (44-66 Hz) arises from the right parietal area correlates with attention, whereas fast amma (70-120 Hz) at central occipito-parietal aids visual grouping (Vidal et al., 2006). Slow gamma (30-48 Hz) is implicated in unconscious learning (Chaumon et al., 2009), whereas higher gamma band (54-64 Hz) increases with conscious stimulus perception, and 76-90 Hz reflects spatial attention (Wyart & Tallon-Baudry, 2008). How the complex roles of fast and slow gamma may relate to those in the hippocampus remains poorly understood.

There is compelling evidence suggesting the presence of a shared mechanism underlying the generation of gamma oscillations between the visual cortex and hippocampus. Optogenetically rhythmic stimulation targets fast spiking parvalbumin-positive (FS-PV+) interneurons in the CA1 region (Iaccarino et al., 2016). These investigations produced results akin to those obtained from studies utilizing rhythmic visual stimulation at the same frequency (Adaikkan et al., 2019; Martorell et al., 2019), showing a similarly favourable mitigation of degenerative diseases markers. Remarkably, the rhythmic visual stimulation predominantly recruits the same type of interneurons – Fs-PV+, in the primary visual cortex (Schneider et al., 2023).

5.2 The propagation of high frequency rhythmic sensory stimulation to deep structures

High frequency RSS does not only act as a frequency tagging tool but have potential to serve as treatment for degenerative disease, because its non-invasive and visually pleasant in delivery is appealing. Yet, the debate surrounding the impact of high frequency stimulation on deep structure remains contentious. Studies measuring multiple structures in rats and human with 40 Hz LED RSS argue for entrainment in both sensory cortex and deep areas like the insula, CA1 and mPFC (Adaikkan et al., 2019; Iaccarino et al., 2016; Khachatryan et al., 2022; Martorell et al., 2019). Similarly, extracellular single unit recordings in macaque V1 illustrates increased spikes time-locked to gratings stimulus displayed on CRT screen at 60 Hz, across all layers (Williams et al., 2004). However, inconsistent findings arise, with some studies using a similar paradigm but shorter stimulation duration failed to find modulation of spike activity beyond V1 (Soula et al., 2023) or even layer 4 in V1 (Schneider et al., 2023). In contrast, several observations indicate that high frequency rhythmic stimulation modulates behaviour (Drijvers et al., 2021; Griffiths et al., 2023; Wang et al., 2023), including the current thesis.

Several factors may contribute to these inconsistencies, including stimulus features, attention, and behavioural tasks. The power, frequency and source of gamma response depend on stimulus characteristics, for example, contrast, motion, location, complexity and size (Hoogenboom et al., 2006; Muthukumaraswamy & Singh, 2013; Tallon-Baudry et al., 2005; Vidal et al., 2006). For instance, the phase locking of V1 spike activities to 60 Hz flickers strengthens with increased contrast (William, 2004). Besides, responses to pure LED light as rhythm stimulation may be attenuated because of repetition suppression, a phenomenon that leads to decreased gamma response (Gruber et al., 2004; Gruber & Müller, 2002). Although these stimulations may not require attention, repetition suppression can also relate to attention-free adaptation (Hsu et al., 2014). Increasing the complexity of stimulus may also benefit the propagation of entrainment and entail effects on behaviour. Martorell and colleagues (2019) observed decreased amyloid in medial prefrontal cortex, of which effect is unique to the multisensory rhythmic stimulation condition compared to unimodality stimulation condition. Drijvers and colleagues (2021) also noticed multisensory rhythmic stimulation results in nonlinear multisensory

integration that connects with speech-gesture integration. Moreover, multisensory rhythmic stimulation improves cognitive function and attenuates Alzheimer's Disease (AD)-related biomarkers in mild AD patients (Chan et al., 2021).

Attention and cognitive tasks also affect gamma phase entrainment (Tallon-Baudry et al., 2005; Vidal et al., 2006). The former is supported by steady-state visual evoked potentials (SSVEPs, Müller et al., 2003, 2006) research, where the main scalp-level response for RSS is modulated by attention (Kashiwase et al., 2012; Morgan et al., 1996). Spatial attention selectively increases both excitatory and inhibitory neurons in V4, facilitating feedback information transition (Spyropoulos et al., 2022), suggesting a role of top-down regulation. Moreover, intracranial study involving an epilepsy patient demonstrates a correlation between cognitive tasks involvement and the propagation of 40 Hz gamma entrainment in deep structures, including the hippocampus, insular, and temporal cortex (Khachatryan et al., 2022). Indirect evidence further underscores this factor by showing strengthened ITPC at the entrainment frequency in the hippocampus when participants remember the audiovisual association (Wang et al., 2023). Together, these studies suggest the impact of attention and task engagement during RSS on the propagation of entrainment.

Disagreement comes from evidence demonstrating that V1 fast-spiking interneurons constitute the dominant response to 40 Hz LED entrainment (Schneider et al., 2023). The engagement of these fast-spiking interneurons potentially alters the balance between excitatory and inhibitory activity, tilting it towards inhibitory influence, as evidenced by stronger phase locking of inhibitory than excitatory neurons. As a consequence, it could impede the propagation of signals beyond the initial input layer (Schneider et al., 2023). This contradicts with the prevailing notion that gamma oscillations intricately regulate the precise timing of information streams and facilitate the feedforward information transition. Thus, it also casts doubt upon the assumed role of gamma synchronization for spike timing-dependent plasticity (STDP) and questions the feasibility in the utilization of high frequency RSS to probe STDP. However, this finding does not eliminate the possibility that fast-spiking interneurons play a role in facilitating pyramidal neurons when task and attention are involved. This assumption finds support in an optogenetic study.

The barrel cortex, responsible for basic sensory processing such as tactile sensation arising from whisker stimulation in rodents, provides insights into this interplay. Optogenetic modification targets FS-PV+ interneurons in the barrel cortex. Driving by 40 Hz light, the FS-PV+ revealed its role in sufficiently generating gamma oscillations (Cardin et al., 2009). In alignment with Schneider and colleagues' (2023) findings, regular spiking neurons (RS, often excitatory neurons) exhibit insensitive to high frequency light stimulation. Significantly, this study also demonstrated that the amplitude of RS response, the timing of sensory response, and the precision of sensory-evoked spikes are regulated by the pairing of whisker stimulation at different evoked gamma phase. This result indicates that FS-PV+ interneurons gates sensory inputs, constraining optimal windows for RS firing. This may in turn facilitate information feedforward to downstream. This study implies that the lack of excitatory response in Schneider and colleagues' (2023) could be attributed to the absence of task engagement. Interestingly, in the research of STDP, the outcomes of paired stimulation similarly depend on the behavioural context. Paired stimulation results in inhibition during rest, while engagement in a visuomotor task leads to excitatory influence (Buch et al., 2011).

The interplay between FS-PV+ and RS outlined above underscores the feasibility of using high frequency RSS to investigate STDP through the presentation of natural stimuli. Additionally, interareal gamma synchronization can induce long-lasting potentiation of recurrent excitatory synapse (Whittington et al., 1997). In our study, manipulation of the inter-hemifield evoked gamma phase lag by RSS likely times the excitatory response to natural scenes. These together contributes to the explanation of the observed enhanced memory recall in the shortest time delay condition. The 0-delay condition did not outperform the other delay conditions might be attributed to the uncertainty at 0-time lag in STDP function. However, it is also worth noted that STDP time window varies across species and brain regions (e.g., for human: Testa-Silva et al., 2010; Stefan et al., 2002; Verhoog et al., 2013; Wolters et al., 2003; for rats: Bi & Poo, 1998; Meliza & Dan, 2006; for locusts: Cassenaer & Laurent, 2007; for cats: Fu et al., 2002; Yao et al., 2004; Yao & Dan, 2001; for frogs: Zhang et al., 1998).

5.3 Slow frequency rhythmic sensory stimulation and the role of beta burst in sensorimotor synchronization

In contrast to the heat debates surrounding high-frequency entrainment, the modulatory effect of low-frequency rhythmic sensory entrainment has been demonstrated in various cognitive processes (Antony & Paller, 2017; Clouter et al., 2017; Wang et al., 2018; Williams, 2001). This phenomenon is likely elucidated by cell-type-specific double dissociation. A study by Cardin and colleagues (2009), involving driven FS-PV+ in rodent sensory cortex from 8-200 Hz, revealed that inhibitory interneurons selectively respond to high frequencies, while pyramidal neurons amplify low frequencies. Further comparison of these neuron responses illustrates the reduction in pyramidal spikes with increased stimulation frequency. Additionally, low frequency is also suggested a binding role for long-distance assembly communication and plasticity (Huerta & Lisman, 1995; Hyman et al., 2003; Pavlides et al., 1998; Siegle & Wilson, 2014). Collectively, these findings suggest that low-frequency entrainment may have the potential to traverse long distances and regulate beta activity in SMS.

Our results demonstrate a relationship relating both movement performance and the stimulating frequency to beta burst. Based on these findings, we propose that beta served as the bridge for sensorimotor coordination. However, it is important to note that our findings are constrained by limitations in spatial resolution and a relatively small sample size. This limitation hinders our ability to differentiate between motor and auditory source activities. The phase locking of beta bursts in relation to predictive finger tapping performance could potentially arise as a result of volume conduction. In other words, beta burst may be phase locked to local low frequency oscillations. Yet, this explanation cannot account the difference observed in movement performance. It remains to answer whether overt movements mediated by beta may prepare a brain state that lowers the threshold for sensory perception, or if the low

frequency entrainment facilitates prediction by regulating the timing of beta bursts, or possibly both. Intracranial recordings and computation modelling may provide insights into the dynamic interplay between motor and sensory assemblies during SMS.

Potential clinical applications and future questions

Numerous factors have the potential to influence the entrainment and propagation facilitated by high frequency RSS. These includes stimulus features, the engagement of attention and behavioural tasks, and the relative timing between flickers and stimulus. Further exploration on these factors can help develop a promising high frequency RSS protocol for its application in research and clinical domains. However, several intriguing questions remain:

- Does the interplay between FS-PV+ and RS indeed facilitate information feedforward and subsequently impact downstream information flow?
- How do FS-PV+ interneurons participate in STDP at the cellular and molecular levels?
- Does fast and slow gamma behave differently in STDP?
- Can RSS induce long-term effects on cognitive functions?

Moreover, the dynamics of propagation – such as from the sensory cortex to the hippocampus – when RSS is paired with informative stimuli, remains poorly understood. Providing the various optimal window for STDP, research using intracranial recordings and laminar measurements may offer valuable insights, potentially examining the efficacy of high frequency RSS in investigating cognitive functions. This could also shed light on the potential of task engagement in shaping RSS-based treatments for degenerative diseases.

Summary

To summarize, the current thesis investigated the role of high frequency oscillations in human episodic memory and SMS, using both fast and very slow RSS. Results demonstrated certain modulation on both SSVEPs and memory performance, and a relation between beta burst phase locking to the slow

rhythms and movement performance. While it has shed light on the potential of RSS for regulating brain activity, there are several factors that need to be taken into account for future studies employ high frequency RSS to explore deep structures. Integrating techniques like optogenetics, neuroimaging, and computational modelling in future investigations could offer a multidimensional view and provide valuable insights into the applications of RSS within research and clinical domains.

APPENDIX A: SUPPLEMENTARY MATEIRALS FOR CHAPTER 2

Supplementary information

Verification of precise timing of the stimulus

A photodiode was attached to the top left of the CRT screen. Each movie (3-second) was displayed at the top left of the screen with an interval of 1 second. Data was recording at a sample rate of 1000 and digitized by the National Instruments USB-6343 multifunction I/O device (see https://www.ni.com/pdf/manuals/377874a.pdf). Since no trigger was implemented during the recording, the trials were defined using the following process. A threshold of 0.7 was used to define 37.5 Hz peaks. Since a quarter cycle of 37.5 Hz is around 6.67 ms, considering the potential noise (e.g., from the sampling position), at least 4 ms of peaks were expected in each cycle of 37.5 Hz. Hence, the point, from which was followed by at least 150 (37.5 times 4) peaks detected in every second of three continuous seconds, was defined as the stimulus onset time. 286 out of 384 trials were detected using this criterium. Time frequency analysis (Morlet wavelet) with a time window from -0.5 to 3.5 upon stimulus onset, in step of 0.02 second, foi from 1 to 200 Hz, in step of 1 Hz revealed a peak at 37.5 Hz (see Fig. S6.5).

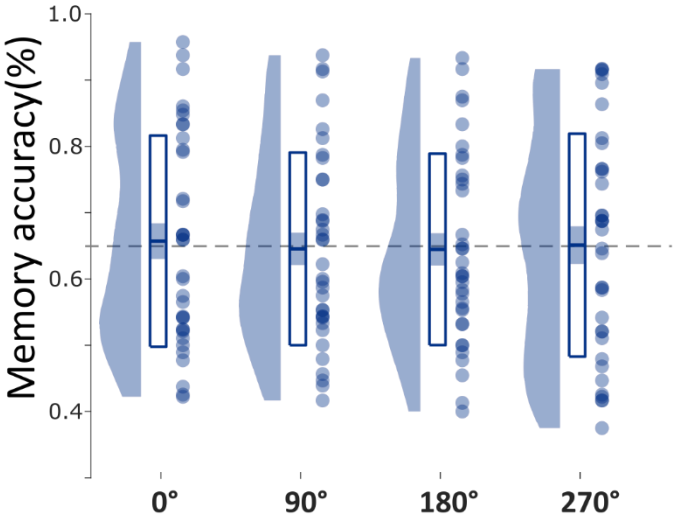

Fig. S6.1. Memory performance across conditions. Except for the dash line, the element representation is the same as Fig. 2.4. The dash line denotes the mean performance across conditions and participants. Without subtraction of individual mean performance across conditions, the trend became less salient.

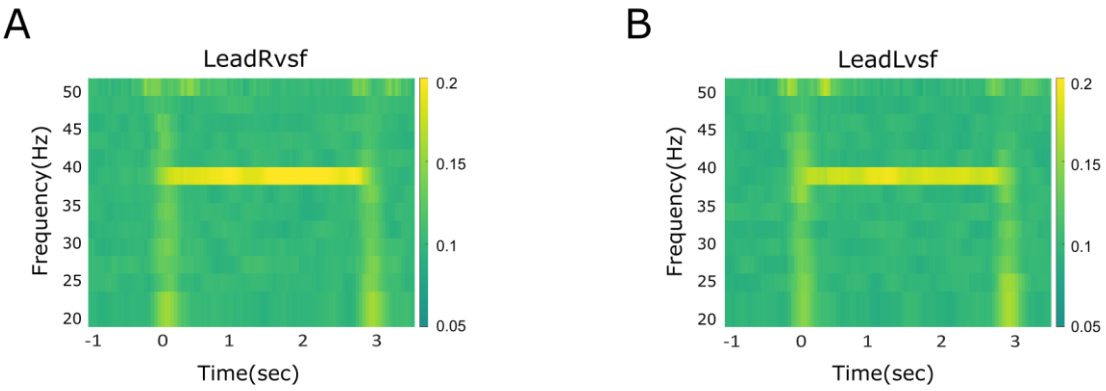

Fig. S6.2. ITPC in other time windows. ITPC from 1s before and 3.75s after stimulus onset in the LeadRvsf (A) and LeadLvsf (B) conditions. ITPC was averaged across electrodes highlighted in Fig. 2.3A and B for LeadRvsf and LeadLvsf, respectively.

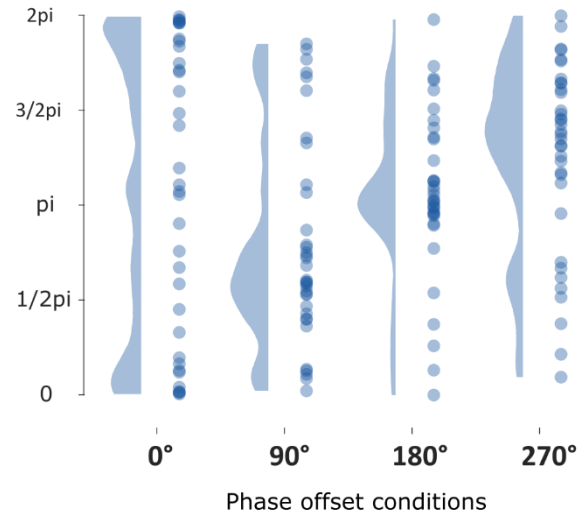

Fig. S6.3. Phase offsets at individual level. Each dot represents a mean phase offset for each participant at the corresponding modulation condition. The calculation of mean phase offset was based on SSVEPs (similar to Fig. 2.5 but at individual level), averaged across the 1s-time interval from 1s to 2s upon stimulus onset.

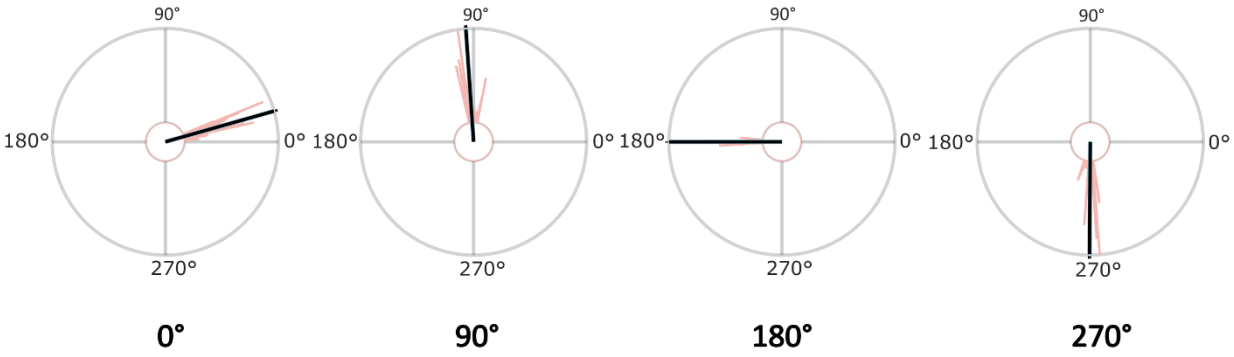

Fig. S6.4. Phase offsets at group level based on group ROI. Group ROI (one electrode) in the left and right hemifield was identified using similar procedure as at the individual level (see Fig. 2). The calculation of mean phase offset was based on SSVEPs (similar to Fig. 2.5 but based on group ROI), averaged across the 1s-time interval from 1s to 2s upon stimulus onset. The mean phase differences with 95% confidence interval are 15.75° ± 0.42°, 93.95° ± 0.64°, 180.04° ± 0.22° and 269.67° ± 0.63° for 0, 90, 180 and 270 phase offset conditions, respectively. The V-test confirmed that the phases from 1s -2s upon stimulus onset were uniformly distributed around their entrained phase offset, with $p = 0$ for all conditions.

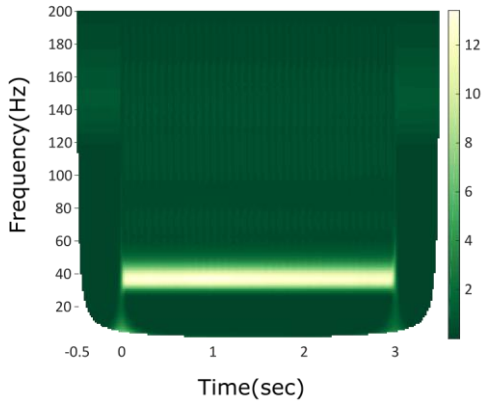

Fig. S6.5. Verification of precise timing of the stimulus. Time frequency analysis revealed a peak at 37.5 Hz.

APPENDIX B: SUPPLEMENTARY MATEIRALS FOR CHAPTER 3

Supplementary information

The raincloud plots in Chapter 3 were processed with the package developed by Allen and colleagues (2021) on the Rstudio platform (R Core Team, 2021).

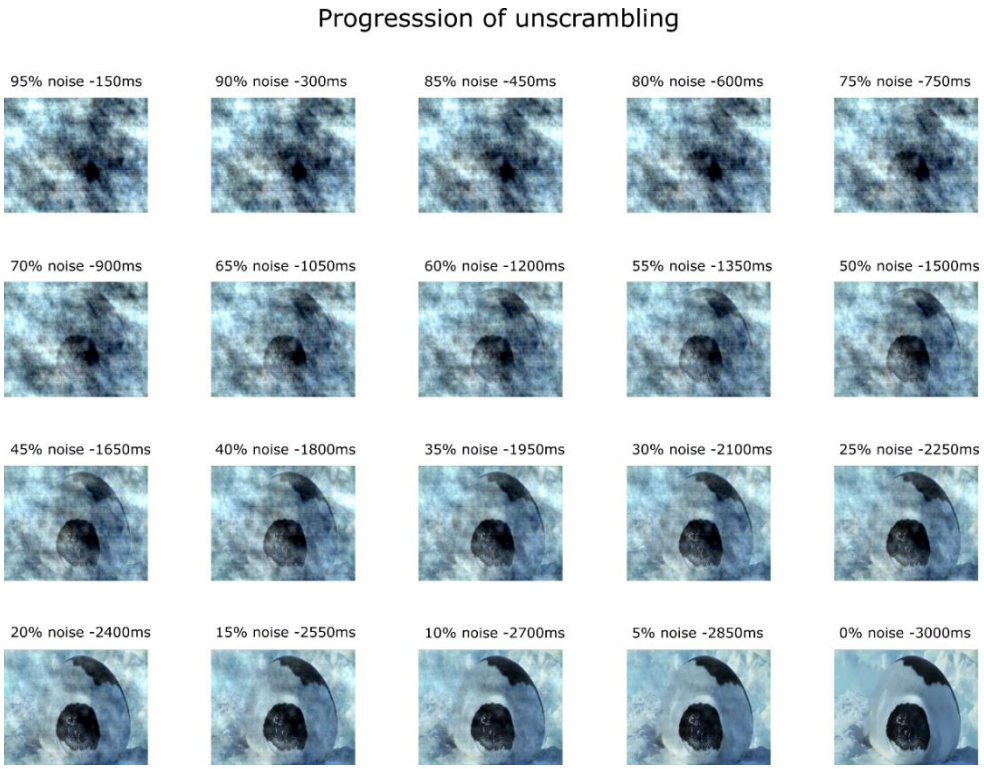

Fig. S7.1. Progression of unscrambling image. The static images were retrieved from the central frame of trailing movies and underwent digitisation from unit8 to double, and then Fourier-transformed to extract phase and amplitude information. Random noise ranging from 0% to 95% was added to the original phase information in 5% increments. The noise-added data was then inverse-Fourier-transformed to create blurred images ranging from 5% to 95% noise. Each blurred image was displayed for 150 ms, gradually transitioning from 95% to 0% noise, resulting in a 3000 ms unscrambling image during the implicit memory test of the retrieval phase.

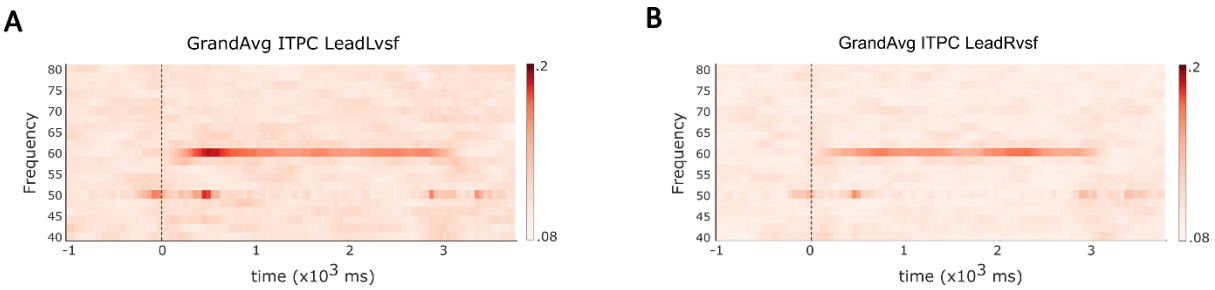

Fig. S7.2. Group ITPC distribution at full epoch length. (A) and **(B)** ITPC from 40-80 Hz spanning from -1 to 3.75s showed a peak at 60 Hz during movie pair presentation for both the LeadLvsf and LeadRvsf conditions. Channels included were the same as Fig. 3.5 (D) and (E).

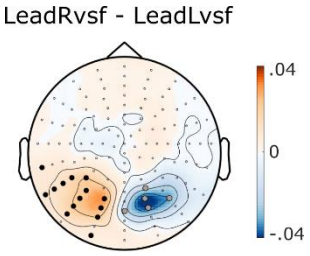

Fig. S7.3. PPC difference between LeadRvsf and LeadLvsf. The topographical distribution of the grand-averaged PPC difference between LeadRvsf and LeadLvsf mirrored the ITPC results. LeadRvsf exhibited stronger PPC in the left hemifield (highlighted by thick black electrodes, *p <0.0001)*, whereas LeadLvsf showed no disparity in the right hemifield for LeadLvsf (highlighted by thick grey electrodes, $p = 0.0935$). Thereby these results substantiated that the absence of a significant LeadLvsf superiority over LeadRvsf in the right hemifield was not influenced by trail number bias.

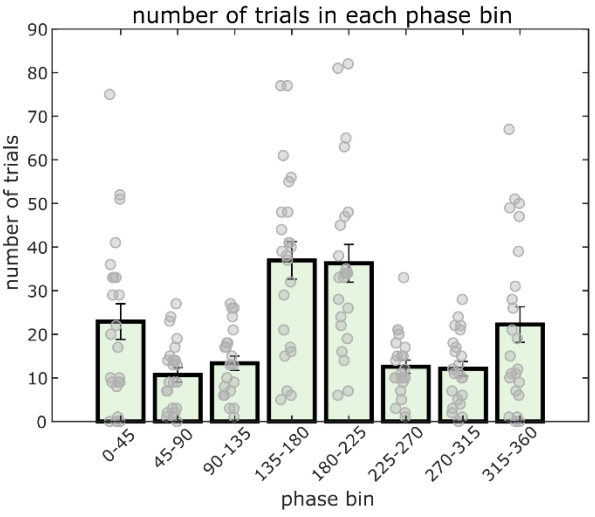

	mean	min	max
0°-45°	22.913	0	75
45°-90°	10.6957	0	27
90°-135°	13.3478	1	27
135°-180°	36.9565	5	77
180°-225°	36.2609	6	82
225°-270°	12.5652	1	33
270°-315°	12.087	0	28
315°-360°	22.2174	0	67

Fig. S7.4. Trial number information in each phase bin. The single-trial instantaneous phase differences between leading and trailing movies were sorted into eight distinct phase bins: 0°-45°, 45°-90°, 90°-135°, 135°-180°, 180°-225°, 225°-270°, 270°-315° and 315°-360°. The bar plot illustrates the distribution of trial numbers across these phase bins for all 23 participants. Most trials were concentrated around the modulation phase lags, i.e., 0° and 180°. In the upper panel, each dot represents an individual participant, while the error bar denotes the stand error. The lower panel provides the mean, minimum and maximum trial number across participants.

REFERENCES

Abbott, L. F., & Nelson, S. B. (2000). Synaptic plasticity: Taming the beast. *Nature Neuroscience*, *3*(11s), 1178–1183. https://doi.org/10.1038/81453

Acuna, O. V., Aqueveque, P., & Pino, E. J. (2014). Eye-tracking capabilities of low-cost EOG system. *2014 36th Annual International Conference of the IEEE Engineering in Medicine and Biology Society, EMBC 2014*, 610–613. https://doi.org/10.1109/EMBC.2014.6943665

Adaikkan, C., Middleton, S. J., Marco, A., Pao, P. C., Mathys, H., Kim, D. N. W., Gao, F., Young, J. Z., Suk, H. J., Boyden, E. S., McHugh, T. J., & Tsai, L. H. (2019). Gamma Entrainment Binds Higher-Order Brain Regions and Offers Neuroprotection. *Neuron*, *102*(5), 929-943.e8. https://doi.org/10.1016/j.neuron.2019.04.011

Adamian, N., Andersen, S. K., & Hillyard, S. A. (2020). Parallel attentional facilitation of features and objects in early visual cortex. *Psychophysiology*, *57*(3), 1–11. https://doi.org/10.1111/psyp.13498

Albouy, P., Weiss, A., Baillet, S., & Zatorre, R. J. (2017). Selective Entrainment of Theta Oscillations in the Dorsal Stream Causally Enhances Auditory Working Memory Performance. *Neuron*, *94*(1), 193-206.e5. https://doi.org/10.1016/j.neuron.2017.03.015

Allen, M., Poggiali, D., Whitaker, K., Marshall, T. R., & Kievit, R. A. (2019). Raincloud plots: a multi-platform tool for robust data visualization. *Wellcome open research*, *4*.

Antony, J. W., & Paller, K. A. (2017). Using oscillating sounds to manipulate sleep spindles. *Sleep*, *40*(3), zsw068.

Arnal, L. H., Doelling, K. B., & Poeppel, D. (2015). Delta-beta coupled oscillations underlie temporal prediction accuracy. *Cerebral Cortex*, *25*(9), 3077–3085. https://doi.org/10.1093/cercor/bhu103

Arnal, L. H. (2012). Predicting "when" using the motor system's beta-band oscillations. *Frontiers in human neuroscience*, *6*, 225.

Arnal, L. H., & Giraud, A. L. (2012). Cortical oscillations and sensory predictions. *Trends in Cognitive Sciences*, *16*(7), 390–398. https://doi.org/10.1016/j.tics.2012.05.003

Auksztulewicz, R., & Friston, K. (2015). Attentional enhancement of auditory mismatch responses: a DCM/MEG study. *Cerebral cortex*, 25(11), 4273-4283.

Axmacher, N., Mormann, F., Fernández, G., Elger, C. E., & Fell, J. (2006). Memory formation by neuronal synchronization. *Brain Research Reviews*, *52*(1), 170–182. https://doi.org/10.1016/j.brainresrev.2006.01.007

Bastos, A. M., Vezoli, J., Bosman, C. A., Schoffelen, J. M., Oostenveld, R., Dowdall, J. R., DeWeerd, P., Kennedy, H., & Fries, P. (2015). Visual areas exert feedforward and feedback influences through distinct frequency

channels. *Neuron*, *85*(2), 390–401. https://doi.org/10.1016/j.neuron.2014.12.018

Bechara, A., Tranel, D., Damasio, H., Adolphs, R., Rockland, C., & Damasio, A. R. (1995). Double dissociation of conditioning and declarative knowledge relative to the amygdala and hippocampus in humans. *Science*, 269(5227), 1115-1118.

Benussi, A., Cantoni, V., Grassi, M., Brechet, L., Michel, C. M., Datta, A., Thomas, C., Gazzina, S., Cotelli, M. S., Bianchi, M., Premi, E., Gadola, Y., Cotelli, M., Pengo, M., Perrone, F., Scolaro, M., Archetti, S., Solje, E., Padovani, A., … Borroni, B. (2022). Increasing Brain Gamma Activity Improves Episodic Memory and Restores Cholinergic Dysfunction in Alzheimer's Disease. *Annals of Neurology*, *92*(2), 322–334. https://doi.org/10.1002/ana.26411

Berens, P. (2009). CircStat: a MATLAB toolbox for circular statistics. *J Stat Softw, 31*(10), 1-21.

Berger, H. (1929). Über das elektroenkephalogramm des menschen. *Archiv für psychiatrie und nervenkrankheiten, 87*(1), 527-570.

Bi, G. Q., & Poo, M. M. (1998). Synaptic modifications in cultured hippocampal neurons: Dependence on spike timing, synaptic strength, and postsynaptic cell type. *Journal of Neuroscience*, *18*(24), 10464–10472. https://doi.org/10.1523/jneurosci.18-24-10464.1998

Biau, E., Wang, D., Park, H., Jensen, O., & Hanslmayr, S. (2021). Auditory detection is modulated by theta phase of silent lip movements. *Current Research in Neurobiology*, *2*, 100014.

Bieri, K. W., Bobbitt, K. N., & Colgin, L. L. (2014). Slow and Fast Gamma Rhythms Coordinate Different Spatial Coding Modes in Hippocampal Place Cells. *Neuron*, *82*(3), 670–681. https://doi.org/10.1016/j.neuron.2014.03.013

Brainard, D. H. (1997) The Psychophysics Toolbox, *Spatial Vision 10*:433-436.

Breska, A., & Deouell, L. Y. (2017). Neural mechanisms of rhythm-based temporal prediction: Delta phase-locking reflects temporal predictability but not rhythmic entrainment. *PLoS Biology*, *15*(2), 1–30. https://doi.org/10.1371/journal.pbio.2001665

Brun, V. H., Otnæss, M. K., Molden, S., Steffenach, H. A., Witter, M. P., Moser, M. B., & Moser, E. I. (2002). Place cells and place recognition maintained by direct entorhinal-hippocampal circuitry. *Science*, *296*(5576), 2243–2246. https://doi.org/10.1126/science.1071089

Buch, E. R., Johnen, V. M., Nelissen, N., O'Shea, J., & Rushworth, M. F. S. (2011). Noninvasive associative plasticity induction in a corticocortical pathway of the human brain. *Journal of Neuroscience*, *31*(48), 17669–17679. https://doi.org/10.1523/JNEUROSCI.1513-11.2011

Buzsáki, G. (2010). Neural Syntax: Cell Assemblies, Synapsembles, and Readers. *Neuron*, *68*(3), 362–385. https://doi.org/10.1016/j.neuron.2010.09.023

Calderone, D. J., Lakatos, P., Butler, P. D., & Castellanos, F. X. (2014). Entrainment of neural oscillations as a modifiable substrate of attention. *Trends in Cognitive Sciences*, *18*(6), 300–309.

https://doi.org/10.1016/j.tics.2014.02.005

Capilla, A., Pazo-Alvarez, P., Darriba, A., Campo, P., & Gross, J. (2011). Steady-state visual evoked potentials can be explained by temporal superposition of transient event-related responses. *PLoS ONE*, *6*(1). https://doi.org/10.1371/journal.pone.0014543

Caporale, N., & Dan, Y. (2008). Spike Timing–Dependent Plasticity: A Hebbian Learning Rule. *Annual Review of Neuroscience*, *31*(1), 25–46. https://doi.org/10.1146/annurev.neuro.31.060407.125639

Cardin, J. A., Carlén, M., Meletis, K., Knoblich, U., Zhang, F., Deisseroth, K., Tsai, L. H., & Moore, C. I. (2009). Driving fast-spiking cells induces gamma rhythm and controls sensory responses. *Nature*, *459*(7247), 663–667. https://doi.org/10.1038/nature08002

Cassenaer, S., & Laurent, G. (2007). Hebbian STDP in mushroom bodies facilitates the synchronous flow of olfactory information in locusts. *Nature*, *448*(7154), 709–713. https://doi.org/10.1038/nature05973

Chan, D., Suk, H. J., Jackson, B. L., Milman, N. P., Stark, D., Klerman, E. B., ... & Tsai, L. H. (2021). Gamma frequency sensory stimulation in probable mild Alzheimer's dementia patients: results of a preliminary clinical trial.

Chaumon, M., Schwartz, D., & Tallon-Baudry, C. (2009). Unconscious learning versus visual perception: Dissociable roles for gamma oscillations revealed in MEG. *Journal of Cognitive Neuroscience*, *21*(12), 2287–2299. https://doi.org/10.1162/jocn.2008.21155

Chen, Q., Wang, D., Shapiro, K. L., & Hanslmayr, S. (2021). Using fast visual rhythmic stimulation to control inter-hemispheric phase offsets in visual areas. *Neuropsychologia*, *157*(August 2020), 107863. https://doi.org/10.1016/j.neuropsychologia.2021.107863

Clouter, A., Shapiro, K. L., & Hanslmayr, S. (2017). Theta Phase Synchronization Is the Glue that Binds Human Associative Memory. *Current Biology*, *27*(20), 3143-3148.e6. https://doi.org/10.1016/j.cub.2017.09.001

Cohen, J. (2013). *Statistical power analysis for the behavioral sciences*. Academic press.

Cohen, M. X., & Gulbinaite, R. (2017). Rhythmic entrainment source separation: Optimizing analyses of neural responses to rhythmic sensory stimulation. *NeuroImage*, *147*(November 2016), 43–56. https://doi.org/10.1016/j.neuroimage.2016.11.036

Colgin, L. L. (2015). Do slow and fast gamma rhythms correspond to distinct functional states in the hippocampal network? *Brain Research*, *1621*, 309–315. https://doi.org/10.1016/j.brainres.2015.01.005

Colgin, L. L., Denninger, T., Fyhn, M., Hafting, T., Bonnevie, T., Jensen, O., Moser, M. B., & Moser, E. I. (2009). Frequency of gamma oscillations routes flow of information in the hippocampus. *Nature*, *462*(7271), 353–357. https://doi.org/10.1038/nature08573

Colling, L. J., Noble, H. L., & Goswami, U. (2017). Neural entrainment and sensorimotor synchronization to the beat in children with developmental dyslexia: An EEG study. *Frontiers in Neuroscience*, *11*(JUL). https://doi.org/10.3389/fnins.2017.00360

Cope, T. E., Grube, M., & Griffiths, T. D. (2012). Temporal predictions based on a gradual change in tempo. *The Journal of the Acoustical Society of America*, *131*(5), 4013-4022.

Cravo, A. M., Rohenkohl, G., Wyart, V., & Nobre, A. C. (2011). Endogenous modulation of low frequency oscillations by temporal expectations. *Journal of Neurophysiology*, *106*(6), 2964–2972. https://doi.org/10.1152/jn.00157.2011

Debanne, D., & Inglebert, Y. (2023). Spike timing-dependent plasticity and memory. *Current Opinion in Neurobiology*, *80*, 102707. https://doi.org/10.1016/j.conb.2023.102707

Draguhn, A., & Buzsáki, G. (2004). Neuronal Oscillations in Cortical Networks. *Science*, *304*(June), 1926–1930.

Drijvers, L., Jensen, O., & Spaak, E. (2021). Rapid invisible frequency tagging reveals nonlinear integration of auditory and visual information. *Human Brain Mapping*, *42*(4), 1138–1152. https://doi.org/10.1002/hbm.25282

Duecker, K., Gutteling, T. P., Herrmann, C. S., & Jensen, O. (2021). No evidence for entrainment: Endogenous gamma oscillations and rhythmic flicker responses coexist in visual cortex. *Journal of Neuroscience*, *41*(31), 6684–6698. https://doi.org/10.1523/JNEUROSCI.3134-20.2021

Elliott, M. A., & Müller, H. J. (1998). Synchronous information presented in 40-Hz flicker enhances visual feature binding. *Psychological Science*, *9*(4), 277–283. https://doi.org/10.1111/1467-9280.00055

Elliott, M. T., Welchman, A. E., & Wing, A. M. (2009). MatTAP: A MATLAB toolbox for the control and analysis of movement synchronisation experiments. *Journal of Neuroscience Methods*, *177*(1), 250–257. https://doi.org/10.1016/j.jneumeth.2008.10.002

Eusebio, A., & Brown, P. (2009). Synchronisation in the beta frequency-band—the bad boy of parkinsonism or an innocent bystander?. *Experimental neurology*, *217*(1), 1-3.

Feingold, J., Gibson, D. J., Depasquale, B., & Graybiel, A. M. (2015). Bursts of beta oscillation differentiate postperformance activity in the striatum and motor cortex of monkeys performing movement tasks. *Proceedings of the National Academy of Sciences of the United States of America*, *112*(44), 13687–13692. https://doi.org/10.1073/pnas.1517629112

Fell, Juergen, & Axmacher, N. (2011). The role of phase synchronization in memory processes. *Nature Reviews Neuroscience*, *12*(2), 105–118. https://doi.org/10.1038/nrn2979

Fell, Jürgen, Klaver, P., Lehnertz, K., Grunwald, T., Schaller, C., Elger, C. E., & Fernández, G. (2001). Human memory formation is accompanied by rhinal-hippocampal coupling and decoupling. *Nature Neuroscience*, *4*(12), 1259–1264. https://doi.org/10.1038/nn759

Fries, P. (2005). A mechanism for cognitive dynamics: Neuronal communication through neuronal coherence. *Trends in Cognitive Sciences*, *9*(10), 474–480. https://doi.org/10.1016/j.tics.2005.08.011

Fries, P., Scheeringa, R., & Oostenveld, R. (2008). Finding gamma. *Neuron*, 58(3), 303-305.

Fries, P. (2015). Rhythms for Cognition: Communication through Coherence. *Neuron*, *88*(1), 220–235.

https://doi.org/10.1016/j.neuron.2015.09.034

Fu, Y. X., Djupsund, K., Gao, H., Hayden, B., Shen, K., & Dan, Y. (2002). Temporal specificity in the cortical plasticity of visual space representation. *Science*, *296*(5575), 1999–2003. https://doi.org/10.1126/science.1070521

Fujii, S., & Wan, C. Y. (2014). The role of rhythm in speech and language rehabilitation: The SEP hypothesis. *Frontiers in Human Neuroscience*, *8*(OCT), 1–15. https://doi.org/10.3389/fnhum.2014.00777

Fujioka, T., Ross, B., & Trainor, L. J. (2015). Beta-band oscillations represent auditory beat and its metrical hierarchy in perception and imagery. *Journal of Neuroscience*, *35*(45), 15187–15198. https://doi.org/10.1523/JNEUROSCI.2397-15.2015

Fujioka, T., Trainor, L. J., Large, E. W., & Ross, B. (2012). Internalized timing of isochronous sounds is represented in neuromagnetic beta oscillations. *Journal of Neuroscience*, *32*(5), 1791–1802. https://doi.org/10.1523/JNEUROSCI.4107-11.2012

Garcia-Argibay, M., Santed, M. A., & Reales, J. M. (2019). Binaural auditory beats affect long-term memory. *Psychological Research*, *83*(6), 1124–1136. https://doi.org/10.1007/s00426-017-0959-2

Grahn, J. A., & Brett, M. (2007). Rhythm and beat perception in motor areas of the brain. *Journal of Cognitive Neuroscience*, *19*(5), 893–906. https://doi.org/10.1162/jocn.2007.19.5.893

Griffiths, B. J., Parish, G., Roux, F., Michelmann, S., van der Plas, M., Kolibius, L. D., Chelvarajah, R., Rollings, D. T., Sawlani, V., Hamer, H., Gollwitzer, S., Kreiselmeyer, G., Staresina, B., Wimber, M., & Hanslmayr, S. (2019). Directional coupling of slow and fast hippocampal gamma with neocortical alpha/beta oscillations in human episodic memory. *Proceedings of the National Academy of Sciences of the United States of America*, *116*(43), 21834–21842. https://doi.org/10.1073/pnas.1914180116

Griffiths, B. J., Weinert, D., Jensen, O., & Staudigl, T. (2023). Imperceptible gamma-band sensory stimulation enhances episodic memory retrieval. *bioRxiv*, 2023-07.

Gruber, T., & Müller, M. M. (2002). Effects of picture repetition on induced gamma band responses, evoked potentials, and phase synchrony in the human EEG. *Cognitive Brain Research*, *13*(3), 377–392. https://doi.org/10.1016/S0926-6410(01)00130-6

Gruber, T., Keil, A., & Müller, M. M. (2001). Modulation of induced gamma band responses and phase synchrony in a paired associate learning task in the human EEG. *Neuroscience letters*, *316*(1), 29-32.

Gruber, T., Tsivilis, D., Montaldi, D., & Müller, M. M. (2004). Induced gamma band responses: An early marker of memory encoding and retrieval. *NeuroReport*, *15*(11), 1837–1841. https://doi.org/10.1097/01.wnr.0000137077.26010.12

Gulbinaite, R., Roozendaal, D. H. M., & VanRullen, R. (2019). Attention differentially modulates the amplitude of resonance frequencies in the visual cortex. *NeuroImage*, *203*(September). https://doi.org/10.1016/j.neuroimage.2019.116146

Hanslmayr, S., Axmacher, N., & Inman, C. S. (2019). Modulating Human Memory via Entrainment of Brain Oscillations. *Trends in Neurosciences*, *42*(7), 485–499. https://doi.org/10.1016/j.tins.2019.04.004

Hanslmayr, S., Matuschek, J., & Fellner, M. C. (2014). Entrainment of prefrontal beta oscillations induces an endogenous echo and impairs memory formation. *Current Biology*, *24*(8), 904–909. https://doi.org/10.1016/j.cub.2014.03.007

Hanslmayr, S., Staresina, B. P., & Bowman, H. (2016). Oscillations and Episodic Memory: Addressing the Synchronization/Desynchronization Conundrum. *Trends in Neurosciences*, *39*(1), 16–25. https://doi.org/10.1016/j.tins.2015.11.004

Hasselmo, M. E., Bodelón, C., & Wyble, B. P. (2002). A proposed function for hippocampal theta rhythm: Separate phases of encoding and retrieval enhance reversal of prior learning. *Neural Computation*, *14*(4), 793–817. https://doi.org/10.1162/089976602317318965

Hasselmo, M. E. (2011). *How we remember: Brain mechanisms of episodic memory*. MIT press.

Helfrich, R. F., Knepper, H., Nolte, G., Strüber, D., Rach, S., Herrmann, C. S., Schneider, T. R., & Engel, A. K. (2014). Selective Modulation of Interhemispheric Functional Connectivity by HD-tACS Shapes Perception. *PLoS Biology*, *12*(12). https://doi.org/10.1371/journal.pbio.1002031

Helfrich, R. F., Breska, A., & Knight, R. T. (2019). Neural entrainment and network resonance in support of top-down guided attention. *Current Opinion in Psychology*, *29*, 82–89. https://doi.org/10.1016/j.copsyc.2018.12.016

Henry, M. J., & Obleser, J. (2012). Frequency modulation entrains slow neural oscillations and optimizes human listening behavior. *Proceedings of the National Academy of Sciences of the United States of America*, *109*(49), 20095–20100. https://doi.org/10.1073/pnas.1213390109

Herrmann, C. S. (2001). Human EEG responses to 1-100 Hz flicker: Resonance phenomena in visual cortex and their potential correlation to cognitive phenomena. *Experimental Brain Research*, *137*(3–4), 346–353. https://doi.org/10.1007/s002210100682

Hoogenboom, N., Schoffelen, J. M., Oostenveld, R., Parkes, L. M., & Fries, P. (2006). Localizing human visual gamma-band activity in frequency, time and space. *NeuroImage*, *29*(3), 764–773. https://doi.org/10.1016/j.neuroimage.2005.08.043

Hsu, Y. F., Hämäläinen, J. A., & Waszak, F. (2014). Repetition suppression comprises both attention-independent and attention-dependent processes. *NeuroImage*, *98*, 168–175. https://doi.org/10.1016/j.neuroimage.2014.04.084

Hyman, J. M., Wyble, B. P., Goyal, V., Rossi, C. A., & Hasselmo, M. E. (2003). Stimulation in hippocampal region CA1 in behaving rats yields long-term potentiation when delivered to the peak of theta and long-term depression when delivered to the trough. *Journal of Neuroscience*, *23*(37), 11725-11731.

Huerta, P. T., & Lisman, J. E. (1995). Bidirectional synaptic plasticity induced by a single burst during cholinergic theta oscillation in CA1 in vitro. *Neuron*, *15*(5), 1053-1063.

Iaccarino, H. F., Singer, A. C., Martorell, A. J., Rudenko, A., Gao, F., Gillingham, T. Z., Mathys, H., Seo, J., Kritskiy, O., Abdurrob, F., Adaikkan, C., Canter, R. G., Rueda, R., Brown, E. N., Boyden, E. S., & Tsai, L. H. (2016). Gamma frequency entrainment attenuates amyloid load and modifies microglia. *Nature*, *540*(7632), 230–235. https://doi.org/10.1038/nature20587

Jacobs, J., Kahana, M. J., Ekstrom, A. D., & Fried, I. (2007). Brain oscillations control timing of single-neuron activity in humans. *Journal of Neuroscience*, *27*(14), 3839–3844. https://doi.org/10.1523/JNEUROSCI.4636-06.2007

Jutras, M. J., & Buffalo, E. A. (2010). Synchronous neural activity and memory formation. *Current Opinion in Neurobiology*, *20*(2), 150–155. https://doi.org/10.1016/j.conb.2010.02.006

Jutras, M. J., Fries, P., & Buffalo, E. A. (2009). Gamma-band synchronization in the macaque hippocampus and memory formation. *Journal of Neuroscience*, *29*(40), 12521–12531. https://doi.org/10.1523/JNEUROSCI.0640-09.2009

Kashiwase, Y., Matsumiya, K., Kuriki, I., & Shioiri, S. (2012). Time courses of attentional modulation in neural amplification and synchronization measured with steady-state visual-evoked potentials. *Journal of* Cognitive Neuroscience, 24(8), 1779–1793. https://doi.org/10.1162/jocn_a_00212

Katz, L., & Cracco, R. Q. (1971). A review of cerebral rhythms in the waking EEG. American Journal of EEG Technology, 11(3), 77-100.

Khachatryan, E., Wittevrongel, B., Reinartz, M., Dauwe, I., Carrette, E., Meurs, A., Van Roost, D., Boon, P., & Van Hulle, M. M. (2022). Cognitive tasks propagate the neural entrainment in response to a visual 40 Hz stimulation in humans. *Frontiers in Aging Neuroscience*, *14*. https://doi.org/10.3389/fnagi.2022.1010765

Kleiner, M., Brainard, D., & Pelli, D. (2007). *What's new in Psychtoolbox-3?*.

Koen, J. D., Barrett, F. S., Harlow, I. M., & Yonelinas, A. P. (2017). The ROC Toolbox: A toolbox for analyzing receiver-operating characteristics derived from confidence ratings. *Behavior Research Methods*, *49*(4), 1399–1406. https://doi.org/10.3758/s13428-016-0796-z

Kok, P., Rahnev, D., Jehee, J. F. M., Lau, H. C., & De Lange, F. P. (2012). Attention reverses the effect of prediction in silencing sensory signals. *Cerebral Cortex*, *22*(9), 2197–2206. https://doi.org/10.1093/cercor/bhr310

Kristjánsson, Á., & Campana, G. (2010). Where perception meets memory: A review of repetition priming in visual search tasks. *Attention, Perception, & Psychophysics*, *72*(1), 5-18.

Kuehl, L. K., Brandt, E. S., Hahn, E., Dettling, M., & Neuhaus, A. H. (2013). Exploring the time course of N170 repetition suppression: A preliminary study. *International Journal of Psychophysiology*, 87(2), 183-188.

Kulashekhar, S., Pekkola, J., Palva, J. M., & Palva, S. (2016). The role of cortical beta oscillations in time estimation. *Human Brain Mapping*, *37*(9), 3262–3281. https://doi.org/10.1002/hbm.23239

Lakatos, P., Gross, J., & Thut, G. (2019). A New Unifying Account of the Roles of Neuronal Entrainment. *Current Biology*, *29*(18), R890–R905. https://doi.org/10.1016/j.cub.2019.07.075

Lakatos, P., Karmos, G., Mehta, A. D., Ulbert, I., & Schroeder, C. E. (2008). Entrainment of neuronal oscillations as a mechanism of attentional selection. *Science*, *320*(5872), 110–113. https://doi.org/10.1126/science.1154735

Lakatos, P., Musacchia, G., O'Connel, M. N., Falchier, A. Y., Javitt, D. C., & Schroeder, C. E. (2013). The Spectrotemporal Filter Mechanism of Auditory Selective Attention. *Neuron*, *77*(4), 750–761. https://doi.org/10.1016/j.neuron.2012.11.034

Large, E. W., & Jones, M. R. (1999). The dynamics of attending: How people track time-varying events. *Psychological review*, *106*(1), 119.

Lee, J. Y., Jun, H., Soma, S., Nakazono, T., Shiraiwa, K., Dasgupta, A., Nakagawa, T., Xie, J. L., Chavez, J., Romo, R., Yungblut, S., Hagihara, M., Murata, K., & Igarashi, K. M. (2021). Dopamine facilitates associative memory encoding in the entorhinal cortex. *Nature*, *598*(7880), 321–326. https://doi.org/10.1038/s41586-021-03948-8

Lewis, A. G., Schriefers, H., Bastiaansen, M., & Schoffelen, J. M. (2018). Assessing the utility of frequency tagging for tracking memory-based reactivation of word representations. *Scientific Reports*, *8*(1), 1–12. https://doi.org/10.1038/s41598-018-26091-3

Little, S., Bonaiuto, J., Barnes, G., & Bestmann, S. (2019). Human motor cortical beta bursts relate to movement planning and response errors. *PLoS Biology*, *17*(10), 1–30. https://doi.org/10.1371/journal.pbio.3000479

Little, S., & Brown, P. (2014). The functional role of beta oscillations in Parkinson's disease. *Parkinsonism & related disorders*, *20*, S44-S48.

Mansvelder, H. D., Verhoog, M. B., & Goriounova, N. A. (2019). Synaptic plasticity in human cortical circuits: cellular mechanisms of learning and memory in the human brain? *Current Opinion in Neurobiology*, *54*, 186–193. https://doi.org/10.1016/j.conb.2018.06.013

Maris, E., & Oostenveld, R. (2007). Nonparametric statistical testing of EEG- and MEG-data. *Journal of Neuroscience Methods*, *164*(1), 177–190. https://doi.org/10.1016/j.jneumeth.2007.03.024

Martorell, A. J., Paulson, A. L., Suk, H. J., Abdurrob, F., Drummond, G. T., Guan, W., Young, J. Z., Kim, D. N. W., Kritskiy, O., Barker, S. J., Mangena, V., Prince, S. M., Brown, E. N., Chung, K., Boyden, E. S., Singer, A. C., & Tsai, L. H. (2019). Multi-sensory Gamma Stimulation Ameliorates Alzheimer's-Associated Pathology and Improves Cognition. *Cell*, *177*(2), 256-271.e22. https://doi.org/10.1016/j.cell.2019.02.014

Mathewson, K. E., Prudhomme, C., Fabiani, M., Beck, D. M., Lleras, A., & Gratton, G. (2012). Making waves in the stream of consciousness: Entraining oscillations in EEG alpha and fluctuations in visual awareness with rhythmic visual stimulation. *Journal of Cognitive Neuroscience*, *24*(12), 2321–2333. https://doi.org/10.1162/jocn_a_00288

McCarthy, M. M., Moore-Kochlacs, C., Gu, X., Boyden, E. S., Han, X., & Kopell, N. (2011). Striatal origin of the pathologic beta oscillations in Parkinson's disease. *Proceedings of the National Academy of Sciences*, *108*(28), 11620-11625.

McMahon, D. B. T., & Leopold, D. A. (2012). Stimulus timing-dependent plasticity in high-level vision. *Current Biology*, *22*(4), 332–337. https://doi.org/10.1016/j.cub.2012.01.003

Meliza, C. D., & Dan, Y. (2006). Receptive-field modification in rat visual cortex induced by paired visual stimulation and single-cell spiking. *Neuron*, *49*(2), 183–189. https://doi.org/10.1016/j.neuron.2005.12.009

Merker, B. (2000). *Synchronous chorusing and human origins*. na.

Meyer, L., Sun, Y., & Martin, A. E. (2020). Synchronous, but not entrained: exogenous and endogenous cortical rhythms of speech and language processing. *Language, Cognition and Neuroscience*, *35*(9), 1089–1099. https://doi.org/10.1080/23273798.2019.1693050

Miltner, W. H. R., Braun, C., Arnold, M., Witte, H., & Taub, E. (1999). Coherence of gamma-band EEG activity as a basis for associative learning. *Nature*, *397*(6718), 434–436. https://doi.org/10.1038/17126

Morgan, S. T., Hansen, J. C., & Hillyard, S. A. (1996). Selective attention to stimulus location modulates the steady-state visual evoked potential. *Proceedings of the National Academy of Sciences of the United States of America*, *93*(10), 4770–4774. https://doi.org/10.1073/pnas.93.10.4770

Milner, B. (1966). Amnesia following operation on the temporal lobes. *Amnesia*.

Miyake, Y., Onishi, Y., & Poppel, E. (2004). Two types of anticipation in synchronization tapping. *Acta neurobiologiae experimentalis*, *64*(3), 415-426.

Molinaro, N., & Lizarazu, M. (2018). Delta (but not theta)-band cortical entrainment involves speech-specific processing. *European Journal of Neuroscience*, 48(7), 2642-2650.

Molle, M., Marshall, L., Gais, S., & Born, J. (2002). Grouping of spindle activity during slow oscillations in human non-REM sleep. *Journal of Neuroscience*, *22*(24), 10941–10947. http://www.jneurosci.org/cgi/content/abstract/22/24/10941

Morillon, B., & Baillet, S. (2017). Motor origin of temporal predictions in auditory attention. *Proceedings of the National Academy of Sciences of the United States of America*, *114*(42), E8913–E8921. https://doi.org/10.1073/pnas.1705373114

Morillon, B., Schroeder, C. E., & Wyart, V. (2014). Motor contributions to the temporal precision of auditory attention. *Nature Communications*, *5*. https://doi.org/10.1038/ncomms6255

Morillon, B., Schroeder, C. E., Wyart, V., & Arnal, L. H. (2016). Temporal prediction in lieu of periodic stimulation. *Journal of Neuroscience*, *36*(8), 2342–2347. https://doi.org/10.1523/JNEUROSCI.0836-15.2016

Müller, M. M., Andersen, S., Trujillo, N. J., Valdés-Sosa, P., Malinowski, P., & Hillyard, S. A. (2006). Feature-selective attention enhances color signals in early visual areas of the human brain. *Proceedings of the National Academy of Sciences of the United States of America*, *103*(38), 14250–14254. https://doi.org/10.1073/pnas.0606668103

Müller, M. M., Malinowski, P., Gruber, T., & Hillyard, S. A. (2003). Sustained division of the attentional spotlight. *Nature*, *424*(6946), 309–312. https://doi.org/10.1038/nature01812

Müller, N. G., Strumpf, H., Scholz, M., Baier, B., & Melloni, L. (2013). Repetition suppression versus enhancement—it's quantity that matters. *Cerebral cortex*, 23(2), 315-322.

Muthukumaraswamy, S. D., & Singh, K. D. (2013). Visual gamma oscillations: The effects of stimulus type, visual field coverage and stimulus motion on MEG and EEG recordings. *NeuroImage*, *69*, 223–230. https://doi.org/10.1016/j.neuroimage.2012.12.038

Niso, G., Rogers, C., Moreau, J. T., Chen, L. Y., Madjar, C., Das, S., Bock, E., Tadel, F., Evans, A. C., Jolicoeur, P., & Baillet, S. (2016). OMEGA: The Open MEG Archive. *NeuroImage*, *124*, 1182–1187. https://doi.org/10.1016/j.neuroimage.2015.04.028

Nordt, M., Hoehl, S., & Weigelt, S. (2016). The use of repetition suppression paradigms in developmental cognitive neuroscience. *Cortex*, 80, 61-75.

Oostenveld, R., Fries, P., Maris, E., & Schoffelen, J. M. (2011). FieldTrip: open source software for advanced analysis of MEG, EEG, and invasive electrophysiological data. *Computational intelligence and neuroscience, 2011*.

Oke, O. O., Magony, A., Anver, H., Ward, P. D., Jiruska, P., Jefferys, J. G. R., & Vreugdenhil, M. (2010). High-frequency gamma oscillations coexist with low-frequency gamma oscillations in the rat visual cortex in vitro. *European Journal of Neuroscience*, *31*(8), 1435–1445. https://doi.org/10.1111/j.1460-9568.2010.07171.x

Papalambros, N. A., Santostasi, G., Malkani, R. G., Braun, R., Weintraub, S., Paller, K. A., & Zee, P. C. (2017). Acoustic enhancement of sleep slow oscillations and concomitant memory improvement in older adults. *Frontiers in Human Neuroscience*, *11*(March), 1–14. https://doi.org/10.3389/fnhum.2017.00109

Patel, A. D. (2011). Why would musical training benefit the neural encoding of speech? The OPERA hypothesis. *Frontiers in psychology*, *2*, 142.

Patel, A. D. (2014). Can nonlinguistic musical training change the way the brain processes speech? The expanded OPERA hypothesis. *Hearing research*, *308*, 98-108.

Park, H., Kayser, C., Thut, G., & Gross, J. (2016). Lip movements entrain the observers' low-frequency brain oscillations to facilitate speech intelligibility. *ELife*, *5*(MAY2016), 1–17. https://doi.org/10.7554/eLife.14521

Pavlides, C., Greenstein, Y. J., Grudman, M., & Winson, J. (1988). Long-term potentiation in the dentate gyrus is induced preferentially on the positive phase of θ-rhythm. *Brain research*, *439*(1-2), 383-387.

Pelli, D. G. (1997) The VideoToolbox software for visual psychophysics: Transforming numbers into movies, *Spatial Vision* 10:437-442

Peykarjou, S., Pauen, S., & Hoehl, S. (2014). How do 9-month-old infants categorize human and ape faces? A rapid repetition ERP study. *Psychophysiology*, 51(9), 866-878.

Pfurtscheller, G., & Da Silva, F. L. (1999). Event-related EEG/MEG synchronization and desynchronization: basic

principles. *Clinical neurophysiology*, *110*(11), 1842-1857.

Pressing, J. (1999). The referential dynamics of cognition and action. *Psychological Review*, *106*(4), 714.

Price, M. H., & Johnson, J. D. (2018). Failure to reactivate salient episodic information during indirect and direct tests of memory retrieval. *Brain Research*, *1699*, 9–18. https://doi.org/10.1016/j.brainres.2018.06.031

R Core Team (2021). R: Alanguage and environment for statistical computing. R Foundation for Statistical Computing. Venna, Austria.

Repp, B. H. (2005). Sensorimotor synchronization: A review of the tapping literature. *Psychonomic Bulletin and Review*, *12*(6), 969–992. https://doi.org/10.3758/BF03206433

Repp, B. H., & Su, Y. H. (2013). Sensorimotor synchronization: A review of recent research (2006-2012). *Psychonomic Bulletin and Review*, *20*(3), 403–452. https://doi.org/10.3758/s13423-012-0371-2

Romei, V., Chiappini, E., Hibbard, P. B., & Avenanti, A. (2016). Empowering Reentrant Projections from V5 to V1 Boosts Sensitivity to Motion. *Current Biology*, *26*(16), 2155–2160. https://doi.org/10.1016/j.cub.2016.06.009

Schneider, M., Tzanou, A., Uran, C., & Vinck, M. (2023). Cell-type-specific propagation of visual flicker. *Cell Reports*, *42*(5), 112492. https://doi.org/10.1016/j.celrep.2023.112492

Schomburg, E. W., Fernández-Ruiz, A., Mizuseki, K., Berényi, A., Anastassiou, C. A., Koch, C., & Buzsáki, G. (2014). Theta Phase Segregation of Input-Specific Gamma Patterns in Entorhinal-Hippocampal Networks. *Neuron*, *84*(2), 470–485. https://doi.org/10.1016/j.neuron.2014.08.051

Schroeder, C. E., & Lakatos, P. (2009). Low-frequency neuronal oscillations as instruments of sensory selection. *Trends in Neurosciences*, *32*(1), 9–18. https://doi.org/10.1016/j.tins.2008.09.012

Sederberg, P. B., Kahana, M. J., Howard, M. W., Donner, E. J., & Madsen, J. R. (2003). Theta and Gamma Oscillations during Encoding Predict Subsequent Recall. *Journal of Neuroscience*, *23*(34), 10809–10814. https://doi.org/10.1523/jneurosci.23-34-10809.2003

Segaert, K., Weber, K., de Lange, F. P., Petersson, K. M., & Hagoort, P. (2013). The suppression of repetition enhancement: a review of fMRI studies. *Neuropsychologia*, 51(1), 59-66.

Sherman, M. A., Lee, S., Law, R., Haegens, S., Thorn, C. A., Hämäläinen, M. S., Moore, C. I., & Jones, S. R. (2016). Neural mechanisms of transient neocortical beta rhythms: Converging evidence from humans, computational modeling, monkeys, and mice. *Proceedings of the National Academy of Sciences of the United States of America*, *113*(33), E4885–E4894. https://doi.org/10.1073/pnas.1604135113

Shin, H., Law, R., Tsutsui, S., Moore, C. I., & Jones, S. R. (2017). The rate of transient beta frequency events predicts behavior across tasks and species. *ELife*, *6*, 1–31. https://doi.org/10.7554/eLife.29086

Siegle, J. H., & Wilson, M. A. (2014). Enhancement of encoding and retrieval functions through theta phase-specific manipulation of hippocampus. *ELife*, *3*, 1–18. https://doi.org/10.7554/elife.03061

Song, S., Miller, K. D., & Abbott, L. F. (2000). Competitive Hebbian learning through spike-timing-dependent

synaptic plasticity. *Nature neuroscience*, *3*(9), 919-926.

Soula, M., Martín-Ávila, A., Zhang, Y., Dhingra, A., Nitzan, N., Sadowski, M. J., Gan, W. B., & Buzsáki, G. (2023). Forty-hertz light stimulation does not entrain native gamma oscillations in Alzheimer's disease model mice. *Nature Neuroscience*, *26*(4), 570–578. https://doi.org/10.1038/s41593-023-01270-2

Spaak, E., de Lange, F. P., & Jensen, O. (2014). Local entrainment of alpha oscillations by visual stimuli causes cyclic modulation of perception. *Journal of Neuroscience*, *34*(10), 3536–3544. https://doi.org/10.1523/JNEUROSCI.4385-13.2014

Spyropoulos, G., Schneider, M., Van Kempen, J., Gieselmann, M. A., Thiele, A., & Vinck, M. (2022). Distinct feedforward and feedback pathways for cell-type specific attention effects. *BioRxiv*. https://doi.org/10.1101/2022.11.04.515185

Staresina, B. P., Bergmann, T. O., Bonnefond, M., Van Der Meij, R., Jensen, O., Deuker, L., Elger, C. E., Axmacher, N., & Fell, J. (2015). Hierarchical nesting of slow oscillations, spindles and ripples in the human hippocampus during sleep. *Nature Neuroscience*, *18*(11), 1679–1686. https://doi.org/10.1038/nn.4119

Stefan, K., Kunesch, E., Benecke, R., Cohen, L. G., & Classen, J. (2002). Mechanisms of enhancement of human motor cortex excitability induced by interventional paired associative stimulation. *Journal of Physiology*, *543*(2), 699–708. https://doi.org/10.1113/jphysiol.2002.023317

Stefanics, G., Hangya, B., Hernádi, I., Winkler, I., Lakatos, P., & Ulbert, I. (2010). Phase entrainment of human delta oscillations can mediate the effects of expectation on reaction speed. *Journal of Neuroscience*, *30*(41), 13578–13585. https://doi.org/10.1523/JNEUROSCI.0703-10.2010

Stefanics, G., Heinzle, J., Czigler, I., Valentini, E., & Stephan, K. E. (2020). Timing of repetition suppression of event-related potentials to unattended objects. *European Journal of Neuroscience*, 52(11), 4432-4441.

Störmer, V. S., Alvarez, G. A., & Cavanagh, P. (2014). Within-hemifield competition in early visual areas limits the ability to track multiple objects with attention. *Journal of Neuroscience*, *34*(35), 11526–11533. https://doi.org/10.1523/JNEUROSCI.0980-14.2014

Suh, J., Rivest, A. J., Nakashiba, T., Tominaga, T., & Tonegawa, S. (2013). Entorhinal Cortex Layer III Input to the. *Science*, *1415*(2011), 1415–1421.

Tadel, F., Baillet, S., Mosher, J. C., Pantazis, D., & Leahy, R. M. (2011). Brainstorm: a user-friendly application for MEG/EEG analysis. *Computational intelligence and neuroscience, 2011*.

Tallon-Baudry, C., Bertrand, O., Hénaff, M. A., Isnard, J., & Fischer, C. (2005). Attention modulates gamma-band oscillations differently in the human lateral occipital cortex and fusiform gyrus. *Cerebral Cortex*, *15*(5), 654–662. https://doi.org/10.1093/cercor/bhh167

Testa-Silva, G., Verhoog, M. B., Goriounova, N. A., Loebel, A., Hjorth, J. J. J., Baayen, J. C., de Kock, C. P. J., & Mansvelder, H. D. (2010). Human synapses show a wide temporal window for spike-timing-dependent plasticity. *Frontiers in Synaptic Neuroscience*, *2*(JUL), 1–11. https://doi.org/10.3389/fnsyn.2010.00012

Thaut, M. H., McIntosh, G. C., & Rice, R. R. (1997). Rhythmic facilitation of gait training in hemiparetic stroke rehabilitation. *Journal of the Neurological Sciences*, *151*(2), 207–212. https://doi.org/10.1016/S0022-510X(97)00146-9

Todorovic, A., Schoffelen, J. M., Van Ede, F., Maris, E., & De Lange, F. P. (2015). Temporal expectation and attention jointly modulate auditory oscillatory activity in the beta band. *PLoS ONE*, *10*(3), 1–16. https://doi.org/10.1371/journal.pone.0120288

Tompary, A., & Davachi, L. (2022). Consolidation-dependent behavioral integration of sequences related to mPFC neural overlap and hippocampal-cortical connectivity. *BioRxiv*, 2022.10.20.513126. https://www.biorxiv.org/content/10.1101/2022.10.20.513126v1%0Ahttps://www.biorxiv.org/content/10.1101/2022.10.20.513126v1.abstract

Tulving, E. (1972). Organization of memory. *Episodic and semantic memory*.

Tulving, E. (1983). Elements of episodic memory.

Tulving, E. (1984). Precis of elements of episodic memory. *Behavioral and Brain Sciences*, *7*(2), 223-238.

Tulving, E. (1993). What is episodic memory?. *Current directions in psychological science*, *2*(3), 67-70.

Van Diepen, R. M., & Mazaheri, A. (2018). The Caveats of observing Inter-Trial Phase-Coherence in Cognitive Neuroscience. *Scientific Reports*, *8*(1), 1–9. https://doi.org/10.1038/s41598-018-20423-z

van Wijk, B. C. M., Beek, P. J., & Daffertshofer, A. (2012). Neural synchrony within the motor system: What have we learned so far? *Frontiers in Human Neuroscience*, *6*(SEPTEMBER), 1–15. https://doi.org/10.3389/fnhum.2012.00252

Verhoog, M. B., Goriounova, N. A., Obermayer, J., Stroeder, J., Johannes Hjorth, J. J., Testa-Silva, G., Baayen, J. C., de Kock, C. P. J., Meredith, R. M., & Mansvelder, H. D. (2013). Mechanisms underlying the rules for associative plasticity at adult human neocortical synapses. *Journal of Neuroscience*, *33*(43), 17197–17208. https://doi.org/10.1523/JNEUROSCI.3158-13.2013

Vidal, J. R., Chaumon, M., O'Regan, J. K., & Tallon-Baudry, C. (2006). Visual grouping and the focusing of attention induce gamma-band oscillations at different frequencies in human magnetoencephalogram signals. *Journal of Cognitive Neuroscience*, *18*(11), 1850–1862. https://doi.org/10.1162/jocn.2006.18.11.1850

Vinck, M., Lima, B., Womelsdorf, T., Oostenveld, R., Singer, W., Neuenschwander, S., & Fries, P. (2010). Gamma-phase shifting in awake monkey visual cortex. *Journal of Neuroscience*, *30*(4), 1250–1257. https://doi.org/10.1523/JNEUROSCI.1623-09.2010

Vinck, M., van Wingerden, M., Womelsdorf, T., Fries, P., & Pennartz, C. M. A. (2010). The pairwise phase consistency: A bias-free measure of rhythmic neuronal synchronization. *NeuroImage*, *51*(1), 112–122. https://doi.org/10.1016/j.neuroimage.2010.01.073

Vivekananda, U., Bush, D., Bisby, J. A., Baxendale, S., Rodionov, R., Diehl, B., Chowdhury, F. A., McEvoy, A.

W., Miserocchi, A., Walker, M. C., & Burgess, N. (2021). Theta power and theta-gamma coupling support long-term spatial memory retrieval. *Hippocampus*, *31*(2), 213–220. https://doi.org/10.1002/hipo.23284

Wang, D., Clouter, A., Chen, Q., Shapiro, K. L., & Hanslmayr, S. (2018). Single-trial phase entrainment of theta oscillations in sensory regions predicts human associative memory performance. *Journal of Neuroscience*, *38*(28), 6299–6309. https://doi.org/10.1523/JNEUROSCI.0349-18.2018

Wang, D., Shapiro, K. L., & Hanslmayr, S. (2023). Altering stimulus timing via fast rhythmic sensory stimulation induces STDP-like recall performance in human episodic memory. *Current Biology : CB*, *33*(15), 3279–3288. https://doi.org/10.1016/j.cub.2023.06.062

Williams, J. H. (2001). Frequency-specific effects of flicker on recognition memory. *Neuroscience*, *104*(2), 283-286.

Wespatat, V., Tennigkeit, F., & Singer, W. (2004). Phase sensitivity of synaptic modifications in oscillating cells of rat visual cortex. *Journal of Neuroscience*, *24*(41), 9067–9075. https://doi.org/10.1523/JNEUROSCI.2221-04.2004

West, T. O., Duchet, B., Farmer, S. F., Friston, K. J., & Cagnan, H. (2022). When do Bursts Matter in the Primary Motor Cortex? Investigating Changes in the Intermittencies of Beta Rhythms Associated with Movement States. *Progress in Neurobiology*, 102397. https://doi.org/10.1016/j.pneurobio.2022.102397

Whittington, M. A., Traub, R. D., Faulkner, H. J., Stanford, I. M., & Jeffers, J. G. R. (1997). Recurrent excitatory postsynaptic potentials induced by synchronized fast cortical oscillations. *Proceedings of the National Academy of Sciences of the United States of America*, *94*(22), 12198–12203. https://doi.org/10.1073/pnas.94.22.12198

Williams, P. E., Mechler, F., Gordon, J., Shapley, R., & Hawken, M. J. (2004). Entrainment to video displays in primary visual cortex of macaque and humans. *Journal of Neuroscience*, *24*(38), 8278–8288. https://doi.org/10.1523/JNEUROSCI.2716-04.2004

Wimber, M., Maaß, A., Staudigl, T., Richardson-Klavehn, A., & Hanslmayr, S. (2012). Rapid memory reactivation revealed by oscillatory entrainment. *Current Biology*, *22*(16), 1482–1486. https://doi.org/10.1016/j.cub.2012.05.054

Wolters, A., Sandbrink, F., Schlottmann, A., Kunesch, E., Stefan, K., Cohen, L. G., Benecke, R., & Classen, J. (2003). A temporally asymmetric Hebbian rule governing plasticity in the human motor cortex. *Journal of Neurophysiology*, *89*(5), 2339–2345. https://doi.org/10.1152/jn.00900.2002

Wright, R. L., Briony Brownless, S., Pratt, D., Sackley, C. M., & Wing, A. M. (2017). Stepping to the Beat: Feasibility and potential efficacy of a home-based auditory-cued step training program in chronic stroke. *Frontiers in Neurology*, *8*(AUG), 1–9. https://doi.org/10.3389/fneur.2017.00412

Wright, R. L., Spurgeon, L. C., & Elliott, M. T. (2014). Stepping to phase-perturbed metronome cues: multisensory advantage in movement synchrony but not correction. *Frontiers in human neuroscience*, *8*, 724.

Wyart, V., & Tallon-Baudry, C. (2008). Neural dissociation between visual awareness and spatial attention. *Journal*

of Neuroscience, *28*(10), 2667–2679. https://doi.org/10.1523/JNEUROSCI.4748-07.2008

Yao, H., & Dan, Y. (2001). Stimulus timing-dependent plasticity in cortical processing of orientation. *Neuron*, *32*(2), 315–323. https://doi.org/10.1016/S0896-6273(01)00460-3

Yao, H., Shen, Y., & Dan, Y. (2004). Intracortical mechanism of stimulus-timing-dependent plasticity in visual cortical orientation tuning. *Proceedings of the National Academy of Sciences of the United States of America*, *101*(14), 5081–5086. https://doi.org/10.1073/pnas.0302510101

Yonelinas, A. P. (1999). The contribution of recollection and familiarity to recognition and source-memory judgments: A formal dual-process model and an analysis of receiver operating characterstics. *Journal of Experimental Psychology: Learning, Memory, and Cognition*, *25*(6), 1415.

Yonelinas, A. P. (2002). The nature of recollection and familiarity: A review of 30 years of research. *Journal of memory and language*, *46*(3), 441-517.

Zago, L., Fenske, M. J., Aminoff, E., & Bar, M. (2005). The rise and fall of priming: how visual exposure shapes cortical representations of objects. *Cerebral Cortex*, 15(11), 1655-1665.

Zhang, L. I., Tao, H. W., Holt, C. E., Harris, W. a, & Poo, M. (1998). and Competition Among Developing. *Metrologia*, *395*(September), 37–44.

Zheng, C., Bieri, K. W., Hsiao, Y. T., & Colgin, L. L. (2016). Spatial Sequence Coding Differs during Slow and Fast Gamma Rhythms in the Hippocampus. *Neuron*, *89*(2), 398–408. https://doi.org/10.1016/j.neuron.2015.12.005

Zheng, C., Bieri, K. W., Trettel, S. G., & Colgin, L. L. (2015). The relationship between gamma frequency and running speed differs for slow and fast gamma rhythms in freely behaving rats. *Hippocampus*, *25*(8), 924–938. https://doi.org/10.1002/hipo.22415

Zhigalov, A., Herring, J. D., Herpers, J., Bergmann, T. O., & Jensen, O. (2019). Probing cortical excitability using rapid frequency tagging. *NeuroImage*, *195*(December 2018), 59–66. https://doi.org/10.1016/j.neuroimage.2019.03.056